Contribution to the Exposure Assessment for the Evaluation of Wind Effects on Buildings

Jianhan Yu

A Thesis

in

The Department

of

Building, Civil and Environmental Engineering

Presented in Partial Fulfillment of the Requirements

For the Degree of

Doctor of Philosophy (Building Engineering) at

Concordia University

Montreal, Quebec, Canada

September 2022

C O N C O R DI A U N I V E R S I T Y

S C H O O L O F G R A D U A T E S T U DI E S

This is to certify that the thesis prepared

By: **Jianhan Yu**

Entitled: **Contribution to the Exposure Assessment for the Evaluation of Wind Effects on Buildings**

and submitted in partial fulfillment of the requirements for the degree of

Doctor of Philosophy Program

Compiles with the regulations of the University and meets the accepted standards with respect to originality and quality.

Signed by the final examining committee:

Dr. Adam Krzyzak Chair

Dr. Theodore Stathopoulos Thesis Supervisor

Dr. Hua Ge Examiner

Dr. Liangzhu Wang Examiner

Dr. Mojtaba Kheiri Examiner

Dr. Forrest J. Masters External Examiner

Approved by Dr. Mazdak Nik-Bakht , Graduate Program Director

«Date» Dr. Mourad Debbabi , Dean

ABSTRACT

Contribution to the Exposure Assessment for the Evaluation of Wind Effects on Buildings

Jianhan Yu, Ph.D.

Concordia University, 2022

The upstream exposure has a major influence on wind loading and on wind environmental conditions around buildings. However, exposure characterization is also a complex and difficult wind engineering problem. The present comprehensive investigation addresses the exposure assessment issue in terms of evaluating the exposure roughness length (z_o) by using various computational approaches.

Countries specify exposure coefficients in wind load provisions to help designers evaluate wind loads on buildings. However, these specifications can include inconsistencies and discrepancies, leading to different results for similar cases while the wind characteristics do not change from country to country. This thesis examines the current wind load provisions of the American Society of Civil Engineers Standard (ASCE 7, 2022), the National Building Code of Canada (NBCC, 2020), the European Standard (EN 1991-1-4, 2005), the Australian/New Zealand Standard (AS/NZS 1170.2, 2021), and the National Standard of the People's Republic of China (GB 50009, 2012) in terms of exposure, and results are compared and discussed. First, the wind load provisions of ASCE 7 (2022) are considered to illustrate the process that most of the provisions follow. For homogeneous exposure, the terrain roughness categories and the corresponding exposure factors are compared. Additionally, the suggested minimum upstream fetch length for different exposure types is discussed by comparing them with the latest research findings. For non-homogeneous

exposure, equations to calculate small-scale roughness change in various provisions are assessed by comparing them with wind tunnel experimental data. The inconsistencies between different provisions are identified, and remedies are proposed to minimize or avoid various errors, which are sometimes subjective. Other approaches such as the internal boundary layer (IBL) theory-based method, the morphometric method, the anemometric method, and the geographic information system (GIS)-based method are reviewed. It was found that it is usually expensive or time-consuming to estimate the exposure coefficients through these methods, particularly in complex terrain. Therefore, an innovative approach to estimate the value of z_o based on Google Earth Pro is proposed, and this approach is efficient and freely available. Two case studies, namely, London, UK and the Tampa International Airport, Florida, were adopted to verify the accuracy of the proposed method and yielded satisfactory results.

This thesis also investigates the effects of upstream exposure on environmental wind engineering problems by taking pedestrian-level wind (PLW) velocity cases as typical examples. The methodology of computational wind engineering (CWE), which works better on environmental challenges than on structural wind engineering problems, is adopted, and the expected discrepancies in the results for typical cases are established and assessed. The sensitivity of the PLW velocity factors to the upstream exposure fetch is documented and discussed. The research presented in the thesis demonstrates a great potential to contribute to further development of wind standards and codes of practice, as far as the characterization of the upstream exposure is concerned, at the national and international level (ISO).

ACKNOWLEDGMENTS

My sincere gratitude goes first to my Professor, Dr. Ted Stathopoulos, for his guidance, encouragement, and support throughout the study. His acceptance letter of my exchange Ph.D. program 6 years ago changed my life and brought me the opportunity of broadening my horizons. I started my second Ph.D. with him, and this was the best decision so far.

I still remember my first year in Canada, at the sunshine afternoon in his office, when he taught me how to organize the structure of my first English manuscript very patiently. Every manuscript, as well as the thesis, he reviewed and modified word by word, despite his overbooked schedule. His serious attitude towards academic work is the goal I will pursue for the rest of my research career. At the first two years and I had my son, he always respected my personal time slot, although he has also been very-very busy. During the pandemic, he supervised me through countless Skype and Zoom meetings when I was in China. He taught me the skills to be a researcher, he gave me confidence, and also taught how to be a nice person. I am extremely lucky to have such a supervisor.

I would like to express my deepest gratitude to Prof. Mingshui Li and Prof. Haili Liao from Southwest Jiaotong University of China, where I completed my first Ph.D. degree. Thanks for their support and suggestions for my wind tunnel tests and investigations during the three years I worked there.

I greatly appreciate and acknowledge the financial support I received from the China Scholarship Council during 2016 - 2018 and Concordia University International Tuition Award of Excellence

during my Ph.D. program.

Many thanks to my colleagues, as well as my dear friends in the wind tunnel lab, Hatem Alrawashdeh, Anastasia Athanasiou, Murad Aldoum, Theodore Potsis, Stephanie Higgins, Sakib Faruk, and Mu'ath Makhadmeh. My special thanks for the help of Hatem and Theodore, whenever I needed their assistance, and for their timely discussions of my wind tunnel tests. Thanks to the friendship of Anastasia, with whom I had small valuable talks during the weekdays to relieve stress and explore Montreal in the weekends.

Further, I would like to express many thanks to my friends Danlin Hou and Tiantian Chen, who also had a baby during the Ph.D. program. You will never know how difficult it is unless you experience it. Girls help girls, we supported and encouraged each other during the most critical times. Special thanks for the support of my friends, Ying Sun, Chao Zeng, Jing Li, Senwen Yang, Hongwen Dou, as well as Mr. J. Guan and his wife during my stay in Montreal. Finally, many thanks for the support of my office roommates, Payam Gholamalipour, Majd Moujahed, and Maher Albettar.

Last but not least, I would like to express my sincere and deep gratitude to my parents for all their sacrifices and unconditional love. Without their caring of my son, I could not focus on the thesis during the last several months. Special appreciation to my husband for his continued and unfailing love and support during my pursuit of the Ph.D. degree; and to my dearest son, who has been the light of my life in the last four years giving me the extra strength and motivation to move forward.

TABLE OF CONTENTS

LIST OF FIGURES

LIST OF TABLES

NOMENCLATURE

Ci	Velocity ratio with and without proposed building
q_z	Velocity pressure at height z
R_i	Velocity ratio with different upstream fetch length
S_{ob}	Frontal area
S_k, S_ε	Source terms of turbulence model equations
H_{max}	Maximum of roughness — obstacles height
H_{ob}	Average height of upstream buildings
H_b	Height of highest building in the computational domain
H_d	Height of the computational domain
I	Importance factor
I_u	Longitudinal component of turbulence intensity
I_g	Turbulence intensity at z_g
I_z	Turbulence intensity at z
k	Turbulence kinetic energy
$K_{33,d}$, $K_{33,u}$	Downwind and upwind exposure coefficients at 33 ft height in ASCE 7 (2022)
K_d	Wind directionality factor in ASCE 7 (2022)
K_e	Ground elevation factor ASCE 7 (2022)
K_z	Exposure factor in ASCE 7 (2022)
K_{zd}	Terrain roughness downwind of the change at height z in ASCE 7 (2022)
K_{zt}	Topographic factor in ASCE 7 (2022)
K_{zu}	Terrain roughness upwind of the change at height z in ASCE 7 (2022)
L_u	Integral scale of turbulence
M_s	Shielding multiplier

$M_{z,cat}$	Exposure factor in AS/NZS 1170.2 (2021)
$S_{(n)}$	Energy spectrum
u	Longitudinal component of fluctuating velocity
U^*_{ABL}	Surface-shear velocity
$u*$	Atmospheric boundary layer friction velocity
$U_{(G)}$	Gradient wind speed
$U_{b,o}$	Fundamental value of the basic wind velocity (10 min mean wind velocity at 10 m above ground level in open country terrain);
U_R	Regional 3 sec gust wind speed.
U_{ref}	Reference velocity
w	Vertical component of fluctuating velocity
x	Upstream patch length
x_r	Upwind extent of rough terrain
z_0	Ground roughness length
z	Vertical elevation height
z_d	Displacement length
z_0	Roughness length
z_g	Gradient height
W	Width of the street
W_b	Width of building groups
W_d	Width of computational domain
α	Power-law index
β	Calibration constants for the Irwin probe
ε	Rate of energy dissipation

λ	Plan area density
λ_F	Frontal area density
ρ	Air density
τ	Turbulence stress
μ	Dynamic viscosity
t	Eddy or turbulence dynamic viscosity
κ	Karman constant (≈ 0.4)
σ_H	Standard deviation of roughness-obstacles height
θ	Angle between vectors

ABBREVIATIONS

3D	Three Dimensional
ABL	Atmospheric Boundary Layer
AIJ	Architectural Institute of Japan
ASCE	American Society of Civil Engineers Standard
ASTER	Advanced Spaceborne Thermal Emission and Reflection Radiometer
AS/NZS	Australian/New Zealand Standard
ASOS	Automated Surface Observing System
BPGs	Best Practice Guidelines
CFD	Computational Fluid Dynamics
CWE	Computational Wind Engineering
DEM	Digital Elevation Model
DSMs	Digital Surface Models
DTMs	Digital Terrain Models
EN	European Standard
ESDU	Engineering Sciences Data Unit
GB	National Standard of People's Republic of China
GCPs	Ground Control Points
GIS	Geographic Information Systems
GDEMs	Global Digital Elevation Models
IBL	Internal Boundary Layers
LiDAR	Light Detecting and Ranging

MAE	Mean Absolute Error
NBCC	National Building Code of Canada
PLW	Pedestrian Level Wind
RADAR	Radio Detecting and Ranging
RANS	Reynolds-averaged N–S equations
RMSE	Root Mean Square Error
SRTM	Shuttle Radar Topography Mission
SIMPLE	Semi-implicit Method for Pressure-linked Equations
UDF	User-defined Functions
UTM	Universal Transverse Mercator
WT	Wind Tunnel

Chapter 1 Introduction

1.1 General

Wind hazards are critical issues. According to the report of the Insurance Bureau of Canada, windstorms caused approximately 26% of insured property losses among the top 10 highest loss years in Canada on record (http://www.ibc.ca/on/resources/media-centre/media-releases/). Structures can be destroyed if the design wind load is inadequate. Wind-induced damage not only causes dramatic economic losses but also threatens the safety of occupants or users. Researchers have conducted many investigations to accurately estimate wind load on structures (e.g., Stathopoulos 1984; Cook 1986; Simiu and Scanlan 1996).

The wind load on buildings is influenced by two types of factors: those related to the building and those related to the wind characteristics. The building-related factors refer to the building shape, building dimension, and natural frequency, while the factors related to the wind characteristics include the wind speed, turbulence intensity, and turbulence integral length scale. These factors are compiled in the formulas of wind load in countries' current wind load provisions to help designers make decisions. Compared with the building-related factors, the wind-related factors are more complex, as they are connected to the local climate, topography, and morphology. The influence of local climate can be obtained by the data recorded at the meteorological station, which is known as basic wind speed. The impact of hills, escarpments, or ridges on wind speed at different locations are provided as topography factors, and the formulas are specified in current provisions. By contrast, the influence of exposure morphology on wind is more complicated and is identified as one of the greatest sources of uncertainty in wind load estimation. The exposure morphology upstream of a building site influences the characteristics of approaching wind, thus affecting the wind load of the site's structures. Additionally, the upstream exposure roughness also influences

the pedestrian-level wind (PLW) velocity, pollutant dispersion, heat island effect, indoor and outdoor natural ventilation, and others. Thus, the accurate specification of exposure factors is a meaningful subject of study.

1.2 Challenges

Parameter z_0 represents the effects of drag of exposure roughness on the wind as it blows over the upstream fetch. It is the only height-independent parameter to determine the exposure roughness (Wamser et al. 1977). A reliable estimation method of z_0 is the basement of the accurate estimation of wind load on structures. In current wind load provisions, z_0 is generally determined according to the exposure categories. However, subjective interpretation of upstream roughness by designers may lead to disagreements of exposure type. Other methodologies to estimate z_0 are the internal boundary layers (IBL) theory-based method, anemometric method, morphometric method, and geographic information systems (GIS) - based method. However, obtaining the raw data through these methods is always expensive and time-consuming.

Moreover, to what extent the upstream exposure influences the results of PLW studies is still a question without a definite answer. Furthermore, the question of using CWE is still debatable. Although various guidelines are proposed to suggest the meshing strategy, the boundary conditions, the turbulence model, and so on, some of the guidelines are far from clear. For example, best practice guidelines by Franke (2004) suggested that, in the area of interest, at least 10 cells per building edge and 10 cells per building separation be used, a suggestion difficult to implement in large-scale urban wind environmental simulations.

1.3 Objectives of the study

The definition of upstream exposure roughness is important in issues related to both wind load estimation and the urban wind environment. This thesis aims to understand the influence of upstream exposure roughness and to determine the exposure coefficient through a variety of approaches.

The main objectives of the present study are to:

1. Examine previous research studies in the field of exposure,
2. Compare and discuss related specifications in current wind load provisions,
3. Propose an improved methodology of determining the value of z_0 that is freely available and easy to implement,
4. Examine the possibility to use numerical methodology in comparison with the experimental approach,
5. Improve the evaluation of the upstream exposure and provide recommendations to assess the effect of urban wind environment for various cases, and
6. Possibly reduce the ambiguities and uncertainties in various wind load provisions.

1.4 Thesis outline

This thesis consists of seven chapters, a list of references and an appendix. Chapter 2 discusses the exposure factors in current wind codes and standards. The inconsistencies between different provisions are identified, and remedies are proposed based on an approach toward resolution. Chapter 3 presents the literature findings on exposure roughness and summarizes the state-of-the-art in this area.

Chapter 4 describes the experimental and numerical methodologies used in this study. The general setting, experimental devices, generation of the atmospheric boundary layer (ABL), and the

building modeling of some case studies of wind tunnel tests are introduced, along with the numerical methodology, namely, Navier–Stokes equations, turbulence models, boundary conditions, and meshing strategies as well as accuracy evaluation performance metrics.

Chapter 5 proposes an exposure roughness length estimation method based on Google Earth Pro. Two case studies of London, UK and the Tampa International Airport in Florida are examined to verify the accuracy of this method. This approach has already been presented in the paper by **Yu, J., Stathopoulos, T., & Li, M. (2021). Estimating Exposure Roughness Based on Google Earth.** ***Journal of Structural Engineering, ASCE*****;** ***147*****(3), 04020353.**

Chapter 6 investigates the application of CWE on PLW velocity studies and the use of upstream exposure metrics as determined in this research study for specific case studies. Chapter 7 summarizes the conclusions and contributions of this study and makes suggestions for future research.

Chapter 2 Exposure Factors in Current Wind Codes and Standards: Inconsistencies and Remedies

2.1 General

The compilation of wind load provisions is a process of continuous improvement based on the latest research results. Therefore, a new version of wind load provisions for different countries is released every few years. In this chapter, the specifications of exposure factors in current wind load provisions are compared and discussed.

Generally speaking, the current wind load provisions follow similar steps to calculate wind load on buildings. In the present study, the wind load provisions of the American Society of Civil Engineers Standard (ASCE 7, 2022) are adopted to illustrate the process. Exposures are divided into homogeneous and non-homogeneous types in various provisions. For homogeneous exposure, several categories are specified according to exposure roughness, and exposure factors for various categories and heights are provided accordingly. In addition, an upstream fetch length that is required to be considered is suggested. For non-homogeneous exposure, formulas are provided in most of the provisions to account for the influence of small-scale roughness change.

However, there remain some inconsistencies among various wind load provisions. In this chapter, the specifications in terms of exposure categories, minimum upstream fetch, and the formulas of non-homogeneous exposure in various wind load provisions are summarized, the inconsistencies are discussed, and remedy suggestions are proposed.

2.2 Wind load code / standard exposure provisions—example: ASCE 7 (2022)

The procedures to calculate design wind pressure in the provisions of the American Society of Civil Engineers Standard (ASCE 7, 2022), the National Building Code of Canada (NBCC, 2020), the Australian/New Zealand Standard (AS/NZS 1170.2, 2021), the European Standard (EN 1991-1-4, 2005), and the National Standard of the People's Republic of China (GB50009, 2012) are summarized in Table 2.1. Each of these provisions follows almost the same procedure: that the design wind pressure is the product of basic wind speed, gust factor, building shape factor, exposure factor, topographic factor, and directional factor, although the symbols are different.

Table 2.1 Calculation method of design wind pressure in current provisions

	ASCE 7 (2022)	NBCC (2020)	AS/NZS 1170.2 (2021)	EN 1991-1-4 (2005)	GB 50009 (2012)
Design wind pressure	$P= q_z[GC_{pf}-GC_{pi}]$	$P= qC_eC_gC_p$	$P= qC_{fig}$	$W_e = qC_eC_p$	$w_k = \beta_z\mu_s\mu_z\, w_0\eta$
Velocity pressure	$q_z = 0.00256K_zK_{zt}K_dK_eU^2$	$q = 0.5\rho U^2I$	$q = 0.5\rho U^2$	$q = 0.5\rho U^2$	$w_0 = 0.5\rho U^2$
Basic wind speed	U	U	$U = U_RM_dM_{z,cat}M_sM_t$	$U = U_{b,o}C_{dir}C_{seas}$	U
Basic wind speed averaging time	*3 s*	*1 h*	*3 s*	*10 min*	*10 min*
Exposure factor	K_z	C_e	$M_{z,cat}$	C_r	μ_z
Topography factor	K_{zt}	C_e^*	M_t	C_o	η
Gust effect factor	G	C_g	-	k_l	β_z
Building shape factor	C_p	C_p	C_{fig}	C_p	μ_s
Directional factor	K_d	-	M_d	C_{dir}	-

Notes: 1. C_e^* is used instead of C_e when the topographic factor is considered in NBCC,

2. I: Importance factor,

3. C_{seas}: Seasonal factor,

4. M_s: Shielding multiplier,

5.$U_{b,o}$: Fundamental value of the basic wind velocity (10 min mean wind velocity at 10 m above ground level in open country terrain), and

6. U_R: Regional 3 sec gust wind speed.

ASCE 7 (2022) is the most explicit and authoritative wind load provision so far. This standard has been taken as an example to illustrate the calculation process of wind load. The wind pressure p is calculated using Eq. 2.1:

$$p = q_z[GC_{pf} - GC_{pi}] \text{ (psf)} \quad (2.1)$$

where q_z is the velocity pressure at height "z," q_z is calculated using Eq. 2.2, and GC_{pf} and GC_{pi} are the external and internal pressure coefficients, respectively. These two factors can be obtained by the figures in the standard:

$$q_z = 0.00256 K_z K_{zt} K_d K_e U^2 \text{ (psf)} \quad (2.2)$$

where K_z is the exposure factor, K_{zt} is the topographic factor, K_d is the wind directionality factor, K_e is the ground elevation factor, and U is the basic wind speed (mph), in other words, a 3-s gust wind speed at 33 ft above ground in Exposure C.

In this study, the focus is on the exposure coefficient K_z, which demonstrates the influence of upstream exposure roughness to the approaching wind speed. K_z varies with height and exposure roughness. The relationship is given by power law or log law in most building codes and standards and is based on the concept of equilibrium state of the ABL. The ABL is directly influenced by the presence of Earth's surface obstacles, of which the drag and friction slow the wind speed and produce turbulence. The wind speed increases in the ABL and becomes constant above the ABL. The equilibrium state is an idealized situation in which the wind environment in the ABL becomes a fairly uniform condition after traveling hundreds or even thousands of kilometers (Irwin, 2006). When determining K_z, the first challenge lies in the selection of consideration region, which is depicted in Figure 2.1. The consideration region is a sector that is determined by the minimum upstream fetch and the sector angle specified as 45° on either side of upwind direction. The lengths

of minimum upstream fetch, varying with exposure types and building heights, are presented in Table 2.2.

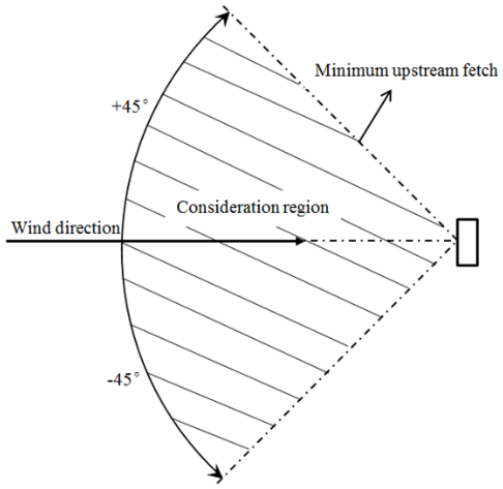

Figure 2.1 Consideration region.

For homogeneous exposure, K_z is determined by the exposure category. In ASCE 7, the surface roughness is divided into three categories (see Table 2.3), then the exposure is classified into three categories according to upstream fetch length and roughness type (see Table 2.4.) Photographs are provided to help designers make choices. Buildings in the foreground are located in Exposure B. Exposure type in the center top is classified as Exposure C when wind comes from the left. After the choice of exposure type, K_z, varying with height, can be calculated using the power law relationship of Eqs. 2.3–2.4. Linear interpolation for intermediate values is acceptable.

Exposure factors have been widely investigated and specified in current wind codes and standards. To determine the exposure factor, for homogeneous exposure, the exposure is usually simplified into three to five categories according to the exposure roughness, and the corresponding z_0 is provided:

$$\text{For } 15 \text{ ft} \leq z \leq z_g \qquad K_z = 2.01\left(z/z_g\right)^{2/\alpha} \tag{2.3}$$

$$\text{For } z \leq 15 \text{ ft} \qquad K_z = 2.01\left(15/z_g\right)^{2/\alpha} \tag{2.4}$$

where α is the exponent coefficient and z_g is the gradient height. The values of α and z_g are estimated according to Eq. 2.5:

$$\alpha = c_1 z_0^{-0.133} \tag{2.5}$$

$$z_g = c_2 z_0^{0.125} \tag{2.6}$$

where $c_1 = 5.65$; $c_2 = 450$.

Figure 2.2 Example of exposure category choice. (ASCE 7, 2022)

Table 2.2 Length of minimum upstream fetch in ASCE 7 (2022)

Terrain type	Building height h	Length of fetch
Urban/suburban area	$h \leq 30$ ft	1,500 ft
	$h > 30$ ft	2,600 ft or 20 h, whichever is greater
Flat area	-	5,000 ft or 20 h, whichever is greater

Table 2.3 Roughness categories in ASCE 7 (2022)

Roughness categories	Description
B	Urban and suburban areas, wooded areas, or terrain with numerous, closely spaced obstructions
C	Open terrain with scattered obstructions, $h \leq 30$ ft
D	Flat, unobstructed area and water surface

Table 2.4 Exposure categories in ASCE 7 (2022)

Exposure categories	Description
Exposure B	Surface roughness B for building height (h) and upstream fetch: for $h \leq 30$ ft:1,500 ft for $h > 30$ ft: 2,600 ft or 20 h, whichever is greater
Exposure C	Where Exposure B or D does not apply
Exposure D:	Surface roughness D: 5,000 ft or 20 h, whichever is greater

For non-homogeneous exposure, the small-scale roughness change directly upstream of the building site should be considered. Formulas to estimate K_z are based on the method of empirically matching the engineering sciences data unit (ESDU) with the power law relationship, which is proposed by Deaves and Harris (1981); see Eq. 2.7:

$$K_z = K_{zd} + \Delta K \tag{2.7}$$

$$\Delta K = \left(K_{33,u} - K_{33,d}\right) \frac{K_{zd}}{K_{33,d}} F_{\Delta K}(x)$$

$$\text{For } x_0 < x < x_1 \qquad F_{\Delta K}(x) = \frac{log_{10}\left(\frac{x_1}{x}\right)}{log_{10}\left(\frac{x_1}{x_0}\right)}$$

$$\text{For } x < x_0 \qquad F_{\Delta K}(x) = 1$$

$$\text{For } x > x_1 \qquad F_{\Delta K}(x) = 0$$

where K_{zd} is the terrain roughness downwind of the change at height z, K_{zu} is the terrain roughness upwind of the change at height z, $K_{33,d}$ and $K_{33,u}$ are downwind and upwind exposure coefficients at 33 ft height, $F_{\Delta K}(x)$ is the function of length, x is the distance between the downstream site and the position of roughness change, and x_1 and x_0 are coefficients specified in the standard. A detailed illustration of exposure categories and transitions of ASCE code can be found in the paper of Irwin (2006).

The accurate estimation of the exposure factor of homogeneous exposure is the foundation of the non-homogeneous exposure factor estimation, as the formulas for small-scale roughness changes are based on the exposure factor of each patch in the considered upstream fetch. There are mainly two approaches to account for exposure factor in various wind load provisions, according to exposure roughness length (z_0) and exposure categories. Research related to these two approaches is introduced in this section.

In ASCE 7 (2022), the exponent coefficient α and gradient height z_g can be obtained according to z_0 (see Eqs. 2.5 – 2.6), then the exposure factor can be calculated directly according to α and z_g (see Eq. 2.7). In EN 1991-1-4 (2005), the exposure factor C_r can also be calculated from z_0. An interpolation method is suggested in AS/NZS 1170.2 (2021) if z_0 falls in the middle of that specified for exposure categories. Traditionally, there are three methods of z_0 estimation: (1) IBLs theory-based method, (2) the anemometric method, and (3) the morphometric method, (4) GIS – based method. A detailed discussion of the development of these methods is introduced in Chapter 3. In

this section, the simple relationship proposed by Lettau (1969) is adopted (see Eq. 2.8); it is the most widely recognized method and has been accepted by ASCE 7 (2022). This method can be adopted to the exposure with low roughness density:

$$z_0 = 0.5 H_{ob} \frac{s_{ob}}{A_{ob}} \tag{2.8}$$

The determination of the exposure factor according to exposure categories is much simpler. Categories are specified according to the description of morphology in terms of average building height, roughness elements, distance, and exposure characteristic. The values of z_o are provided in most of the exposure category methods, and the exposure factors or velocity profiles can be calculated accordingly.

2.3 Homogeneous exposure

2.3.1 Exposure categories

To determine the exposure factor in homogeneous terrain, exposure is usually classified into three to five categories according to its roughness, and the exposure factor is provided for each category. The optimal exposure categories should feature a balance of accuracy of definition and simplicity of application, and they should meet the following conflicting requirements (Wieringa, 1980; Choi, 2009):

(a) The definitions of exposure types should be clear and cause no difficulty in choice. This means that the exposure should also not be divided exaggeratedly for the requirement of simplicity.

(b) The exposure categories should encompass the full range of exposure roughness, from open seas to urban areas with densely arranged high-rise buildings. Additionally, there should be enough categories that an error in category choice will not lead to severe consequences when the characteristic of the objective exposure lies between two exposure types.

The exposure factor is always associated with roughness length z_0. The provisions of ASCE 7 (2022), EN 1991-1-4 (2005), AS/NZS 1170.2 (2021), and GB 50009 (2012) specify z_0 for each exposure category. ASCE 7 (2022) and EN 1991-1-4 (2005) directly calculate exposure factors according to z_0. In AS/NZS 1170.2 (2021) and GB 50009 (2012), exposure factors are provided in the form of tables for various exposure categories, and the height and interpolation method is suggested for an intermediate z_0 value between the two exposures. NBCC (2020) has only two exposure categories, open terrain and rough terrain, and the value of z_0 does not specify. The exposure categories specified in various wind load codes are similar, which are flat or sea, open, urban/suburban, and large city center. The comparison of the specifications in the current wind provisions of each exposure type with the range of z_0 value from small to large is listed in Tables 2.5–2.8.

Table 2.5 Exposure categories of flat or sea

z_0 (m)	Code	Type name	Description
0.002	AS/NZS 1170.2 (2022)	Flat	Exposed open terrain with few or no obstructions and water surfaces at serviceable wind speeds
0.003	EN 1991-1-4 (2005)	Sea	Sea or coastal area exposed to the open sea
0.005	ASCE 7 (2022)	Flat	Flat, unobstructed areas and water surfaces outside hurricane-prone regions
0.01	EN 1991-1-4 (2005)	Flat	Lake or flat and horizontal area with negligible vegetation and without obstacles
	GB 50009 (2012)	Sea	The sea and island, coast, shore, and desert

Table 2.6 Exposure categories of open

z_0 (m)	Code	Type name	Description
0.02	AS/NZS 1170.2 (2021)	Open	Water surfaces, open terrain, grassland with few, well-scattered obstructions having heights generally from 1.5 m to 10 m
0.03	ASCE 7 (2022)	Open	Open terrain with scattered obstructions with heights generally less than 30 ft (9.1 m)
0.05	EN 1991-1-4 (2005)	Open	Area with low vegetation such as grass and isolated obstacles (trees, buildings) with separations of at least 20 obstacle heights
	GB 50009 (2012)	Open	Countryside, jungle, hills, sparse houses and suburbs

Table 2.7 Exposure categories of urban or suburban

z_0 (m)	Code	Type name	Description
0.2	AS/NZS 1170.2 (2021)	Urban/Suburban	Terrain with numerous closely spaced obstructions 3m to 5m high, such as a suburban housing area
0.3	ASCE 7 (2022)	Urban/Suburban	Urban and suburban areas, wooded areas, or other terrain with numerous closely spaced obstructions with the size of single-family dwellings or larger
	EN 1991-1-4 (2005)	Urban/Suburban	Area with regular vegetation cover or buildings or with isolated obstacles with separations of a maximum of 20 obstacle heights
	GB 50009 (2012)	Urban/Suburban	Urban area with densely packed buildings

Table 2.8 Exposure categories of large city center

z_0 (m)	Code	Type name	Description
1	EN 1991-1-4 (2005)	Large City Center	Area in which at least 15% of the surface is covered with buildings whose average height exceeds 15 m
	GB 50009 (2012)	Large City Center	Densely populated urban area with high buildings
2	AS/NZS 1170.2 (2021)	Large City Center	Terrain with numerous large, high (10 m to 30 m high) and closely spaced obstructions
	ASCE 7 (2022)	Large City Center	City centers with mixture of low-rise and high-rise buildings or large forests of irregular height with many clearings.

In general, the categories proposed by these various provisions are coherent with each other. For example, the ASCE 7 and AS/NZS 1170.2 specify the category of open with the same roughness length z_0 of 0.02 m for obstacle heights of 9.1 m and 1.5–10 m, respectively. Moreover, the revised Davenport method and the EN 1991-1-4 feature descriptions of separation distance of at least 50 h, at least 20 h and about 15 h separately with roughness lengths of 0.03 m, 0.05 m, and 0.25 m. However, there are some discrepancies and inconsistencies across different provisions. For instance, Table 2.6 indicates that z_0 ranges from 0.0002 m to 0.01 m in nearly the same description of open sea and water surfaces. The value of z_0 for large city center also differs greatly from one code to the next; for example, EN 1991-1-4 describes this exposure type as having an average building height more than 15 m, and AS/NZS 1170.2 defines the building height as ranging from 10 m to 30 m. However, the two codes provide the value of z_0 with large discrepancies of 1.0 m and 2.0 m, respectively. Similarly, though providing the same description of separations of at least 20 obstacle heights, the value of z_0 is 0.05 m and 0.1 m in the EN 1991-1-4 code and the revised

Davenport method, respectively. An incorrect choice of exposure category will lead to a huge deviation of wind load. For homogeneous exposure, the deviation may come from two parts. First, the values of z_0 of similar specification in current provisions are various, which will lead to different results from the same target issue. Second, the judgment is based on the designers' experience, which may have subjective errors. Photographs, together with the prescription, are a beneficial way to help designers make the correct choice. ASCE 7 and EN 1991-1-4 all provide photos of different exposure types. Moreover, for the exposure with easy acquisition of the layout and shape of all obstacles, the morphometric formulas of Lettau (1969) could be used to estimate the value of z_0, which is suggested by ASCE 7.

2.3.2 Minimum upstream fetch

Table 2.9 is a summary of minimum upstream fetch length in current wind load provisions. It should be noted that the specification of minimum upstream fetch length in NBCC and AS/NZS 1170.2 are provided regardless of exposure type. There is no minimum upstream fetch length in the provisions of GB 50009. Indeed, the fetch length in other provisions is the extending distance of the roughness exposure directly upstream of the building site that determines the exposure category. Only the static procedure without the consideration of wind velocity fluctuation is discussed.

Table 2.9 Specification of minimum upstream fetch length in wind load provisions

Min fetch	Flat/Open	Urban/Suburban
ASCE 7 (2022)	Max (1,524 m, 20 h)	Max (792 m, 20 h), with exception of 457 m for $h < 9.2$ m
NBCC (2020)	Max (1,000 m, 20 h)	Max (1,000 m, 20 h)
AS/NZS 1170.2 (2021)	1,000 m for $h < 50$ m 2,000 m for 50 m $\leq h < 100$ m 3,000 m for 100 m $\leq h < 200$ m	1,000 m for $h < 50$ m 2,000 m for 50 m $\leq h < 100$ m 3,000 m for 100 m $\leq h < 200$ m
EN 1991-1-4 (2005)	Flat terrain: 500 m–50,000 m Open terrain: 300 m–50,000 m for 5 m $\leq h \leq 50$ m	200 m – 20,000 m for 5 m $\leq h \leq 50$ m
GB 50009 (2012)	No mention	

Generally speaking, the lower the roughness and the higher the building, the longer the minimum upstream fetch is required, but there are deviations across various provisions. To illustrate the differences, the specification of minimum upstream fetch in current provisions of various building heights in terms of open or flat exposure and urban or suburban exposure types are illustrated in Tables 2.10 and 2.11.

For low-rise buildings with the height of 5 m, with regard to flat or open exposure, the required minimum upstream fetch ranges from 500 m by EN 1991-1-4 to 1,000 m by NBCC and AS/NZS 1170.2 and to 1,524 m by ASCE 7. Moreover, the minimum upstream fetch required to qualify the exposure as urban or suburban exposure for the same buildings' height ranges from 200 m in EN 1991-1-4 to 457 m in ASCE 7 and to 1,000 m in NBCC and AS/NZS 1170.2. The specification of minimum upstream fetch length for urban or suburban exposure of 1,000 m and for flat and open exposure of 1,524 m is large compared with the wind tunnel test result of Wang and Stathopoulos

(2006) that the wind load on low-rise building roofs with the height of 15.2 m is determined by a fetch as short as 300–400 m regardless of the upstream morphology.

For buildings with the height of 25–75 m, the minimum upstream fetch ranging from 1,000 m to 2,000 m in the provisions of ASCE 7, NBCC, and AS/NZS 1170.2 for both exposure types agree with the field measurement data by Letchford et al. (2001) that a 1,000–1,500 m fetch needs to be considered for grass upstream roughness and with the wind tunnel test results obtained by Yu et al. (2021) that the fetch length of 750 m directly upstream determines the mean velocity profile in urban exposure. By contrast, the fetch length specified in EN 1991-1-4 of approximately 22,000 m for a building height of 25 m and 50,000 m for a building height of 50 m is too large.

Discrepancies can be found between the wind load provisions and previous investigations for super-high-rise buildings of 100 m and 200 m height, which is 3,000 m in AS/NZS 1170.2 for a building height higher than 100 m and as large as 4,000 m in ASCE 7 for a building height of 200 m for both exposure types. However, Yu et al. (2021) found that the mean velocity profiles will not be influenced by upstream morphology when the fetch length goes farther than 1,250 m for urban exposure. Unfortunately, the investigation for super-high-rise buildings in a flat or open exposure is insufficient. EN 1991-1-4 does not provide the minimum upstream fetch length for a building height higher than 50 m.

Table 2.10 Minimum upstream fetch length of flat or open exposure (Unit: m)

Building heights (m)	Minimum upstream fetch length of flat or open exposure (Unit: m)			
	ASCE 7 (2022)	NBCC (2020)	AS/NZS 1170.2 (2021)	EN 1991-1-4 (2005)
5	1,524	1,000	1,000	300 (open) and 200 (flat)
25	1,524	1,000	1,000	22,500
50	1,524	1,000	1,000	50,000
75	1,524	1,500	2,000	-
100	2,000	2,000	3,000	-
200	4,000	4,000	3,000	-

Table 2.11 Minimum upstream fetch length of urban or suburban exposure (Unit: m)

Building heights (m)	Minimum upstream fetch length of urban or suburban exposure (Unit: m)			
	ASCE 7 (2022)	NBCC (2020)	AS/NZS 1170.2 (2021)	EN 1991-1-4 (2005)
5	457	1,000	1,000	200
25	792	1,000	1,000	22,388
50	1,000	1,000	2,000	50,000
75	1,500	1,500	2,000	-
100	2,000	2,000	3,000	-
200	4,000	4,000	3,000	-

Moreover, compared with the detailed specification of minimum upstream fetch by the current wind provisions, the angle of the considered upstream exposure sector is specified only in the EN 1991-1-4 and ASCE 7, which, extending to either side of the wind direction to be considered, are 15° and 45° separately. In contrast, the NBCC, AS/NZS 1170.2, and GB 50009 do not mention the

sector angle at all. The sector angle should also be defined along with the upstream fetch length to determine the scope need to be considered.

From the discussion results of this section, it can be concluded that the specification of minimum upstream fetch length in most of the current wind load provisions is large for low-rise buildings, especially the code of EN 1991-1-4. It is reasonable that the fetch length is provided according to building height, however, the specification by AS/NZS 1170.2 and NBCC of the fetch length of 1,000 m for the $h < 50$ m is a bit cursory, as there are many low-rise buildings with heights lower than 50 m and a shorter minimum upstream fetch length. Moreover, the specification of minimum upstream fetch is important for the accurate estimation of wind load. Lack of this specification may cause confusion when designers are making decisions. Therefore, it is suggested that China's wind load code include the specification of minimum upstream fetches according to building heights and exposure types. It should be pointed out that the minimum upstream fetch length discussed in this investigation is applicable only to the static analysis. Longer upstream fetch lengths are required to estimate the dynamic response of a high-rise building.

2.4 Non-homogeneous exposure

Table 2.12 summarized the methods of calculating exposure factors for non-homogeneous upstream exposures. ASCE 7 (2022), NBCC (2020), and AS/NZS 1170.2 (2021) all provide formulas for change in roughness. The ASCE 7 method is based on matching the ESDU model (Deaves and Harris, 1981) with the power law relationship. NBCC uses a formula to calculate the exposure factor C_e when the upwind extension of the roughness exposure is greater than 0.05 km and less than 1 km. In AS/NZS 1170.2, the lag distance x_i of each exposure of oncoming wind direction is considered for the new fetch length at different heights, then the weighted average method is used to calculate the exposure factor $M_{z,cat}$. The EN 1991-1-4 code adopted the category

with the lowest roughness length to account for the exposure factor, which results in an unreasonably larger wind force. GB 50009 does not provide a method for non-homogeneous exposure. These methods are further discussed and evaluated in the wind tunnel experimentation discussed in Chapter 3.

Table 2.12 Method of calculating roughness change in various codes

Code/Method	Procedure
ASCE 7 (2022)	Mentioned previously
NBCC (2020)	x_r>1,000 m $C_e = C_{er}$ 50 m < $x_r \leq$ 1,000 m, $C_e = C_{er}\left(0.816 + 0.184\log_{10}\left(\frac{10}{x_r - 0.05}\right)\right) \leq C_{eo}$ $x_r \leq$ 50 m, $C_e = C_{eo}$ x_r : upwind extent of rough terrain; C_{er} : Ce for rough terrain; C_{eo} : C_e for open terrain.
AS/NZS 1170.2 (2021)	First calculate the lag distance: $x_i = z_{0,x}\left(\frac{z}{0.3z_{0,x}}\right)^{1.25}$ 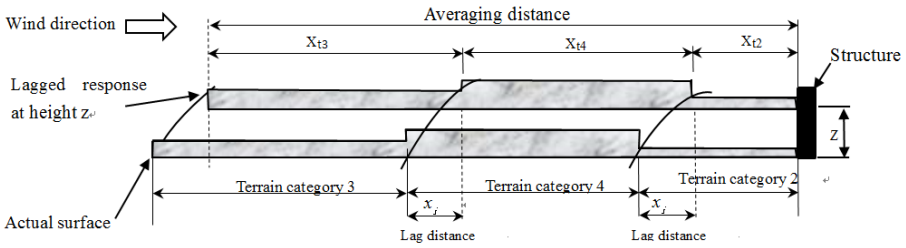 $M_{z,cat} = \frac{M_{Z,2}x_{t2} + M_{Z,4}x_{t4} + M_{Z,3}x_{t3}}{Averagingdistance}$
EN 1991-1-4 (2005)	When there is a choice between two or more terrain categories in the definition of a given area, then the area with the lowest roughness length should be used.
GB 50009 (2012)	No mention.

2.5 Summary

The specifications of exposure factors in current wind provisions of ASCE 7 (2022), NBCC (2020), AS/NZS 1170.2 (2021), EN 1991-1-4 (2005), and GB 50009 (2012) have been presented and discussed in this chapter. First, the steps to estimate wind loading in various provisions are introduced by taking the ASCE 7 as an example, with emphasis on the determination of exposure factors. For homogeneous exposure, inconsistencies of exposure categories among different code or standard provisions and the potential error sources are pointed out. The discrepancies among minimum upstream fetch specified in various provisions are discussed. For non-homogeneous exposure, the methodology to calculate the exposure coefficient in various wind load provisions is summarized, and these inconsistencies are further addressed in Chapter 3. The development of wind load provisions is a process of harmonizing and adopting the ongoing investigations. It is hoped that this research will be helpful in the future compilation of wind load provisions to allow designers to make more accurate decisions.

Chapter 3 Literature Review

3.1 Overview

The two most significant aspects of wind engineering are wind loading on structures and wind environment, both of which are determined by wind velocity. To estimate wind load on structures, the approach wind profile must first be obtained. The wind profile is determined by the drag effect of the upstream exposure roughness of mesoscale. It can be calculated by the log law and power law relationship, in which the parameters can be arrived at by the exposure coefficient. To determine the exposure coefficient, the exposure is classified into homogenous exposure and non-homogeneous exposure and codified in current wind load codes and standards. The exposure coefficients are provided for each category for the reference of designers. For non-homogenous exposure, the IBL theory-based method, the morphometric method, the anemometric method, and the GIS-based method have been proposed to determine the exposure coefficient. Additionally, formulas are provided in various wind load provisions to consider small-scale roughness changes. Upstream exposure influences the wind profile approach, thus affecting the wind loading and the wind environment around buildings. Low wind velocity in urban areas leads to poor pollutant ventilation and the heat island effect, while large wind velocity at pedestrian-level height may cause comfort problems or even result in concerns about safety. This influence is usually investigated by wind tunnel experiments and through the numerical simulation method. In this chapter, previous investigations related to the determination of exposure coefficient are reviewed, and the influence of upstream exposure on wind loading and the wind environment is examined.

3.2 Homogeneous exposure

3.2.1 Exposure categories

For homogeneous exposure, the velocity profile can be calculated according to the exposure coefficient, which represents the influence of exposure morphology roughness on the characteristics of the approaching wind. It is usually calculated by two parameters: the power law exponent (α) of the wind profile and the surface roughness length (z_0). The exponent (α) is considered to be non-physical and inaccurate when height intervals are not accounted for (Panofsky 1984; Peterson, 1997). The roughness length (z_0) represents the effects of drag of exposure roughness on the wind as it blows over the upstream fetch. This is the only height-independent parameter to determine the exposure roughness (Wamser et al., 1977).

The influence of exposure roughness was first considered by Davenport (1960), who classified the exposure into eight categories in terms of power law exponent (α) based on the published wind data records. In 1980, Davenport's power-law exponent classification was redefined in z_o terms by Wieringa (1980) with the help of experimental data. An example illustrated by Simiu and Scanlan (1996) also proves that terrain roughness has an enormous effect on mean wind speed. In the 30 years following Davenport's 1960 classification, dozens of exposure roughness field measurements were conducted. Wieringa (1992, 1993) summarized this wealth of material and put it into practical engineering. Davenport et al. (2000) later proposed a revised eight-grade classification method that is referenced in ASCE Engineering Practice No. 67 (Isyumov, 1999); see Table 3.1. Other studies on exposure types and terrain roughness have since been proposed by Deaves (1981), Cook (1986), Schmid and Oke (1990), and Choi (2009). Wieringa (1992) summarized previous field measurement materials and proposed a revised eight-grade classification method based on

Davenport's classification, which is presented in Table 3.1. This revised Davenport classification method is considered to be the most authoritative classification method so far.

Table 3.1 Exposure classification of the revised Davenport method

z_0 (m)	Type name	Description
0.0002	Sea	Open sea or lake, tidal flat, snow-covered flat plain, featureless desert, tarmac, and concrete with a free fetch of several kilometers
0.005	Smooth	Featureless land surface without any noticeable obstacles and with negligible vegetation
0.03	Open	Level country with low vegetation (e.g., grass) and isolated obstacles with separations of at least 50 obstacle heights
0.1	Roughly open	Cultivated area with regular cover of low crops or moderately open country with occasional obstacles at relative horizontal distances of at least 20 obstacle heights
0.25	Rough	High crops or crops of varying height, with scattered obstacles at relative distances of about 15 obstacle heights
0.5	Very rough	Large obstacle groups separated by open spaces of about 10 obstacle heights. Large, low vegetation with small interspaces
1	Closed	Landscape totally and uniformly covered with large obstacles of similar size and open spaces comparable to the obstacle heights
2	Chaotic	Large town centers with a mixture of low-rise and high-rise buildings. Also, irregular large forests with many clearings.

Previous exposure classification methods are summarized and compiled in the wind load provisions of various countries. For example, as referenced in Isyumov et al. (1999), the revised Davenport classification by Wieringa (1992) is adopted in the ASCE Engineering Manual of Practice No. 67 as well as in wind design standards such as ASCE 7-16 and ASCE 49-12. Exposure is classified into three to five upstream roughness categories in the wind load provisions of various countries, and the classifications are similar: flat, sea, open; urban or suburban; large city centers,

etcetera. Exposure factors are usually provided according to the exposure category to help designers more easily determine the wind load. Most of the categories are given in terms of z_0, and estimation of z_0 according to the exposure categories of wind load codes and standards is the most traditional and convenient method. Figure 3.1 depicts a sketch of the variation of wind velocity with height and the corresponding z_0 value for typical homogeneous exposure types, and Figure 3.2 presents photographs of four typical exposure types. The exposure classification methods in various provisions are generally consistent with each other, although some inconsistencies still exist.

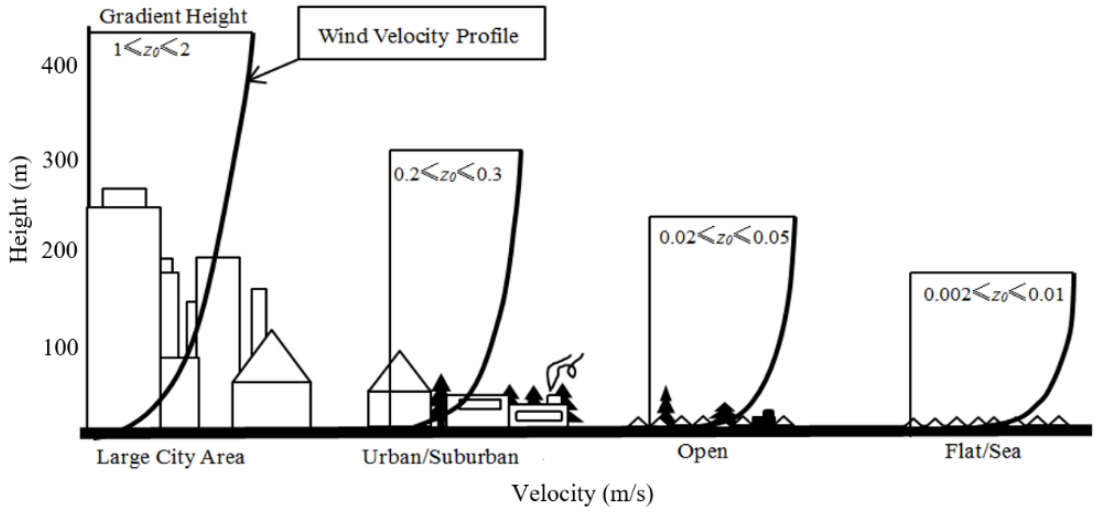

Figure 3.1 Wind velocity profiles and the corresponding z_0 for typical exposure types. (based on Davenport, 1960)

(a) Flat/Sea

(b) Open

(c) Urban or suburban

(d) Large city center

Figure 3.2 Typical exposure categories

However, the selection of exposure categories by designers is sometimes subjective, and this may be critical, since an improper exposure coefficient adoption may strongly influence the value of the design wind load. The best way to resolve this issue is to directly estimate the value of z_0. Then, the velocity variation with height can be calculated according to the power law or log law wind profile.

3.2.2 Minimum upstream fetch

"Wind has poor memory," (Stathopoulos, et al. 2009). The velocity profile is determined only by a certain length of upstream exposure patch and its roughness directly upstream of the building

site. The length of this area is called the minimum upstream fetch. A reasonable minimum upstream fetch length is the basis for the accurate estimation of the exposure factor. In the past 20 years, researchers have conducted wind tunnel experiments, field measurements, and numerical simulations to investigate the influence of upstream exposure fetch.

The experimental investigations focus mainly on the impact of exposure roughness on the wind loads of buildings. Tsutsumi et al. (1992) concluded that the average wind pressure coefficient becomes steady when the upstream fetch is greater than about 6 h (with h being the height of the building), regardless of volume ratio and the arrangement of roughness elements. Kiefer and Plate (1998) found that for homogeneous exposure, the upwind roughness changes have significant impacts only on mean pressure coefficients within 9 h. Wang and Stathopoulos (2006) concluded that the peak pressure coefficient on roofs can be determined by a fetch as short as 300–400 m, regardless of the configuration of the terrain further upwind. Kim et al. (2012, 2015) found that the profiles of mean wind speed and turbulence intensity vary little in shape and values for changes beyond 15 h, and this was also found to be true for the peak wind pressure coefficients. Yu et al. (2021) conducted a real urban morphology wind tunnel test and concluded that, in typical urban exposure, the fetch length of 750 m directly upstream of the building site typically determines the mean velocity.

Field measurements have been conducted to evaluate the effect of upstream open or suburban terrain based on the measured wind characteristics. Letchford et al. (2001) concluded from the observation data that for grass upstream roughness, a 1,000–1,500 m fetch needs to be considered. Tamura et al. (2001) conducted simultaneous observations over two sites with different roughness and found that the velocity profile of the city exposure type needs a shorter fetch to develop than the suburban exposure type. Weng et al. (2010) conducted a numerical test and concluded that an

upstream distance on the order of 500–1,000 m is necessary for full development of friction velocity when the exposure changes from rough to smooth. Miller et al. (2015) summarized and analyzed the wind-speed records data at 10 m height from 56 mobile weather stations along the Gulf of Mexico and Atlantic Ocean coasts of the United States. It was found that an upstream fetch of at least 1,000 m is required to evaluate turbulence intensity for a change of terrain from rough to open, which is comparable to the values suggested by Wieringa (1993) and Jedege and Foken (1999).

In summary, the wind tunnel experimentation focused mainly on urban or suburban exposure, and attention was paid mainly to wind loads on buildings. Generally, it has been found that wind loads on buildings are sensitive to small-scale upstream roughness close to the site (9–15 h or 300–400 m), while the velocity profile of urban or suburban exposure required a longer fetch length to be fully developed, as long as 750 m. In contrast, field measurement studies were carried out for open or flat to suburban exposure types and concluded that an upstream fetch of 1,000–1500 m should be considered for adequate representation of velocity profile and turbulence intensity profile. Additionally, a shorter upstream fetch is needed for city exposure compared to suburban exposure. A detailed summary of the influence of upstream fetch length can be found in Yu et al. (2021). Some of the early investigation results have been incorporated into the current wind code and standard provisions to help designers estimate exposure roughness according to the minimum upstream fetch, so that the wind load on buildings could be estimated accordingly.

3.3 Non-homogeneous exposure

In practice, the common situation is usually non-homogeneous exposure, and neglecting small-scale roughness change will lead to significant errors in the estimation of wind load (Schmid and Bunzli, 1995). There are four main methods to address non-homogeneous exposure, namely, the

IBL theory-based method, the morphometric method, the anemometric method, and the GIS-based method.

3.3.1 Internal boundary layers theory-based method

For non-homogeneous exposure, the effect of exposure on wind profile was primarily specified according to IBL theory in provisions (see Figure 3.3). The IBL appears because of the downwind roughness change, which results in an outer original boundary layer and a new internal boundary layer. The concept of transition region is introduced to account for multiple exposure roughness changes in the IBL model. The change of exposure roughness stratifies the atmosphere into an unmodified outer sub-layer flow and a set of corresponding independent IBLs. In the transition region, the flow is neither in equilibrium with the new exposure nor does it retain the upstream character over the old exposure. The depth of a single patch of IBL g(x) is determined by the distance from the exposure roughness change to the building site x and representative exposure roughness length z_0. The IBL flow will not be influenced by the upstream exposure any longer when its fetch extends to a certain length, which is called the minimum upstream fetch length.

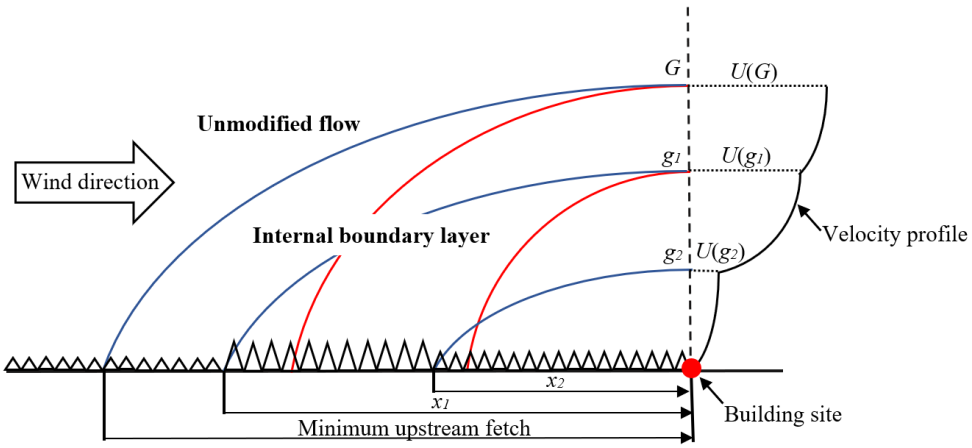

Figure 3.3 Schematic boundary layer above an upstream fetch of non-homogeneous exposure. (based on Wang and Stathopoulos, 2007)

The most well-known IBL model is the Deaves and Harris model (1981a and 1981b), which was adopted by ASCE 7. Some earlier IBL theory-based methods were reviewed by Garratt (1990), and models of $g(x)$ were suggested by Antonia and Luxton (1971, 1972) and Wang and Stathopoulos (2007).

3.3.2 Anemometric method

The anemometric method is also called the micrometeorological method. In this method, z_0 is determined from field measurement data. There are mainly three types of anemometric methods: the profile method, the variance method, and the gustiness method. The profile method uses the mean velocity data recorded at multiple heights, while the variance method and the gustiness method require turbulent fluctuation velocity measured at a single height. To observe the real-time wind speed data, a tower and anemometers are required. The equipment used for data observation is depicted in Figure 3.4.

(a) Tower for data observation (b) Anemometer

Figure 3.4 Equipment of anemometric method. (https://www.windfarmbop.com/tag/anemometer/)

Comparisons of different anemometric methods can be found in the research of Barthelmie et al. (1993) and Verkaik and Holtslag (2007). Review of the anemometric-based estimation of z_0 has been reviewed and summarized by Grimmond and Oke (1999). Recent studies concerning the estimation of z_0 by anemometric methods were conducted in Chicago, Los Angeles, Miami, and Vancouver by Roth and Oke (1993), Grimmond and Oke (1995), Grimmond (1998), and King and Grimmond (1997); at several airports along the coastline extending from Texas to New York by Lombardo et al. (2017) and Master et al. (2010); in Hong Kong by He et al. (2017); and in London by Kent et al. (2017, 2018). The roughness length z_0 obtained by anemometric methods is assumed to be representative of the most reliable data. However, instrumentation and a tower are needed, and a long period of measurement time is required.

3.3.3 Morphometric method

Compared with the anemometric method, the morphometric method is more convenient, as it uses analytical formulas to estimate z_0 based on height, surface area, and spatial distribution of roughness elements. The algorithms of morphometric methods were deduced by means of wind tunnel tests, numerical simulations, field measurements, and analytical methodology.

The definition of parameters in the morphometric algorithms is depicted in Figure 3.5, in which H_{ob} is the average height of the obstacles upstream of the building site; S is the horizontal dimension of roughness elements; and S_{ob} is the frontal area, which is the average area of each obstacle's projection onto a vertical plane normal to wind direction, $S_{ob} = \overline{S_x} H_{ob}$; A is the horizontal distance between centers of consecutive roughness elements; A_{ob} is the average ground area of each roughness element, including its surrounding open area, $A_{ob} = \overline{A_x A_y}$; λ_P and λ_f are the plan and frontal area index of roughness elements, respectively: $\lambda_P = \overline{S_x S_y}/A_{ob}$ and $\lambda_f = S_{ob}/A_{ob}$; and z_d is the zero-plane displacement height. The effective frontal areas of plants are reduced as they are porous and are deformed in wind (Raymer 1962). No more than about 50% of the frontal area should be considered for evergreen plants and no more than about 15% of that should be considered for deciduous trees.

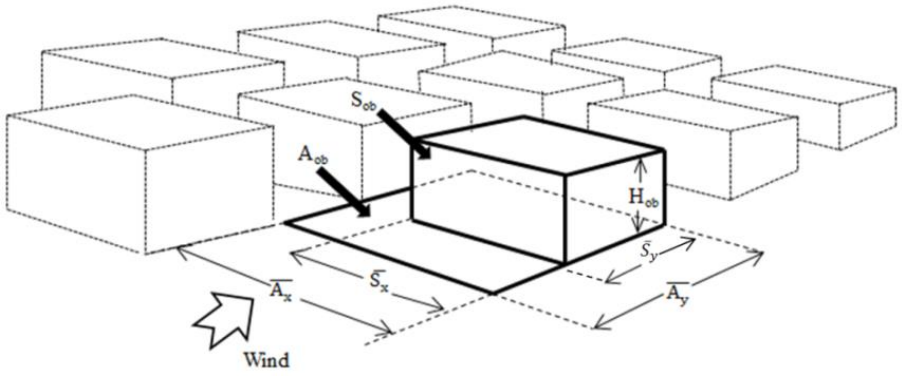

Figure 3.5 Parameters in morphometric methods. (based on Grimmond and Oke, 1998)

There are three types of morphometric methods, namely, height-based methods (Garratt, 1992; Raupach et al., 1991; Hanna and Chang, 1992; and Taylor, 1988), height and plan areal fraction-based methods (Counihan, 1971; Kondo and Yamazawa, 1986; and Bottema, 1995), and height and frontal area index-based methods (Lettau, 1969; Macdonald et al., 1998; and Raupach, 1994).

An explicit summary and comparison of morphometric methodologies can be found in Grimmond et al. (1998) and Kent et al. (2017). A brief introduction of these methods follows:

Height-based method

The height-based method is the most common morphometric method, in which z_0 and z_d are simply dependent on the average height of the roughness elements:

$$z_d = f_d \overline{z_H} \tag{3.1}$$

$$z_0 = f_0 \overline{z_H} \tag{3.2}$$

where f_d and f_0 are empirical coefficients derived from field measurement or wind tunnel test observation. The values of f_d and f_0 are suggested by Garratt (1992) and Hanna and Chang (1992).

Height and plan areal fraction-based (λ_p) method

Kutzbach (1961) and Counihan (1971) first incorporated the plan areal fraction $\lambda p = A_p/A_T$ into the morphometric formulas. The equations of their formula are presented in Eqs. 3.3–3.4 and Eq. 3.5.

Kutzbach's method:

$$z_d = \lambda_x^{0.29} \overline{z_H} \qquad \lambda_x \leq 0.29 \tag{3.3}$$

$$z_0 = \lambda_x^{0.13} \overline{z_H} \qquad \lambda_x \leq 0.29 \tag{3.4}$$

Counihan's method:

$$z_0 = \left(1.08\lambda_p - 0.08\right)\overline{z_H} \qquad 0.1 < \lambda_p \leq 0.25 \tag{3.5}$$

Height and frontal area index-based (λ_f) method

Lettau (1969) developed the morphometric formula in consideration of height and λ_f for irregular arrays' reasonably homogenous elements:

$$z_0 = 0.5 \overline{z_H} \lambda_f \tag{3.6}$$

Lettau's formula is the most widely recognized method and has been adopted by ASCE 7 (2022). Other height- and λ_f-based methods were proposed by Raupach (1994), Bottema (1995, 1997), and Macdonald et al. (1998).

3.3.4 GIS-based method

The morphometric method is indeed more accurate to estimate z_0 than referring to the wind load provisions and more convenient than the anemometric method. However, the difficulty lies in the acquisition of morphometric parameters of all roughness elements in such a large upstream exposure area. Until early in the 21st century, these formulas have been restricted to simple geometry due to the lack of 3D structure models of urban areas. Unlike the application in regular structures, there are two challenges to apply the formulas in real urban areas: the acquisition of 3D models and the extraction of the morphometric parameters. With the development of the digital elevation model (DEM) database produced by light detecting and ranging data (LiDAR) and radio detecting and ranging (RADAR) data, this gap became possible to close. DEM is a compact way of storing urban 3D information using a 2D matrix of elevation values, as each pixel represents building height and is displayed in gray shades as a digital image. DEM includes both digital surface models (DSMs) (ground and roughness-element heights) and digital terrain models.

Grimmond and Oke (1999) were among the first researchers to combine morphometric formulas and DEM to estimate z_0. Nine morphometric formulas were verified with the field observation of North American cities to analyze their sensitivity. Unfortunately, after the application of quality control criteria (Wieringa 1993, Bottema 1997), only very few field measurement studies were acceptable to assess the formulas.

Ratti et al. (2006) proposed a guideline to calculate morphometric parameters based on the urban DEM with an image processing technique, the Fourier transform and variance plot. This method

was adopted by Di Sabatino et al. (2008) to estimate the velocity profiles through λ_f and λ_p of London, Toulouse, Berlin, and Salt Lake City. The results reveal that DEM is a promising simple tool for wind prediction, but no verification was made.

Di Sabatino et al. (2010) proposed a method to promote and improve city DEMs' analysis by combining raw building height collection and image analysis. The field data collection of building height took about three months for three of areas of the urban areas of Lecce, Italy. The parameters of λ_f, λ_p, and z_0 derived by Macdonald's formula are compared with those of three northern European cities and two North American cities. Results revealed that the proposed method is an effective tool to derive the parameterization of a real urban canopy. However, the wind direction is not considered.

Leo et al. (2018) extended the method used by Di Sabatino et al. (2010) and proposed a scale-adaptive morphometric analysis method to estimate aerodynamic roughness parameters. This method was validated by the CFD simulation results of downtown Oklahoma City in the United States. It is suggested that the adopted grid provides the best agreement with data from laboratory experiments when the selection of grid size is made based on maximum building height and the spatial profile of building height standard deviation.

Kent et al. (2018) assessed three global digital elevation models (GDEMs) for the determination of urban morphology and wind speed, namely, advanced spaceborne thermal emission and reflection radiometer (ASTER), shuttle radar topography mission (SRTM), and TanDEM-X. Geometric and aerodynamic parameters derived from these models are compared with those derived from benchmarks, and the wind profiles are compared with field measurement data. The errors in z_0 and average directional wind speed are underestimated by up to 40% and 30% due to

the apparent merging of roughness elements in all GDEMs. The results can be improved with the proposed corrections to 10% compared with observation.

The satellite images were also combined recently with morphometric formulas to estimate z_0. Darmanto et al. (2017) derived λ_p and λ_f from eight Landsat satellite images and H_{ave} from night light images. Values of z_0 were then estimated following the formula of Kanda et al. (2013). The proposed method can provide more wind-speed estimation than the use of a forecasting model for weather research. However, the roughness length z_0 is not quantitatively assessed.

Xu et al. (2017) proposed a novel satellite-based approach to extract 3D urban morphology parameters and applied it to Kowloon, Hong Kong. Results were compared with the benchmark data. The average differences of the above urban morphology parameters of building coverage, building height, frontal area index, and z_0 (calculated by Macdonald et al., 1998) were between 22% and 30%. The underestimation of building height in high-density locations and the potential overestimation of lower buildings is due to the imperfect building boundaries.

Other researchers have used meteorological models to estimate z_0. Ketterer et al. (2017) implemented three morphometric formulas in the SkyHelios (Matzarakis and Matuschek, 2011) model, a microscale model used in complex urban environments, to calculate z_0 on the microscale. Spatial information of urban structures can be exported as ASCII grids, which are supported by most of the commercial or open-source GISs. The investigated urban area is divided into reference areas for each of the obstacles using a Voronoi diagram to apply the model. The proposed method was used to estimate z_0 of Stuttgart, Germany, but no assessment was made.

Godlowska and Kaszowski (2019) tested various morphometric formulas for wind-speed determination in Krakow, Poland, using a hybrid modeling system based on the numerical weather prediction system. Their results reveal that research by Kanda et al. (2013) provided more

appropriate results for wind speed estimation. An inevitable error in this method is that the maximum and standard deviation of tree heights are not included due to the limitation of the adopted morphometric database.

3.4 Influence of upstream exposure on wind environment

The rapid urbanization process in numerous cities around the world has brought the improvement of infrastructure and rapid economic growth but, at the same time, urban construction leading to significant changes in upstream exposure, which will affect the wind environment. The large PLW speed will affect pedestrian comfort and safety as well as reduce residents' pleasant and healthy feelings.

The investigation of the influence of upstream exposure on the PLW environment consists of three steps: the determination of statistical meteorological data, the aerodynamic information of upstream exposure, and the local wind statistics at the building site. The statistical meteorological data is obtained by a mereological station that is usually located in open area far from the city center to represent the oncoming wind of the area. However, the wind speed will change according to aerodynamic information, which is the combination of terrain-related and design-related contributions to the wind profile between the metrological station and the investigated area. The transformation of statistical data from the meteorological site to the building site is depicted in Figure 3.6. The determination of terrain-related contributions can be found in the reference of Simiu and Scanlan et al. (1986), and the design-related contribution can be obtained by either a wind tunnel test or CFD methodology. After the acquisition of local wind statistical data at the pedestrian-level height, wind comfort and safety are assessed by existing criteria that usually include a threshold wind speed value and an allowed exceedance probability of this threshold.

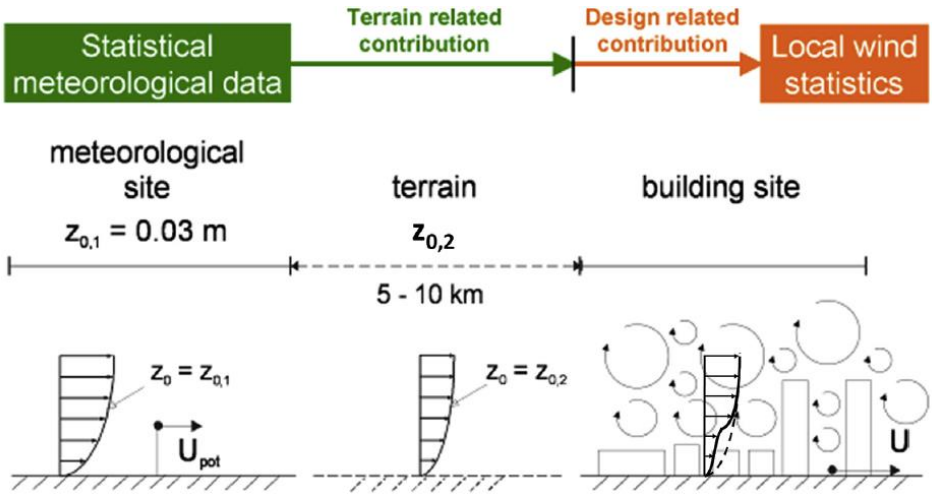

Figure 3.6 Transformation of statistical data from the meteorological site to the building site. (by Blocken et al., 2016)

Traditionally, aerodynamic data is usually obtained by a wind tunnel test (Irwin, 1981; Kubota et al., 2008), with the measurement of PLW velocity usually performed by hot-wire or hot-file anemometry (Isyumov and Davenport, 1975; Stathopoulos and Storms, 1986; Ratcliff and Peterka, 1990; Jamieson et al., 1992; and Blocken et al., 2008), pulsed-wire anemometry (Bradbury and Castro, 1971; Britter and Hunt, 1979; and Castro, 1992), or Irwin probes (Irwin, 1981; Wu and Stathopoulos, 1994; Van Beeck, et al., 2009; and Tsang et al., 2012). In comparison, the CFD method can provided detailed information of the flow field in a complex urban area and can be conducted at full scale. Due to these advantages, CFD is increasingly being adopted to investigate issues relating to wind environment in an urban area that cannot provide a flow field image and where the observation points are limited. Additionally, the size and scaling of the experimental model is restricted to the width of the wind tunnel. The previous investigations of the influence of upstream exposure on wind environment in terms of street scale, neighborhood scale, and city scale are summarized in this section.

3.4.1 Influence of street design

The street design also influences the wind environment of the street climate, for example, street aspect ratios, street width, and the passage configuration. Figure 3.7 is a schematic diagram of the most common case of a geometrically symmetrical street. In cross wind direction, the airflow in the street canyon is affected mainly by the wake behind the upwind building. In oblique or along wind directions, the flow is compressed by the street canyon and is accelerated. In the case of gradual changing of street width, the expansion or contraction roads in the existing studies are defined according to wind directions (see Figure 3.8). Moreover, street intersections (Figure 3.9) also affect the wind environment. Relevant research conclusions are summarized in Table 3.2.

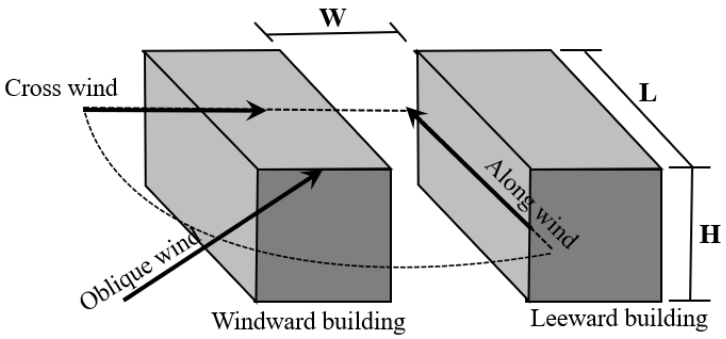

Figure 3.7 Geometrically symmetrical street.

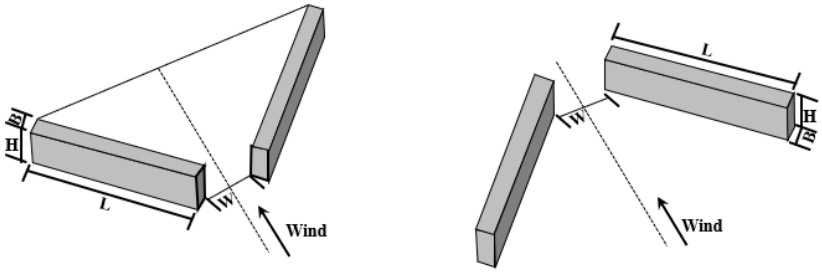

(a) Diverging (b) Converging

Figure 3.8 Diverging and converging street configurations.

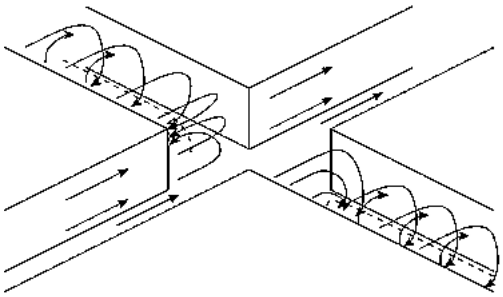

Figure 3.9 Visualisation of the main flow structure in a street connected to an intersection. (Soulhac et al., 2009)

Table 3.2 The influence of street design by various authors

Street design		Authors	Comments
Symme-trical	Along Wind	Oke, 1988 (review)	The airflow is the same as that of a single building for H/W = 0.1667. The airflow in the street will be affected by the building wake for H/W = 0.25. The upper airflow cannot enter the street interior for H/W = 1.
		Shishegar, 2013 (review)	The deeper street leads to lower internal airflow velocity and more stable flow. When there are tall buildings along the street, the airflow velocity will increase significantly.
		He et al., 2017 (CFD)	Leeward-side pollutant exposures are much larger than windward-side as H/W = 1-4 while oppositely as H/W = 5-6. Road barriers slightly increase pollutant exposure in near-road buildings with H/W = 1 and reduce it with H/W = 3 and 5.
	Oblique /Cross Wind	Stathopoulos and Storms, 1986 (WT)	The most critical wind velocity conditions occur for a wind direction skewed by 30° from the passage center line. The larger the passage width, the lower the velocity amplifications in the passage.
		Hang et al., 2012 (CFD)	Streets with taller buildings may capture more rural air through the windward entry but also drive more air out of the street. Mean flows along the streets dominate pollutant removal.
		Kuo et al., 2015 (WT)	A higher podium creates stronger wind speeds of the flow within the street canyon, and different approaching wind directions change the high-wind-speed zone within the street canyon accordingly.
Converging/ Diverging		Blocken et al., 2008 (CFD)	Wind speed amplification factors in diverging passages are generally larger than in converging passages. The maximum wind speed amplification factors increase with a decrease in passage width.
		Li et al., 2014 (CFD)	Converging passages have higher wind-blocking effect than diverging passages. A converging passage with α = 15° is recommended for cold regions, while a diverging passage with α = 150° is better for ventilation.
		Allegrini and Lopez, 2016 (CFD)	The wind speeds in the passage are increasing with increasing angles between the buildings for the converging cases, while they are decreasing for the diverging cases.
Intersection		Dobre et al., 2005 (WT)	Main features of the flow in the streets are similar to idealized 2D street canyons. The in-street flows can be explained by a linear superposition of the parallel and perpendicular rooftop wind components.
		Carpentieri et al., 2009 (WT)	In the complex and realistic situation, some details of the upwind flow, such as the presence of two tall towers, is significant in defining the flow field within the intersection, particularly at roof level.

	Soulhac et al., 2009 (WT and CFD)	Flow and dispersion at the entrance to crosswind streets is dominated by a large vertical-axis recirculating vortex that forms at the interface between the intersection and the street.

3.4.2 Influence of neighborhood parameters

The relationship of the neighborhood parameters—such as building density, building height deviation and layout, and wind environment—are studied by researchers. In the case of the same average height, the greater the deviation in height, the better the ventilation. Lower building density and a scattered, irregular layout are more conducive to ventilation, and ventilation also improves when the layout of open space is aligned with the dominant local wind direction. Furthermore, L-shaped buildings are better for pollutant diffusion than square, U-shaped, and I-shaped buildings, but this may lead to excessive wind speed at pedestrian height, thus affecting pedestrian comfort. Ventilation will decrease with the expansion of the city area. Table 3.3 presents a brief summary of the previous research results.

Table 3.3 Influence of neighborhood parameters by various authors

Para -meter	Authors	Comments
Height/ Density	Jiang et al., 2008 (CFD)	Wind velocity within arrays rises with an increase in the variation degree of building height. Tall buildings have greater disturbance on wind than low buildings do.
	Yim et al., 2009 (CFD)	The PLW velocity ratio was reduced 40% and the retention time of pollutants increased 80% when high-rise buildings four times the height of the street canyon were aligned as a "wall" upstream.
	Hang and Li, 2010 (CFD)	The ventilation in both the main and secondary streets becomes better if the base of all buildings is open from z = 0 to 0.33B.
	Hang et al., 2012 (WT and CFD)	Larger standard deviations tend to induce better pedestrian ventilation. For arrays with uniform heights, lowering aspect ratios or increasing street lengths may enhance the contribution of removing pollutants.
	Kubota et al., 2008 (WT)	An increase of the gross building coverage ratio reduced the mean wind velocity ratio. The mean wind velocity ratio in apartment houses was found to be 0.24 higher than that in detached houses.
Layout	Zhang et al., 2005 (CFD)	Wind environment for arrangements with lower interval-to-height ratio is better than that for the reference layout with a higher aspect ratio in terms of the natural ventilation.
	Xie et al., 2008 (CFD)	The canopy flow local to any individual block can be significantly influenced by relatively remote blocks. This highlights the importance of undertaking simulations of entire domains.
	Asfour, 2010 (CFD)	Configurations that contain a central space articulated by buildings and oriented toward the prevailing wind can offer better exposure to air currents and better containment of wind.
	Zaki et al., 2011 (WT)	The higher the building density is, the smaller the deviation of building height in the block influences the surface roughness.
	Gu et al., 2011 (CFD)	The separation of stepup and stepdown notches in non-uniform street canyons might be a good choice for uneven building layout arrangements from the point of view of pollutant dispersion and human health.
	Lin et al., 2014 (CFD)	The air change rates per hour decrease and overall urban canopy layer ventilation becomes worse if urban size rises from 390 m to 5 km.
	Iqbal and Chan, 2016 (WT)	The wind speed circulation at the corner of L-shaped buildings is the strongest compared with square, U-shaped, L-shaped, and I-shaped buildings, which are conducive to ventilation. The ventilation will be affected by the wind direction.

3.4.3 Influence of urban layout

In recent years, the influence of the urban layout in a city scale on wind environment has also been emphasized. The high building density of large cities results in a poor ventilation effect, which can be alleviated by improving building layout and urban planning. The study of He et al. (2018) demonstrates that ventilation can be improved by reducing road density and increasing road width in urban centers with high building density. Open space also improves ventilation when it is in line with the dominant wind direction, and buildings with podiums should be avoided as much as possible. He et al. (2019) analyzed the ventilation characteristics of various urban layouts in the city center of Sydney, Australia, and proposed an urban ventilation evaluation system composed of "compactness + building height + street structure" to provide a reference for urban planners. Li et al. (2019) studied the influence of the urban street layout on ventilation performance.

As discovered in the previous investigations, it is known that the building shape, street design, building layout, and urban expansion all affect the airflow characteristics at the pedestrian level. However, building construction and urban planning in large city centers are highly complex, for which the wind environment is not the linear combination of various factors.

3.5 Approach in various wind load provisions

The determination of exposure roughness of upstream small-scale roughness change specified in the wind load provisions of various countries is summarized in Chapter 2. In this section, the wind tunnel tests conducted by Wang and Stathopoulos (2006) are selected for comparison to the current wind load provisions in terms of the specification of small-scale upstream roughness change. The set-up of the wind tunnel test is introduced first. Then, the wind loads are calculated according to the specification of current wind load provisions for comparison purposes. The discrepancies are revealed and discussed.

- **Wind tunnel experimentation**

The experiment was carried out in the Building Aerodynamics Laboratory at Concordia University in Montreal, Canada. The scaling down of the model is 1:400. Three exposure types are used—open, suburban, and urban—with the corresponding roughness lengths z_0 of 0.024 m, 0.42 m, and 1 m in full scale, respectively. A sketch of the exposure roughness is depicted in Figure 3.10. The model selected for study was a 15.2 m height low-rise building model with a 4:12 gable roof slope; the tap locations on the model surface are presented in Figure 3.11. The pressure data of 13 wind directions—specifically, 0°, 35°, 40°, 45°, 50°, 55°, 90°, 125°, 130°, 135°, 140°, 145°, and 180°—were collected to indicate the most critical pressure coefficient of each tap.

The r-o case and o-r case are used to investigate the influence of small-scale roughness change directly upstream of the building site, which is depicted in Figure 3.12. The r-o case is an open exposure type of variable length directly upwind of the building with urban exposure farther upstream. On the contrary, the o-r case is a suburban exposure type of variable length directly upwind of the building with open exposure farther upstream. The length of the exposure directly

upwind of building site is x, which is changeable, and the variation of roof pressure with x is measured accordingly.

The mean value of the most critical pressure coefficients of all types is adopted for study. The pressure coefficient of the open exposure upstream of the building site was used as a reminder, which is $C_{p\ mean,\ o}$. The pressure coefficient ratios of the case of small-scale roughness change to the case of open upstream exposure were adopted for comparison, which are $R_{r\text{-}o}$ and $R_{o\text{-}r}$, respectively (see Eqs. 3.7–3.8). By means of the pressure coefficient ratio, the influence of other factors such as wind direction, gust effect factor, and building shape factor can be avoided.

$$R_{r-o} = \left(C_{p\ mean,r-o}/C_{p\ mean,o}\right)_{most\ critical} \tag{3.7}$$

$$R_{o-r} = \left(C_{p\ mean,o-r}/C_{p\ mean,o}\right)_{most\ critical} \tag{3.8}$$

where $C_{p\ mean,\ r\text{-}o}$ and $C_{p\ mean,\ o\text{-}r}$ are the mean pressure coefficient of r-o case and o-r case, respectively; $C_{p\ mean,\ o}$ is the mean pressure coefficient of the open exposure case; and "most critical" means the most critical value of all wind directions.

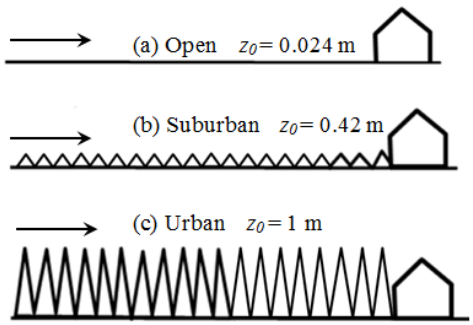

Figure 3.10 Roughness length of different cases reference.

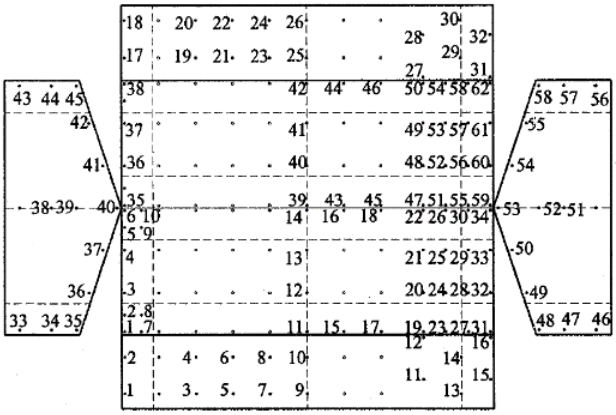

Figure 3.11 Unfolded view of the pressure model with the tap locations. (from Wang and Stathopoulos, 2006)

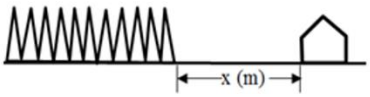

(a) r-o case

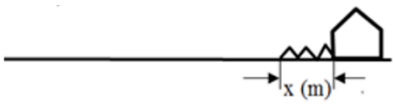

(b) o-r case.

Figure 3.12 Upstream exposure setup in the wind tunnel test.

- **Results analysis**

A brief introduction of the calculation steps in various provisions is provided first, followed by a detailed discussion of the comparison with the wind tunnel test results. In the provisions of ASCE 7 (2022), NBCC (2020), and EN 1991-1-4 (2005), the ratio of pressure coefficient is equal to the ratio of exposure factors, the symbols of which are K_z, C_e and C_e, respectively, while the pressure coefficient ratio of AS/NZS 1170.2 (2021) is equal to the square of exposure – $M_{z,cat}$.

The calculation steps of ASCE 7 (2022) are illustrated in Eq. 2.5. The exponent coefficient α and gradient height z_g of different exposure types are calculated first according to z_0. Then, K_z of the

single exposure type is obtained. The exposure factor estimation method of two roughness changes is provided and the K_z can be calculated accordingly.

The exposure factor C_e calculation method in NBCC (2020) is specified as follows:

(a) $(h/10)^{0.2}$ but not less than 0.9 for open terrain,

(b) $0.7(h/12)^{0.3}$ but not less than 0.7 for rough terrain, and

(c) An appropriate interpolation method is used if a value intermediate between the two exposures defined in Clauses (a) and (b) in cases where the site is less than 1 km or 10 times the building height from a change in terrain conditions, whichever is greater.

The exposure factor of open exposure and urban exposure at the building roof height are, respectively, 1.087 and 0.751 calculated from Clauses (a) and (b), and the C_e of suburban exposure is 0.951, according to interpolation if $C_e = 1.087$ for the case of $z_0 = 0.0024$ and $C_e = 0.751$ for the case of $z_0 = 1$. For upstream exposure roughness change, there are three types of situations according to the length of rough terrain x_r. An open terrain exposure factor is adopted for $x_r \leq 50$ m and a roughness terrain exposure factor is adopted for $x_r > 1{,}000$ m, resulting in constant values of $R_{r\text{-}o}$ and $R_{o\text{-}r}$. The formula in Table 2.12 is used if $50 \text{ m} < x_r \leq 1{,}000$ m.

The exposure factor $M_{z,cat}$ in AS/NZS 1170.2 (2021) is specified according to building height and exposure type. Linear interpolation is suggested for intermediate values. The $M_{z,cat}$ of open, suburban, and urban exposure of the wind tunnel test of Wang and Stathopoulos (2006) is 1.011，0.841, and 0.796, respectively, by interpolation. Then, the weighted average value is used to calculate $M_{z,cat}$ for non-homogeneous exposure (see Table 2.12).

It is specified in EN 1991-1-4 (2005) that the exposure factor resulting in the largest wind load should be used when there is a choice between two or more terrain categories. As a result, the exposure factor of open terrain is used for both cases and the pressure coefficient ratio is always 1.

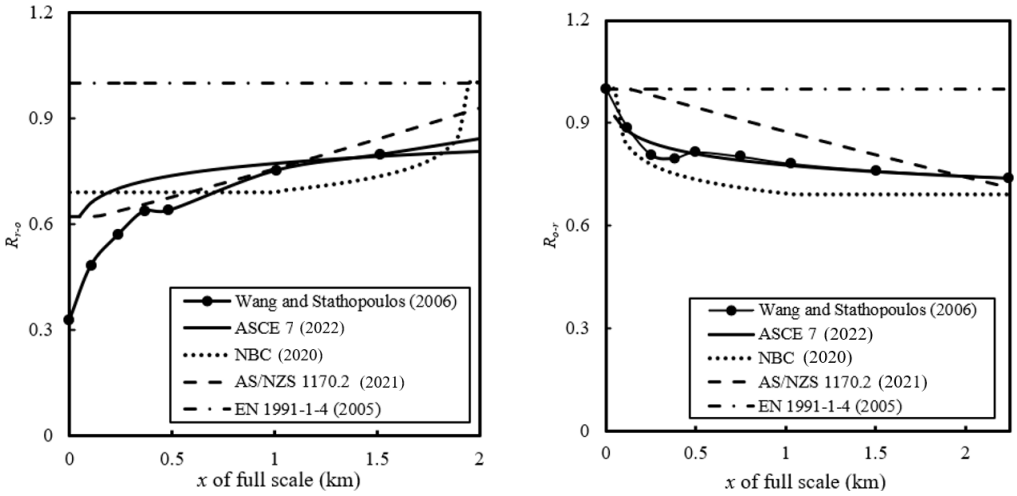

(a) r-o case (b) o-r case

Figure 3.13 Ratio of most critical pressure coefficients

The results of various provisions and wind tunnel tests are depicted in Figure 3.13. Clearly, the curve variation tendency of all studied provisions fit the wind tunnel test results except for EN 1991-1-4 (2005), which uses the lowest roughness length to calculate the exposure factor. The results of ASCE 7 (2022) correspond best with the wind tunnel test results with an average deviation of approximately 4.5%, followed by the results of NBCC (2020) with an average deviation of 8%. The results of AS/NZS 1170.2 (2021) fit well for the r-o case, while they overestimate wind load for o-r case with the largest deviation of 15%. The overestimate of AS/NZS 1170.2 when the rough exposure is short is due to the reason that, for low-rise buildings, the fetch length that determines the peak load is as short as 300–400 m regardless of the exposure type, while the positions of upstream exposure terrain are considered equally in all studied provisions. The reason for the underestimate of wind load by NBCC (2020) is because the exposure factor of rough exposure is suggested to be adopted when its fetch length is larger than 1,000 m. However, the results indicate that further upstream exposure change also influences the wind load. Except the

calculation steps, other deviations between different provisions are discussed. The conclusions from the discussions are as follows:

(1) Exposure factors for buildings of different height are calculated by formulas directly according to z_0 in ASCE 7 (2022). The exposure factor for buildings of different heights and exposure categories are provided in the form of a table in AS/NZS 1170.2 (2021). Interpolation can be used, as the z_0 of different exposure categories is provided. However, it should be noted that the relationship of z_0 and exposure factor at the same height is not linear, and this relationship should be obtained first. Although an appropriate interpolation method is suggested in NBCC (2020), it is somewhat difficult to be adopted, as the exposure factors are specified only for two exposure categories, and the corresponding z_0 values are not provided. It is better to specify exposure categories according to z_0, as its value can be obtained in many ways.

(2) The arrangement of different exposure types is considered in the provisions of ASCE 7 (2022) and AS/NZS 1170.2 (2021), while the NBCC (2020) estimates the exposure factor only depending on the total length of rough terrain. Moreover, NBCC (2020) specifies that "the value of C_e for rough terrain can be used when the rough terrain extends in the upwind direction for at least 1 km or 20 times the building height, whichever is greater." A condition is suggested to be added for this specification. For example, EN 1991-1-4 (2005) specified that "the sea and water that extend more than 1 km when closer than 1 km in wind direction could be classified as the terrain type of sea." A similar specification with "closer than 1 km to the site" is suggested for addition.

(3) The estimation method of only two upstream exposure roughness changes is provided in ASCE 7 (2022), while NBCC (2020) and AS/NZS 1170.2 (2021) can be used to calculate multiple upstream exposure roughness changes.

(4) The roughness that led to the largest wind load is adopted in EN 1991-1-4 when there is a roughness change. This will result in a too-conservative result of the most critical wind pressure value. Moreover, the GB 50009 does not specify the method of small-scale roughness change. Small improvements to these specifications have significant potential to enhance the economic efficiency of wind load design.

It should be noted that the case study used in this section is an ideal situation, and the morphology is more complex in real terrain. The determination of single exposure roughness is significant for the accurate estimation of wind load for non-homogeneous exposure. Moreover, the wind direction with the largest local wind speed combined with the corresponding exposure roughness should be considered in practical engineering applications.

3.6 Summary

A detailed review of the past research related to exposure morphology and its influence on the PLW environment is presented in this chapter. The previous investigations are demonstrated in terms of homogeneous exposure and non-homogeneous exposure and are summarized in Chapters 3.2 and 3.3, respectively. For homogeneous exposure, the development of exposure category method is reviewed, and the minimum upstream fetch by previous researchers is summarized. Additionally, the discrepancies among exposure classification and minimum upstream fetch specified in various provisions are clarified. For non-homogeneous exposure, four methods to account for the exposure factor of upstream small-scale roughness change have been presented, namely, the IBL theory-based method, the anemometric method, the morphometric method, and the GIS-based method. The disadvantages of these methods are that they may be difficult, time-consuming, and/or quite expensive.

In Chapter 3.4, previous investigations of the influence on upstream exposure on PLW are summarized in terms of street design, neighborhood parameters, and urban layout. The formulas accounting for small-scale roughness change in current wind load provisions have been checked by the wind tunnel tests carried out by Wang and Stathopoulos (2006), and inconsistencies found are discussed and concluded by the author in Chapter 3.5.

Chapter 4 Experimental and Numerical Methodologies

This chapter is a detailed introduction of all necessary information concerning the experimental and numerical tests. Experimental tests were carried out in the wind tunnel of the Building Aerodynamics Laboratory at Concordia University and the XNJD-III wind tunnel at Southwest Jiaotong University for parallel comparison and validation purposes. Case I is a building complex of low-rise to medium-rise buildings located sparsely in Westmount, Montreal, which was conducted at the wind tunnel of Concordia University. This wind tunnel test was designed to verify the accuracy of the computational method. Case II is a dense high-rise building complex in Kowloon, Hong Kong, which was conducted at the Southwest Jiaotong University. In this wind tunnel test, two different upstream fetch lengths were adopted to investigate the influence of upstream exposure. Additionally, numerical simulations were carried out for the Westmount, Montreal, wind tunnel test for the purpose of the investigation of the effect of upstream roughness on wind environment. After the validation of the numerical method by comparing the wind tunnel test, different upstream fetch lengths were adopted to investigate the influence of upstream exposure on environmental issues.

4.1 Experimental methodology

4.1.1 Instrumentation

- **Velocity profile measurement**

The mean velocity profile was measured by the self-designed pressure pipe and Scanivalve electronic scanners (DSM4000) - see Figure 4.1. Compared with the Cobra three-dimensional fluctuating anemometer, this equipment can simultaneously measure multiple locations. The calibration of probe sensors was carried out prior to the wind tunnel test. The pressure pipes and the pitot tube were both connected to the scanner during the calibration. The pressure P_i of each

pipe and the total pressure P and the static pressure P_0 of the pitot tube were measured simultaneously. Then, the calibration parameter C_i of each pipe can be obtained according to the equation $P_i - P_0 = 1 / 2 \rho V^2 C_i$.

Figure 4.1 Pressure probe for velocity profile measurement.

- **Turbulence intensity profile measurement**

The Cobra three-dimensional fluctuating anemometer was used to observe the turbulence intensity profiles. The measurement wind speed range of Cobra was between 2 and 40m/s and the wind direction measurement range was ±45°. The wind speed measurement accuracy was not less than ±0.3m/s and the measurement of turbulence was less than 30%. Multiple Cobra probes were installed on an iron bar to simultaneously measure the turbulence intensity profile (see Figure 4.2). The sampling frequency was set as 512 Hz and the sampling time was 60 s.

Figure 4.2 Multiple Cobras installed on an iron bar.

- **PLW velocity measurement**

The observation of PLW was conducted by Irwin probes, which are surface wind sensors that can be used to observe the mean wind speed in a wind tunnel test. An Irwin probe, depicted in Figure 4.3 (a), is suitable for measuring the velocity of approaching flow in any direction within a range of 360°. Compared with other anemometers, an Irwin probe is small and can be easily fixed into the ground, allowing a multi-point wind speed observation without affecting the flow characteristics. Each probe consists of a round sensor hole and a sensor tube that protrudes above the ground to a desired height, for the measurement of p_A and p_B; see Figure 4.3 (b). The pressure difference Δp between p_A and p_B was used to calculate the wind speed according to the simple relationship indicated in Eq. 4.1. The results of the PLW velocity ratio of U/U_{ref} are adopted for further investigation, for which U is the PLW velocity measured at the 2 m height in full scale with buildings and U_{ref} is the velocity measured at the same height without buildings.

$$U = \alpha + \beta\sqrt{\Delta p} \tag{4.1}$$

where α and β are the calibration constants that can be determined using velocity measured by the Cobra probes.

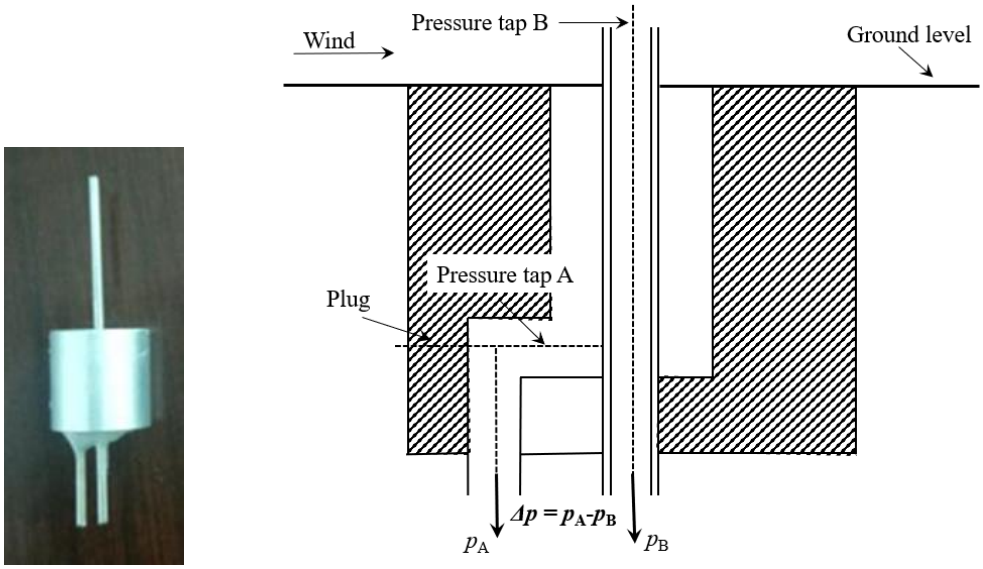

(a) Irwin probe (b) Cross-sectional drawing of the Irwin probe

Figure 4.3 Cross-section drawing of Irwin probe. (based on Irwin, 1981)

4.1.2 Wind tunnel test of Westmount, Montreal

- **Wind tunnel of Building Aerodynamics Laboratory at Concordia University**

The Building Aerodynamics Laboratory of Concordia University is in Montreal, Canada; see Figure 4.4 (a). The working section of the wind tunnel is 1.8 m wide and 12.2 m long, depicted in Figure 4.4 (b). The adjustable roof height allows the negligible pressure gradient along the streamwise direction. The maximum air speed at the test section of the tunnel is approximately 14.0 m/s and varies in the range of 4.7 to 14.0 m/s. A turntable is set at the test section so that the influence of wind direction is considered during model testing. Wind profiles over urban, suburban, and open terrains can be simulated at a geometric scale of 1/400–1/500. The floor of the wind tunnel is carpet, which is appropriate for the exposure type of open country.

This wind tunnel is an open-circuit, blowdown tunnel. The advantage of an open-circuit wind tunnel is that its construction cost is relatively low and there is no accumulation of exhaust products of smoke visualization. The disadvantage is that it is sensitive to the ambient conditions of air, temperature, and the pressure gradient between the room and the wind tunnel, and it is noisy during operation. More details about this wind tunnel can be found in the reference of Stathopoulos (1984).

(a) Picture of wind tunnel

(b) Working section

Figure 4.4 Wind tunnel of the Building Aerodynamics Laboratory at Concordia University (https://www.concordia.ca/research/zero-energy-building.html)

- **Generation of ABL**

The case study of Westmount, Montreal, was conducted in the boundary layer wind tunnel of the Building Aerodynamics Laboratory at Concordia University, Montreal, Canada. The scaling down of the investigative area model is 1:400, and the blockage ratio of the test is 3%, which is less than 10% to minimize the constraining effects (ASCE, 1999). The Reynolds number during the test was over 4.3×10^4, which is sufficiently large to meet the Reynolds number independent requirement. The neutral atmosphere boundary layer in the wind tunnel is reproduced by spires and roughness cubes. Based on similarity requirements, the calibrated mean wind speed and turbulence intensity profiles were simulated according to the suburban exposure type. The approaching wind velocity

and intensity profile were measured by the Cobra probe at the test location without the model, which is depicted in Figure 4.5. Both profiles fit the power law relationship of Eqs. 4.2–4.3. The turbulence spectrum measured at the height of 0.33 m in the wind tunnel is depicted in Figure 4.6, and the longitudinal integral length scale L_u is 0.3368 m. This corresponds to the L_u of 126.7 m at 132 m height in full scale.

$$\bar{u}_z = \bar{u}_g \left(\frac{z}{z_g}\right)^{\alpha} \tag{4.2}$$

$$I_z = I_g \left(\frac{z}{z_g}\right)^{-\alpha} \tag{4.3}$$

where $\bar{u}_g$ = 10.3 m/s is the mean wind speed at gradient height of z_g = 0.58 m in the wind tunnel, and the power law coefficient of the velocity profile is α = 0.19. I_g = 10.3% is the turbulence intensity at z_g.

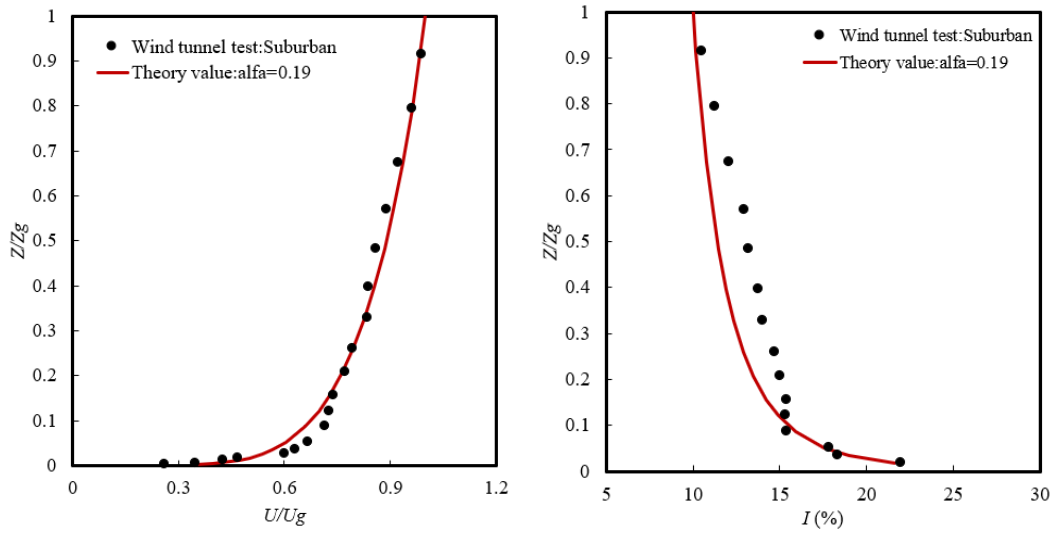

(a) Velocity profile (b) Turbulence intensity profile

Figure 4.5 Comparison of regenerated atmospheric boundary and theory data

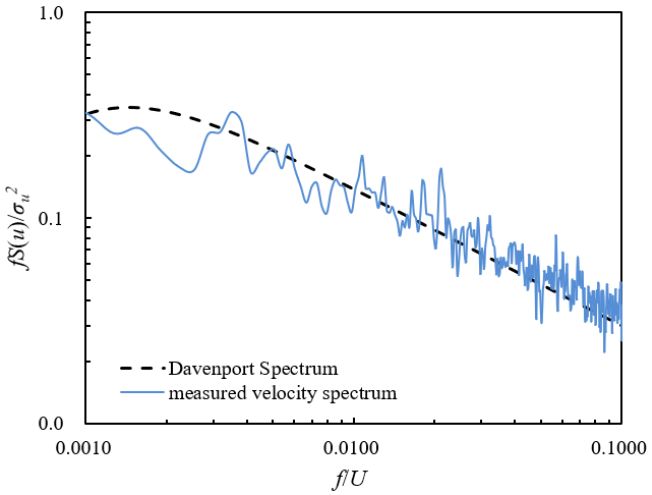

Figure 4.6 Longitudinal turbulence spectrum.

- **PLW velocity test**

A photo of the wind tunnel test model is presented in Figure 4.7. The building models were made of foam and ignore the details of the building figure, which will not have any influence on the PLW velocity. The diameter of the investigated area was 700 m in full scale, and 16 measurement points at the pedestrian level were chosen in this study (see Figure 4.8). The PLW velocities were measured by the Cobra probe at the height of 0.005 m above the ground in the scaled model, corresponding to 2 m of pedestrian level at full scale. The figure indicates that the test points are uniformly distributed in the main street, secondary street, and a nearby park, which are the areas that frequently host human activities.

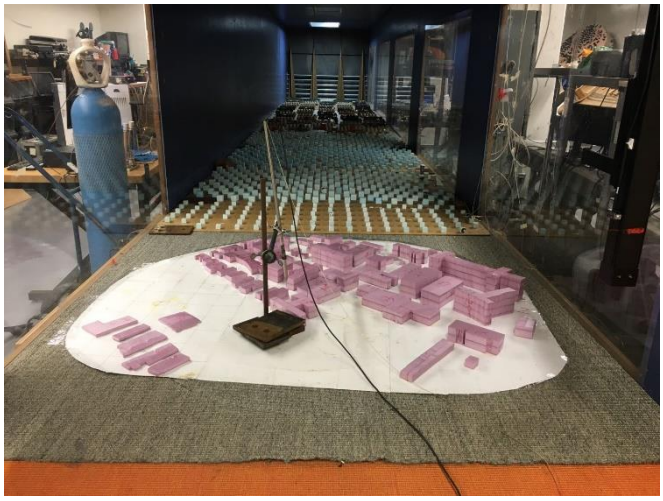

Figure 4.7 Wind tunnel test of Westmount, Montreal.

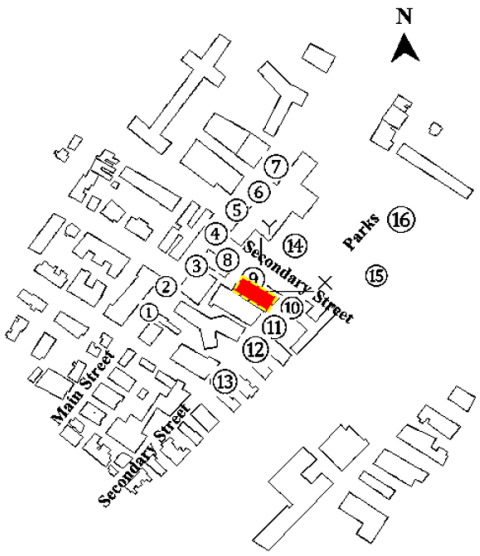

Figure 4.8 Measurement points location of Westmount, Montreal.

4.1.3 Wind tunnel test of Kowloon, Hong Kong

- **XNJD-III boundary layer wind tunnel at Southwest Jiaotong University**

The XNJD-III boundary layer wind tunnel at Southwest Jiaotong University is in Chengdu, China; see Figure 4.9 (a). The size of the test section of the wind tunnel is 22.5 m wide, 4.5 m tall and 36 m long, and the generated wind speed ranges from 1.0 m/s to 16.5m/s. The ABL is simulated by

wood towers and three types of wood cubes arranged in the upstream of the wind tunnel section with the dimensions of 0.15 m, 0.1 m, and 0.06 m, respectively, as seen in Figure 4.9 (b). The approaching wind profiles can be simulated at a scale of 1:200–1:800. The bottom wall of the wind tunnel is equipped with a turntable plate, which can realize the conversion of wind direction from 0° to 360°.

This is a closed-circuit wind tunnel, which has the advantage of producing higher-quality flow in the test section at a lower operational cost than that of an open-circuit wind tunnel. However, construction costs are higher, and there must be a way to purge the tunnel for smoke flow visualization tests.

(a) Picture of wind tunnel (b) Working section

Figure 4.9 Wind tunnel of XNJD-III at Southwest Jiaotong University.

- **Generation of ABL**

The case study of Kowloon, Hong Kong, was conducted in the XNJD-III wind tunnel at Southwest Jiaotong University, Sichuan, Chengdu. The ABL was simulated by wood spires and roughness elements arranged in the upstream of the wind tunnel section, as depicted in Figure 4.10. The scaling down is 1:800 in consideration of the wind tunnel size and model dimensions.

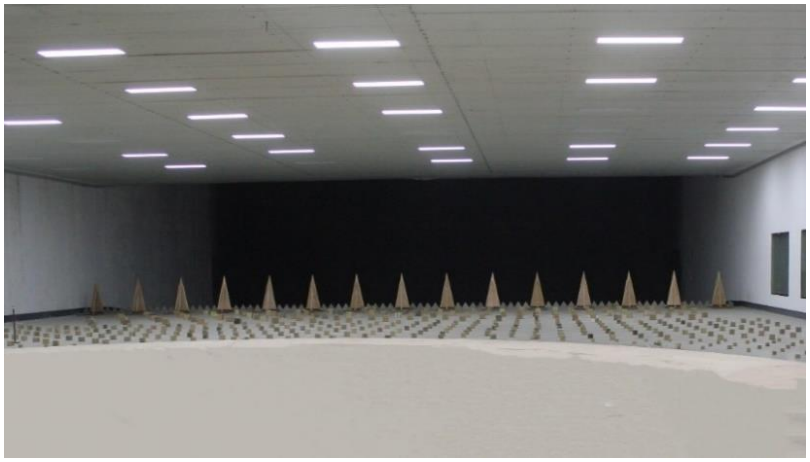

Figure 4.10 ABL setup of the wind tunnel test of Kowloon, Hong Kong.

Based on similarity requirements, the calibrated mean wind speed and turbulence intensity profiles were simulated according to the Code of Practice on Wind Effects in Hong Kong (2004); see Eqs. 4.4–4.5. The code recommends that the design wind speed be increased by 5% above the derived 50 years return wind speed, taking into consideration that Hong Kong is in a typhoon wind climatic area. Therefore,

$$\bar{u}_z = 1.05\bar{u}_g \left(\frac{z}{z_g}\right)^{\alpha} \tag{4.4}$$

$$I_z = I_g \left(\frac{z}{z_g}\right)^{-\alpha} \tag{4.5}$$

where u_g = 56.6 m/s is the hourly mean wind speed at gradient height, z_g = 500 m is the gradient height, α = 0.11 is the power law exponent for mean velocity, and I_g = 0.087 is the turbulence intensity at gradient height.

The mean velocity and turbulence intensity profiles were measured at the test location without the model by self-designed pressure pipes and Cobra probes installed on an iron bar. The measurement results of the calibrated profiles and the target profiles from the wind load code of Hong Kong are compared in Figure 4.11. The gradient height of the regenerated ABL is 0.55 m, with the corresponding velocity of 8 m/s. The values of turbulence intensity near the ground and at gradient height are approximately 18% and 9%, respectively. The turbulence spectrum measured at the

height of 0.3 m in the wind tunnel is presented in Figure 4.12, and the longitudinal integral length scale L_u is 0.34 m. This corresponds to the L_u of 272 m at 240 m height in full scale.

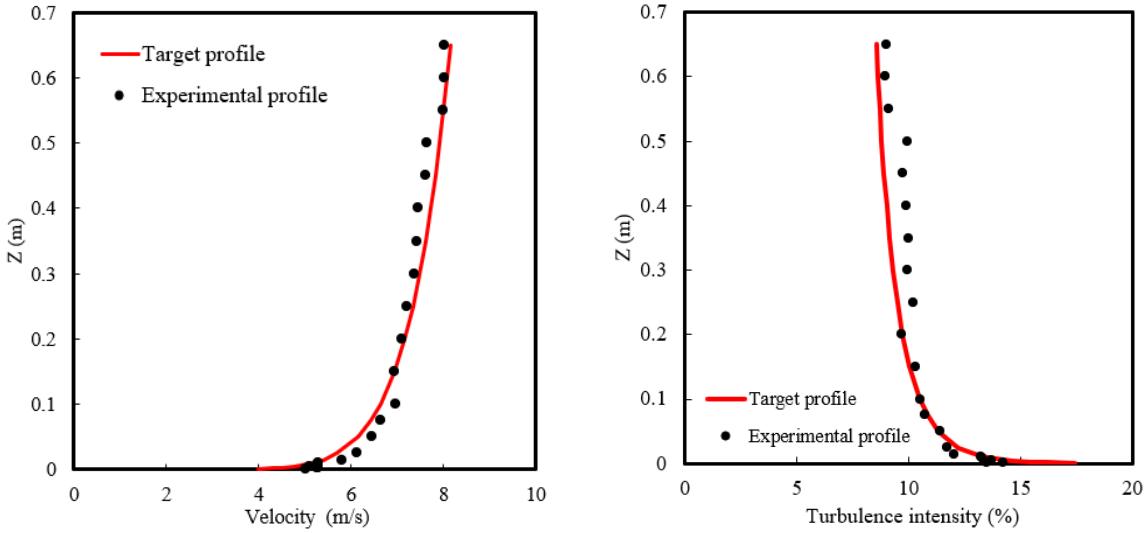

(a) Velocity profile (b) Turbulence intensity profile

Figure 4.11 Comparison of regenerated atmospheric boundary and meteorological data similar title.

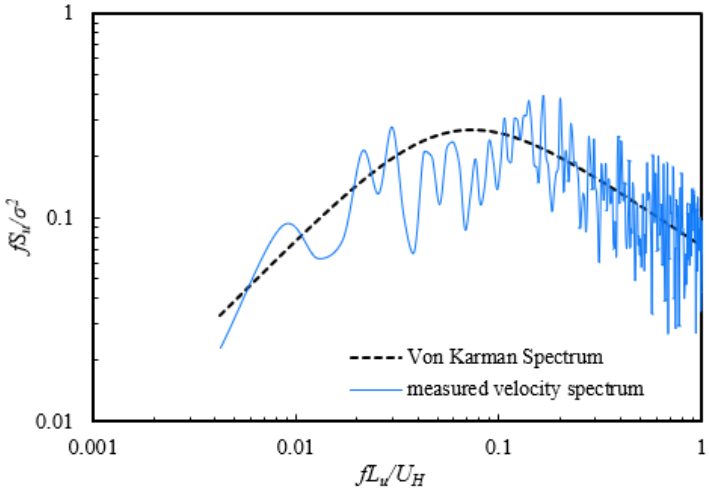

Figure 4.12 Longitudinal turbulence spectrum.

- **PLW velocity test**

A photo of the wind tunnel test model of Kowloon, Hong Kong, is presented in Figure 4.13. The building models were made of foam and the details of the buildings, which have less influence on the PLW, were ignored. In this case study, only the wind direction of 260° was investigated. The radius of the interested area where the wind velocities were observed is 450 m, and the velocities were observed with both the upstream fetch length of 450 m and 3,300 m (see Figure 4.13). Observation points of 50 locations at the pedestrian level were chosen in this study (see Figure 4.14). The velocities were measured at the height of 0.004 m above the ground in the scaled model, corresponding to 3.2 m at pedestrian level in full scale. The PLW velocity was measured by Irwin probes. The figure indicates that the tests points were uniformly distributed in the main street and the secondary street, which are the areas that see frequent human activities.

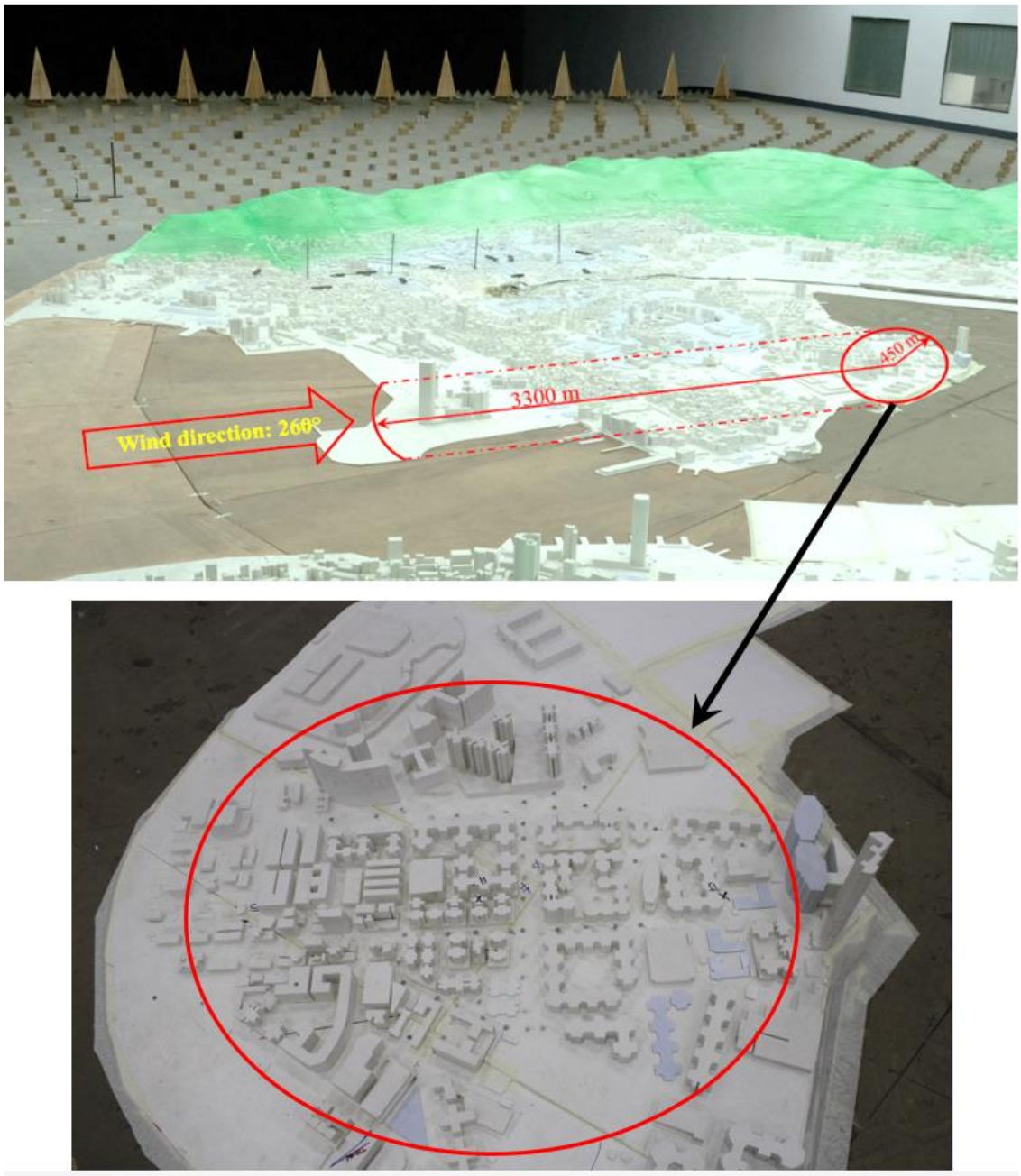

Figure 4.13 Wind tunnel test of Kowloon, Hong Kong.

Figure 4.14 Measurement points location of the Kowloon, Hong Kong.

4.2 Numerical methodology

4.2.1 General

CWE is primarily defined as "the use of computational fluid dynamics (CFD) for wind engineering applications, although it also includes other approaches of computer modeling as well as field and wind tunnel measurements supporting CWE model development and evaluation" (Murakami, 1990,1997; Stathopoulos, 1997, 2002; Baker, 2000; Murakami et al., 2008, etc.). In recent years, with the development of high-performance computers, CWE has been widely adopted in the investigation of wind environment problems. The CFD simulation of wind flow over urban areas is a useful tool for a variety of applications of PLW comfort, dispersion of pollutants, urban ventilation, and wind energy resource assessment. Compared with a wind tunnel test, the CFD method can provided detailed information of a flow field in a complex urban area and can be conducted at full scale. Additionally, the size and scaling of an experimental model is restricted to the width of the wind tunnel, and these issues can be easily addressed in a numerical test. With the increasing accuracy of the CFD method, it is gradually being adopted as equivalent to the experimental methodology.

This chapter describes the numerical methodology of PLW velocity estimation. The governing equations and turbulence model are introduced, then the setup computational domain size and meshing strategies are illustrated, followed by the selection of various boundary conditions.

4.2.2 Governing equations

The governing equations of incompressible turbulent flow are the Navier–Stokes (N–S) equations:

$$\frac{\partial u_i}{\partial x_i} = 0 \tag{4.6}$$

$$\rho\frac{\partial u_i}{\partial t}+\rho\frac{\partial\left(u_i u_j\right)}{\partial x_j}=-\frac{\partial p}{\partial x_i}+\frac{\partial}{\partial x_i}\left(\mu\frac{\partial u_i}{x_j}\right) \tag{4.7}$$

Where u_i, p, ρ, and μ are the velocity component, pressure, air density, and dynamic viscosity, respectively (i = 1, 2, 3).

The steady-state Reynolds-averaged N–S equations (RANS) are commonly used for the simulation of wind flow around bluff bodies that model the flow quantities decomposed into time-averaged and fluctuating components (Reynolds decomposition). The N–S equations are not closed due to the presence of Reynolds stresses. According to the method of closure for the time-averaged N–S equations, various turbulence models have been developed.

4.2.3 Turbulence models

Turbulence models include one-equation models, for example, the Spalart–Allmaras model by Spalart and Allmaras (1992), and two-equation models, for example, the standard k-ε model by Jones and Launder (1972), the Renormalization group (RNG) k-ε model by Yakhot et al. (1986), the Realizable k-ε model by Shih et al. (1995), and the k-ω shear stress transport (SST) model by Menter (1994). For the problem of urban wind flow, the 3D RANS numerical approach is adopted in most cases. The most commonly used turbulence models for the simulation of urban physics and wind engineering problems are the k-ε and k-ω models. The realizable k-ε model was adopted in the present investigation. Its governing equations are as follows:

$$\rho\frac{\partial k}{\partial t}+\rho div\left(k\vec{V}\right)=div\left(\mu+\frac{\mu_t}{\sigma_k}gradk\right)+P_k+P_b-\rho\varepsilon-Y_M+S_k \tag{4.8}$$

$$\rho\frac{\partial \varepsilon}{\partial t}+\rho div\left(\varepsilon\vec{V}\right)=div\left(\mu+\frac{\mu_t}{\sigma_\varepsilon}grad\varepsilon\right)+\rho C_1 S_\varepsilon-\rho C_{2\varepsilon}\frac{\varepsilon^2}{k+\sqrt{\nu\varepsilon}}+C_{1\varepsilon}\frac{\varepsilon}{k}C_{3\varepsilon}P_b+S_\varepsilon \tag{4.9}$$

where μ and μ_t are the molecular dynamic viscosity and the eddy or turbulence dynamic viscosity, respectively; P_k is the generation of k due to the mean velocity gradients; S_k and S_ε are source terms;

and Y_M is the dilatation dissipation term. The constants such as C_μ, σ_k, σ_ε, $C_{2\varepsilon}$ in the transport equations assume different values for different applications.

4.2.4 Computational domain

The size of the computational domain can affect the development of PLW flow, which, in turn, can affect the predicted accuracy of the wind environment. The width of the computational domain should be chosen carefully to avoid the artificial acceleration due to the close distance between the building models and the lateral domain. According to best practice guidelines (BPGs); (Blocken, 2012; Franke et al., 2010; Tominaga et al., 2008), the length of the upstream fetch should be as short as possible to avoid unintended streamwise gradients, and the length of the downstream fetch should be long enough for the full development of wake flow. In this study, $5H_b$ (H_b is the height of tallest building in the area) is chosen for the upstream length, and $25H_b$ is chosen for the downstream length.

The width and height are chosen to meet the BPGs that the directional blockage ratio should be less than 3% in lateral and vertical direction. Since the square root of 3% is 17%, the following equations should be satisfied:

$$W_b/W_d \leq 17\% \tag{4.10}$$

$$H_b/H_d \leq 17\% \tag{4.11}$$

where W_b and W_d are the width of building groups and the computational domain, respectively, and H_b and H_d are the height of the highest building and the computational domain, respectively. The width of the computational domain is chosen as W_b/17% and the height of the domain is chosen as H_b/17%. A schematic view of the computational domain is depicted in Figure 4.15.

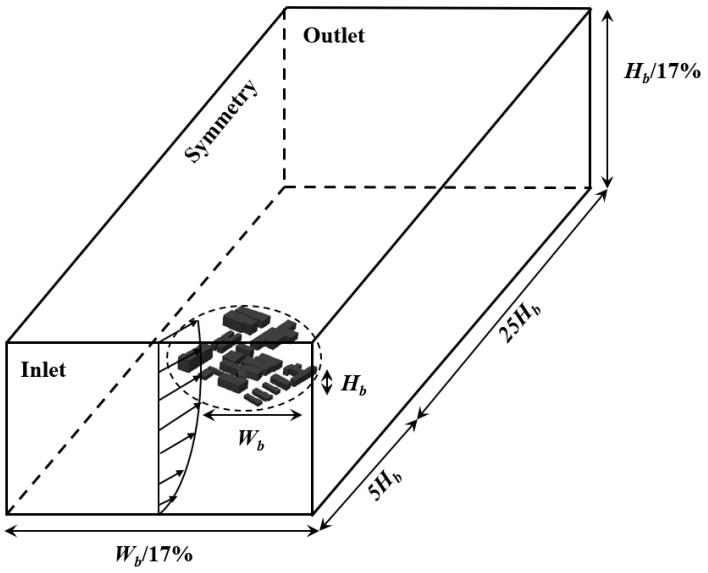

Figure 4.15 Schematic view of the computational domain.

4.2.5 Meshing strategy

Mesh quality is essential for accurate simulation results. Frank (2007) and Tominage et al. (2008) summarized cross-comparison results for a simple building model (Mochida et al., 2002, Yoshie et al., 2005) and suggested in the Architectural Institute of Japan (AIJ) guideline and in the BPGs that a minimum of 10 grids is required on one side of a building to reproduce the separation flow around the upwind corners. In the regions with a steep velocity gradient, it is desirable to set a stretching ratio of adjacent cells of 1.3 or less. For a building complex, COST suggests that at least 10 cells should be used per building side and 10 cells per cube root of building volume as an initial choice. Moreover, the evaluation height (1.5–5.0 m above ground) is suggested located at the third or higher grid from the ground surface (Yoshie et al., 2005; Tominaga et al., 2005). Du et al. (2018) investigated the influence of meshing quality on the PLW environment by taking the case study of the Hong Kong Polytechnic University campus and proposed a near-wall mesh generation technique to provide sufficient near-wall mesh density for the simulation requirement.

In this section, the appropriate meshing strategy is obtained by independent tests. The entire computational domain is divided into inner region and outer region. A high-resolution and high-quality grid is generated in the inner region. Most of the cells are hexahedral and the others are prismatic, and this meshing strategy can avoid the convergence problems caused by tetrahedral or pyramid cells. The meshing strategy is presented is Figure 4.16 with the meshing near buildings in detail. To meet the requirement of BPGs, five cell layers are set below the pedestrian height. The height of the first layer is 0.03 m with the according corresponding $y+ \approx 10–30$.

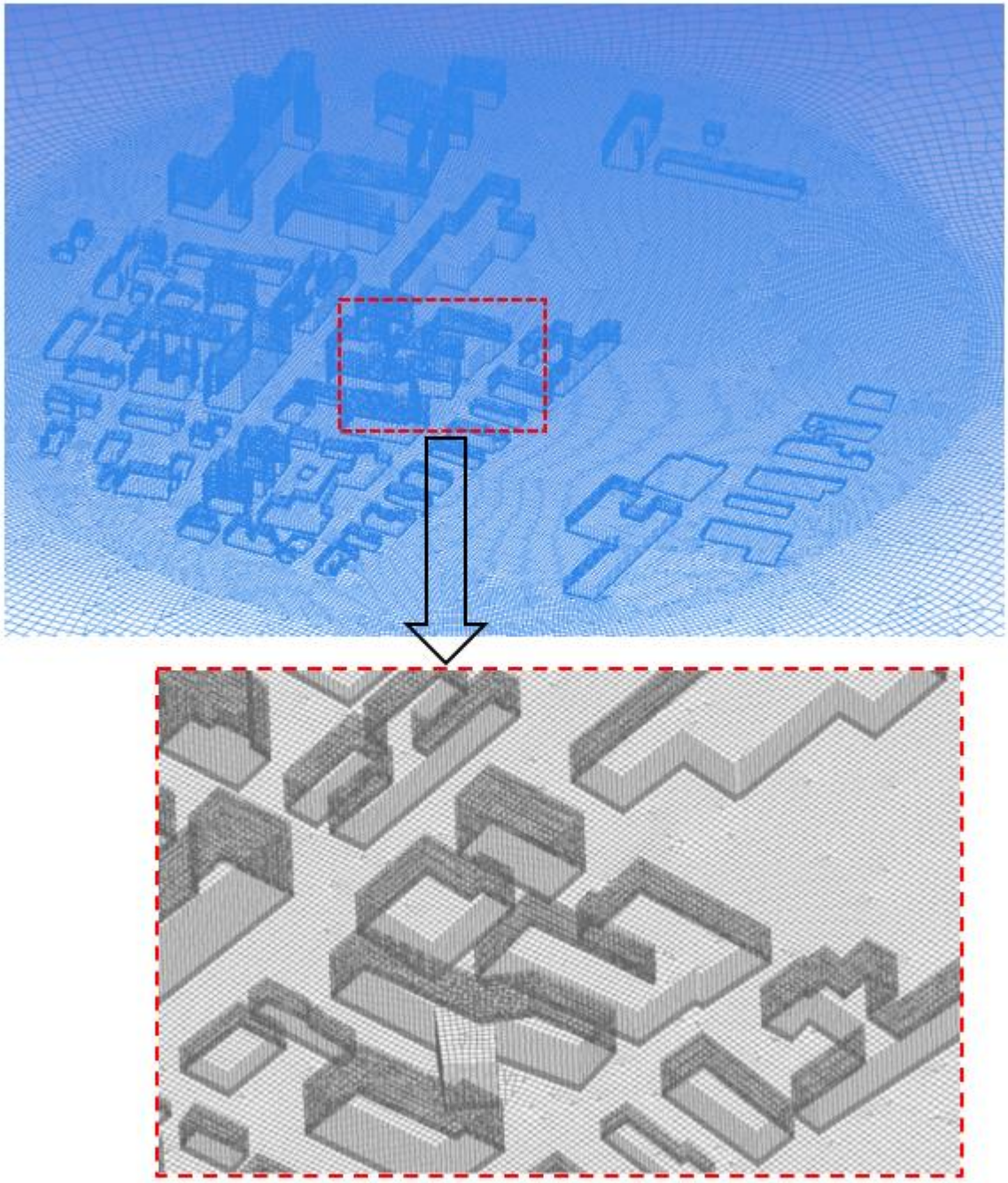

Figure 4.16 Meshing strategy.

4.2.6 Boundary conditions

- **Inlet boundary conditions**

A reasonable setup of the inlet boundary conditions of the computational domain will increase the accuracy of PLW simulation results to a large extent. The inlet formula of approaching wind velocity U, turbulence kinetic energy k, and turbulence dissipation rate ε of the RANS turbulence model are all related to the value of exposure roughness z_0. The inlet condition of computational domain is imposed by user-defined functions (UDF), consisting of the profiles of mean wind speed, turbulence kinetic energy, and turbulence dissipation rate. The inlet boundary conditions proposed by Tominaga et al. (2008) are adopted in the present numerical test; see Eqs. 4.12–4.16. This inlet profile setup is based on the Architectural Institute of Japan Recommendations for Loads on Buildings (2004). The k profile can be calculated according to the observation data if a wind tunnel test or a field measurement is available.

$$U(z) = U_S \left(\frac{Z}{z_S}\right)^{\alpha} \tag{4.12}$$

$$I(z) = \frac{\sigma_u(z)}{U(z)} = 0.1 \left(\frac{z}{z_G}\right)^{(-\alpha-0.05)} \tag{4.13}$$

$$k(z) = \frac{\sigma_u^2(z) + \sigma_v^2(z) + \sigma_w^2(z)}{2} \cong \sigma_u^2(z) = \left(I(z)U(z)\right)^2 \tag{4.14}$$

$$\varepsilon(z) \cong C_\mu^{1/2} k(z) \frac{dU(z)}{dz} \tag{4.15}$$

When the vertical gradient of the velocity can be expressed by a power law with α

$$\varepsilon(z) \cong C_\mu^{1/2} k(z) \frac{U_S}{z_S} \alpha \left(\frac{z}{z_S}\right)^{(\alpha-1)} \tag{4.16}$$

Where U_S is the velocity at the reference height, z_S; z_G is the boundary layer height; σ_u is the RMS value of velocity fluctuation in streamwise direction; $C_\mu = 0.09$ is the model constant; and $\alpha = 0.19$ by fitting the curve of mean velocity profile.

- **Ground roughness setup**

At the building's surface, the non-slip wall with standard wall functions by Launder and Spalding (1974) were employed. For the ground roughness, the input parameters of wall functions are equivalent sand-grain roughness height k_s and roughness constant C_S.

Blocken et al. (2007) investigated the manifest of vertical mean wind speed and turbulence profiles as they travel through the computational domain. He proposed the relationship of exposure roughness parameters of k_S and Cs and z_0 in Fluent is $k_S = 9.793\ z_0 / Cs$ with the requirement of $y_P > k_S$, where y_P is the distance from the first layer center to the wall. Ai and Mark (2013) investigated the effect of the inhomogeneous ABL and near-wall treatment on a CFD simulation of the flow and dispersion ground surface. Liu et al. (2017) found that it is better to vary C_s while keeping $k_s = 1$ to provide satisfactory wind information close to the ground. Ricci et al. (2020) found that the ground roughness setup may influence the PLW comfort studies with open areas as squares and wide streets. Its influence on high-density cities is less where local scale-forcing effects are dominant.

In this study, C_S was set to 1 to meet the necessary condition $y_p > k_s$, where y_p is the distance between the wall and the center point of the wall-adjacent cell. The equivalent sand-grain roughness height k_s was calculated according to the relationship of $k_s = 9.793\ z_0/C_s$ and C_s is 1.0. Zero statistic pressure is specified on the domain outlet. Symmetry boundary conditions with zero normal velocity and gradient are imposed at the top and sides of the domain.

4.2.7 Discretization method

All simulations were performed using second-order discretization schemes for the convection and viscous terms. The SIMPLE (semi-implicit method for pressure-linked equations) algorithm with second-order upwind discretization schemes was used for pressure-velocity coupling. Second-order upwind and spatial discretization were used for pressure and momentum, respectively. The velocity magnitude on several observation points was monitored for the purpose of confirming convergence, and the integrations were terminated when the velocity magnitude did not change.

4.3 Summary

This chapter has summarized the experimental setups and the numerical parameters. The wind tunnel test general setting of the case studies of Westmount, Montreal, and Kowloon, Hong Kong, are both introduced, conducted in the Building Aerodynamics Laboratory at Concordia University and in the XNJD-III boundary layer wind tunnel at Southwest Jiaotong University, respectively. The measurement instrument and the approaching wind profile are also illustrated. Additionally, the numerical methodology for the simulation of PLW velocity is introduced in terms of governing equations, turbulence models, computational domain, meshing strategy, boundary conditions, and discretization method.

Chapter 5 Estimation Exposure Roughness Length Based on Google Earth Pro

The methodology of estimation z_0 in various wind load provisions and literature are summarized and reviewed in Chapter 2 and 3. In this chapter, an efficient and freely available method to estimate the value of z_0 by Google Earth Pro is proposed. This chapter is taken from the reference of ***Estimating Exposure Roughness Based on Google Earth*** (Yu, J., Stathopoulos, T., & Li, M, 2021) that published on the *Journal of Structural Engineering*, *147*(3), 04020353. The context is exactly the same with the reference except the number of equations, figures, and tables.

5.1 Introduction

The determination of exposure roughness is essential for both the estimation of wind load on buildings and the investigation of wind environment. The value of exposure roughness can be calculated by morphometric method. However, the difficulty of the usage of morphometric methods lie in the estimation of the parameters λ_f, λ_P, H_{ob}, H_{max}, and σ_H relating to the size, shape, and distribution of a large-scale area. To identify these parameters, the 3-dimensional model is needed. Traditionally, methods of 3-dimensional modeling are based on ground survey, aerial observation, or online database. Such methods may be expensive and time-consuming. Besides, with the rapid development of urbanization, these current 3-dimensional model data can be easily out-of-date. Currently, the data source for the reconstruction of 3D model can be divided into three categories, which are DEM, satellite images and meteorological model. However, these resources used in current research and practice are expensive and unavailable for some rural areas. Among all the data source, Google Earth Pro is widely used in recent years, which can provide freely available 3D geo-referenced images with high spatial resolution.

The images provided by Google Earth Pro are obtained by satellite imagery, aerial photography, and GIS data over days or months, and have global coverage. By early 2022, 3D imagery has been

expanded to hundreds of cities in over 40 countries, including major cities of the United States and encompassing every continent except Antarctica. According to the Google Earth Blog (https://www.gearthblog.com/), data updates in some large city areas usually take place about once a month, and a little bit slower in remote areas. Imagery resolution ranges from 15m to 15 cm.

In this chapter, a 3-dimensional model building approach based on the rapidly developed high-discretization GIS software of Google Earth Pro is proposed, which could be used in a large-scale area in most places of the world conveniently and efficiently. Together with the morphometric method, the value of z_0 could be estimated. The workflow chart of the z_0 estimation process is shown in Figure 5.1. The process can be divided into three steps, which are extracting data from Google Earth Pro, reconstructing 3D model in Agisoft Metashape, and calculating morphometric parameters by MATLAB.

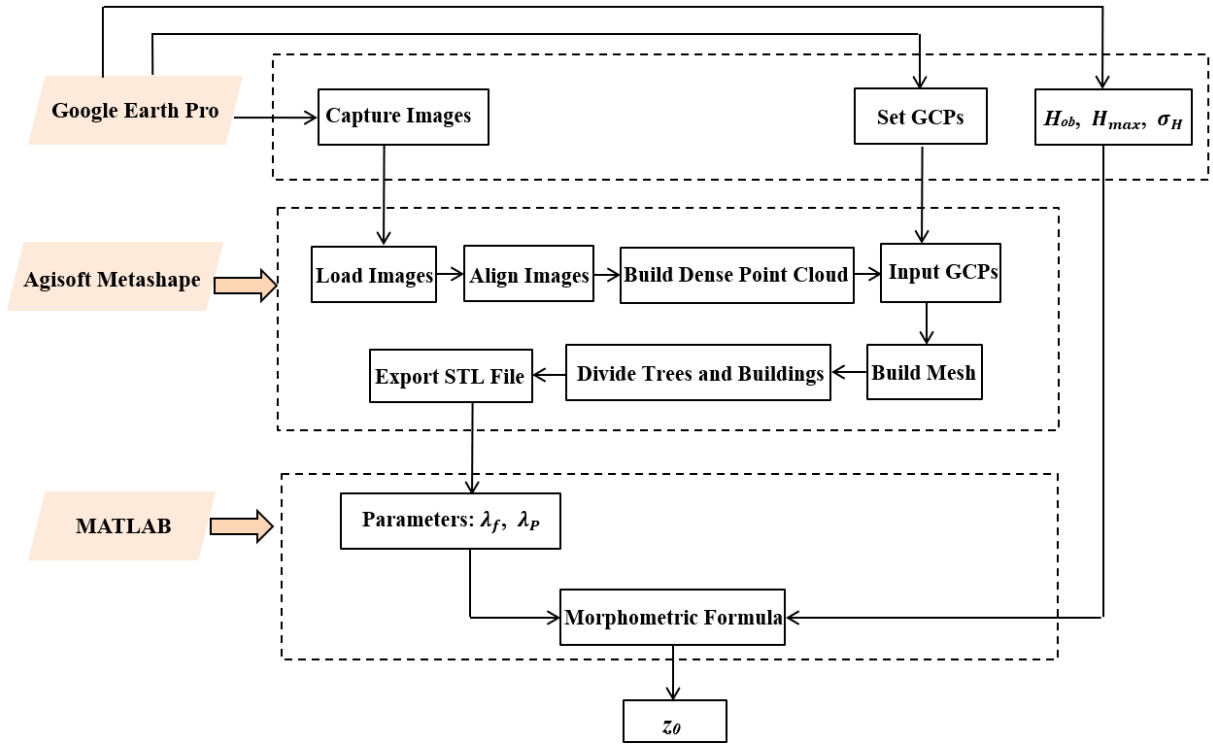

Figure 5.1 Workflow of z_0 estimation process.

5.2 Methodology

5.2.1 Extracting data from Google Earth Pro

The first step of extracting GIS information is to capture the images of the investigated area in Google Earth Pro. The captured images require 60% of side overlap and 80% of forward overlap. The number of "blind-zones" should be minimized since Agisoft Metashape is able to reconstruct geometry visible structures from at least two images.

In order to obtain an accurate estimation of dimension and size of this area, at least 10 ground control points (GCPs) across the area are required. The coordinate values of GCPs are obtained from Google Earth Pro and imported into the reconstructed model to ensure the magnitude of the reconstructed model is accurate and consistent. GCPs should be uniformly distributed in the area and the Universal Transverse Mercator (UTM) coordinate should be used instead of latitude and longitude.

5.2.2 Reconstructing 3D model in Agisoft Metashape

In this step, the images and GCPs are loaded into the Agisoft Metashape software which can generate the 3D model with various spatial data through photogrammetric processing of a series of high-resolution digital images taken from different perspectives. Agisoft Metashape is normally used for drone-based aerial survey, but in this investigation, the high-resolution images captured from Google Earth Pro are used. The city center of London, UK is taken as an example to show the process of the 3D model reconstruction. The area in Google Earth Pro is shown in Figure 5.2.

Figure 5.2 Map of city center of London, UK (from Google Earth Pro).

The images are aligned and checked after inputting into the software. At this stage, the camera position and orientation for each image are identified, and a sparse point cloud model is built accordingly – see Figure 5.3 (a). Then depth and coordinate information are calculated for each image based on the estimated camera position. All this information is combined together with the sparse points cloud and a dense point cloud is generated containing the details of the exposure characteristics of the investigated area, as shown in Figure 5.3 (b). Based on the dense point cloud, a triangular mesh surface is reconstructed by Agisoft Metashape, which depicted the characters of the investigate area – see Figure 5.3 (c). After inputting the GCPs into the mesh surface, a geographic and geometric accurate 3D model of the studied area is reconstructed. Finally, a STL file of the mesh surface containing information of the normal vector and the coordinate value of three vertices of each triangle mesh of the surface is exported. This file format can be processed by MATLAB. It should be noted that the models of plants and buildings need to be separated as only the part of the frontal area of plants is considered to estimate z_0. Indeed, to obtain the model of buildings, the mesh of plants is deleted; similarly, to obtain the model of plants, the mesh of buildings is deleted.

The reconstructed 3D model, which can provide detailed exposure information, is the foundation of investigations concerning urban and city areas, for example, the ventilation, pollutant diffusion, and relevant CFD (Computational Fluid Dynamics) simulation.

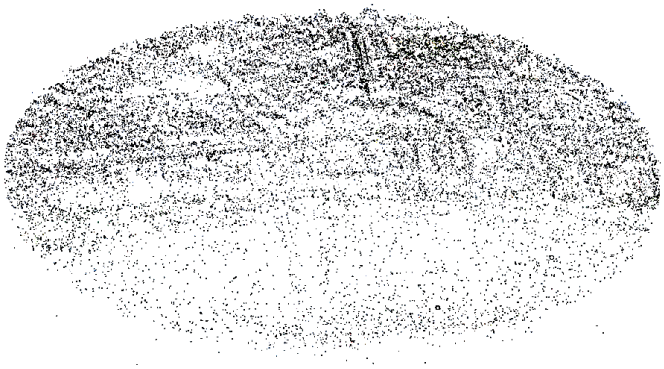

(a) Sparse points cloud model

(b) Dense point cloud model

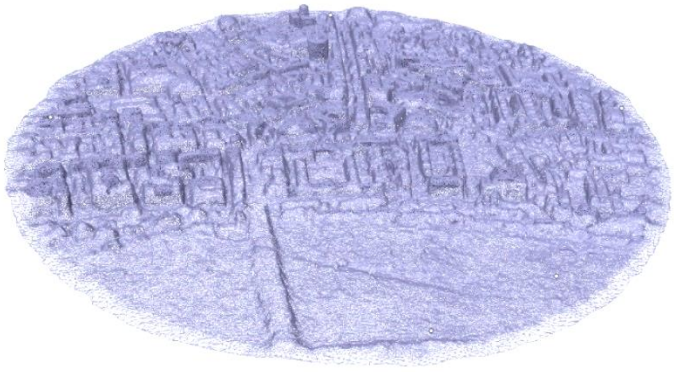

(c) Polygonal model

Figure 5.3 3-dimensional reconstruction process in Agisoft Metashape.

5.3 Morphometric method

The simple relationship proposed by Lettau (1969), is the most widely recognized method and has been adopted by ASCE 7 (2022). However, this algorithm is based on empirical relations derived from wind tunnel work concerning idealized flow over simplified array of roughness elements, which is different from real urban or suburban areas. The basic assumption of this model is that the wake interference between roughness elements is negligible and that the mean velocity profile towards each element is logarithmic. According to the assumption, this model is only valid when λ_f is less than 0.3 - 0.5, because the mean velocity profile towards each structure is not logarithmic with λ_f increasing as the recirculation flow caused by the interference among structures will be dominant.

Macdonald et al. (1998) found that z_0/z_h will increase with increasing the height variability because of the interference among structures. The study introduced the displacement height (z_d) into the logarithmic velocity profile in order to account for the high building density area and determine z_0 more accurately. The frontal area density above the displacement height $\lambda_f{}^{*}= [H_{ob}/(H_{ob} - z_d)]\lambda_f$ could be better to estimate z_0 than λ_f.

$$Mac_{z_d} = \left[1 + \alpha_M{}^{-\lambda_P}(\lambda_P - 1)\right]H_{ob} \tag{5.1}$$

$$Mac_{z_0} = \left(\left(1 - \frac{z_d}{H_{ob}}\right) exp\left[-\left\{0.5\beta_M \frac{C_{Db}}{k^2}\left(1 - \frac{z_d}{H_{av}}\right)\left(\frac{H_{ob}}{H_{ob} - z_d}\right)\lambda_f\right\}^{-0.5}\right]\right)H_{ob} \tag{5.2}$$

where C_{Db} = 1.2, α_M = 4.43, and β_M = 1.0 are empirical constants.

Moreover, the variation of height should also be considered in morphometric algorithms. Kanda et al. (2013) proposed a method that incorporates height variability and zero-plane displacement of Mac_{z0}, such that:

$$Kan_{z_d} = \left[c_0 X^2 + \left(a_0 {\lambda_P}^{b_0} - c_0\right)X\right]H_{max}, \quad X = \frac{\sigma_H + H_{ob}}{H_{max}} \tag{5.3}$$

$$Kan_{z_0} = (b_1 Y^2 + c_1 Y + a_1)Mac_{z_0}, \; Y = \frac{\lambda_P \sigma_H}{H_{ob}} \tag{5.4}$$

where $0 \leq X \leq 1$, $0 \leq Y$, and a_0, b_0, c_0, a_1, b_1 and c_1 are constants equal to 1.29, 0.36, -0.17, 0.71, 20.21, and -0.77, respectively. H_{max} and σ_H are the maximum and the standard deviation of roughness-obstacles height.

Ideally, the complex factors that influence z_0, which are the size, shape, distribution and variation of height, should be all included in the morphometric method. In this regard, Kanda's algorithm is the most extensive method so far. In this investigation, the morphometric formulas of Lettau (1969) and Kanda et al. (2013) are both adopted.

5.4 Calculating key parameters by MATLAB

The key parameters need to be calculated in the morphometric formulas are frontal area index λ_f, plan area index λ_P, and those related to height (H_{ob}, H_{max}, and σ_H), which can be easily obtained from Google Earth Pro by subtracting the ground altitude from the altitude of building roof. The other two parameters can be calculated by geometric method based on the STL file with the help of MATLAB.

To calculate λ_f, the first step is to figure out all the mesh facing the wind. This judgement depends on the angle θ between vectors $\vec{n}$ and $\vec{m}$, which are the unit vector of the wind direction and the normal vector of each mesh respectively. θ is calculated by Eq. 6.5. Meshes with $0 < \theta < \pi/2$ are against the wind direction and meshes with $\pi/2 < \theta < \pi$ are those facing the wind and need to be considered.

$$\theta = arccos \frac{\vec{n} \cdot \vec{m}}{|\vec{n}||\vec{m}|} \tag{5.5}$$

Secondly, the coordinates of these triangle mesh vertex projection points on the plan perpendicular to the wind direction are calculated. As shown in Figure 6.4, if the equation of the plane is $Ax + By + Cz + D = 0$ and the coordinates of the vertex outside of the plane is (x_{o1}, y_{o1}, z_{o1}), the coordinates of the points on the plane (x_{p1}, y_{p1}, z_{p1}) can be calculated as follows:

$$x_{p1} = \frac{(B^2 + C^2)x_{o1} - A(By_{o1} + Cz_{o1} + D)}{A^2 + B^2 + C^2} \tag{5.6}$$

$$y_{p1} = \frac{(A^2 + C^2)y_{01} - B(Ax_{01} + Cz_{01} + D)}{A^2 + B^2 + C^2} \tag{5.7}$$

$$z_{p1} = \frac{(A^2 + B^2)z_{01} - C(Ax_{01} + By_{01} + D)}{A^2 + B^2 + C^2} \tag{5.8}$$

The projection area s_{ob} can be calculated by Eq. 5.9. The total area S_{ob} is obtained by adding all the projected areas of each mesh facing the wind. Then λ_f is calculated by dividing S_{ob} with the area of horizontal plane.

$$s_{ob} = \frac{(x_{p1}y_{p2} - x_{p2}y_{p1}) + (x_{p2}y_{p3} - x_{p3}y_{p2}) + (x_{p3}y_{p1} - x_{p1}y_{p3})}{2} \tag{5.9}$$

For λ_P, the mesh above the ground is figured out by the height. The area of projection to the horizontal plane can be calculated by the same way through Eq. (5.8) and Eq. (5.9). Then λ_P can be calculated by dividing the total projection area by the area of the horizontal plane.

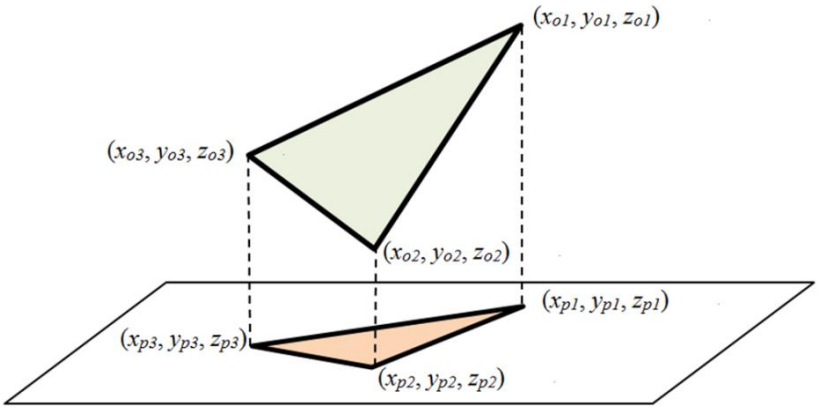

Figure 5.4 The projection of mesh on a plane.

5.5 Case studies

To verify the accuracy of the proposed z_0 estimation method, two cases, for which results are available from previous studies, have been considered. The first case is the area of city center of London, UK, one of most high-density and populated cities in the world, so it belongs to the exposure type of Urban. This study was conducted by Kent et al. (2018). z_d and z_0 are calculated according to Kanda's morphometric formula. The spatial data were acquired using an Optech ALTM 3033 LiDAR system at an altitude of 900 m above ground level (Lindberg and Grimmond, 2011). The upstream fetch to be considered is variable, i.e. 170 m, 1 km, 1.8 km, 2.6 km, 3.4 km, 4.2 km, and 5 km. The field observation data by Doppler LiDAR were used to testify the accuracy of the estimated z_d and z_0, which were measured at 141 m, 171 m, and 201 m. The position of the observation points is 51°30'N, 00°07'W. More details about these measurements can be found in Kotthaus and Grimmond (2012, 2014a, and 2014b) and Kent et al. (2017).

Case II is the Tampa International Airport (KTPA), a suburban area along the Gulf Mexico coastline. This study was conducted by Masters et al. (2010). Field measurement data recorded by Automated Surface Observing System (ASOS) stations along the Gulf of Mexico coastline are studied. This system records surface meteorological conditions and provides minute-to-minute weather updates. z_0 values were estimated according to averages of neutrally stratified mean gust factors (GFs) by an objective, automated, and data-driven technique. GFs are peak gust ($\hat{u}$) to mean wind speed ($\overline{U}$) ratios of stationary wind speed segments determined from wind speed records at a single height. KTPA is chosen to testify the proposed method because z_0 is relatively larger than the other area. The position of data collection is 27°57'N and 82°32'W.

In both studies, z_0 of 16 wind directions of upstream exposure are provided. To be consistent with the available data, the same wind directions are considered in this investigation for comparison

purposes. For each direction, a 45° sector of each side is considered according to ASCE 7-16. Such a large exposure area is chosen for a comprehensive consideration of morphometric features. All geometric features of obstacles at different positions in the sector are treated equally. The wind direction and the corresponding considered area are shown in Figure 5.5. The z_0 values of the two cases are also compared with the revised Davenport's classification method (Wieringa 1992).

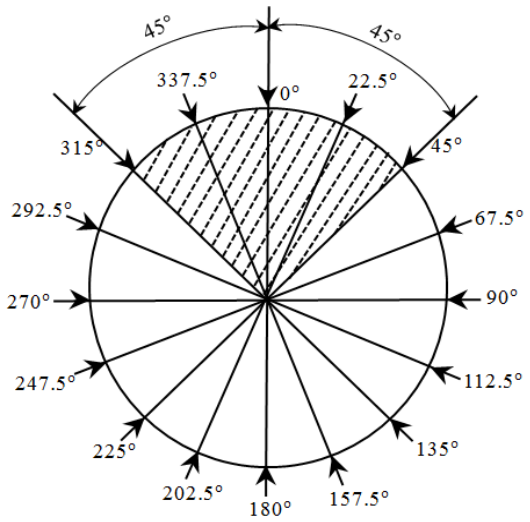

Figure 5.5 Wind direction and corresponding considered area.

5.5.1 Case I: London, UK

The results of 1000 m upstream fetch are compared with Kent's study. The upstream fetch length is determined according to ASCE 7 (2022): for buildings or other structures with a mean roof height greater than 9.1 m, a distance greater than 792 m or 20 times the height of the building or structure should be considered. The map of the investigated area from Google Earth Pro and the wind directions to be considered are shown in Figure 5.6.

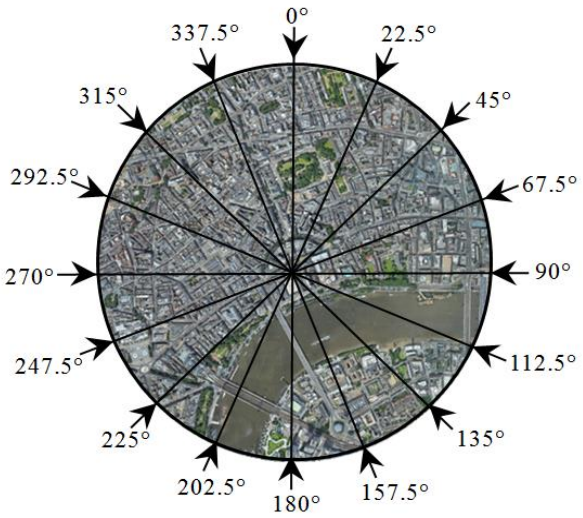

Figure 5.6 Map of London, UK. (from Google Earth Pro).

Morphometric parameters are extracted from the reconstructed 3D model. The variations of λ_f and λ_P with different wind directions are displayed in Figure 5.7. For λ_f, the values from 90°–202.5° are clearly lower than the other directions, which is due to the open area of river. A similar trend was found for λ_P. The gap between 90° – 202.5° and other directions are as a result of the high-rise buildings with small roof area.

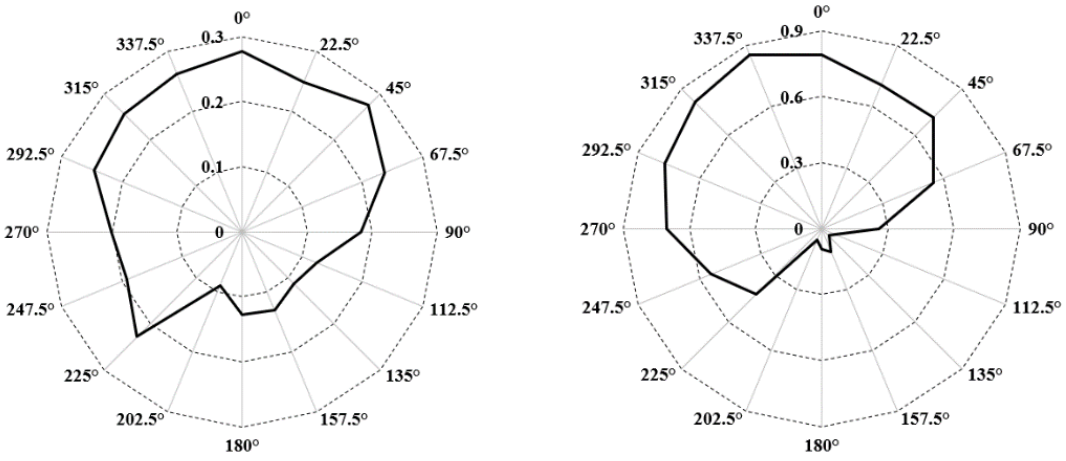

(a) The variation of λ_f with wind direction (b)The variation of λ_P with wind direction

Figure 5.7 Morphometric parameters of λ_f and λ_P extracted from 3D model - Case I: London, UK.

Comparisons are shown in Figure 5.8. The data of Kent's study in the figure show the range of the estimated results obtained for different upstream fetches with considerably more data available. The results determined by both Lettau's and Kanda's formula fall in the range of Kent's results except for the wind direction of 135º, 202.5º and 247.5º. In general, Lettau's results are more accurate than those of Kanda except for the direction of 247.5º, in which z_0 estimated by Lettau's formula and Kanda's formula are 44% and 17% higher than Kent's results. This may be due to the small variation of building heights in this area except for the direction of 247.5º in which the buildings are staggered, and the heights vary significantly. The variation of building heights is considered in Kanda's formula as opposed to the Lettau's formula.

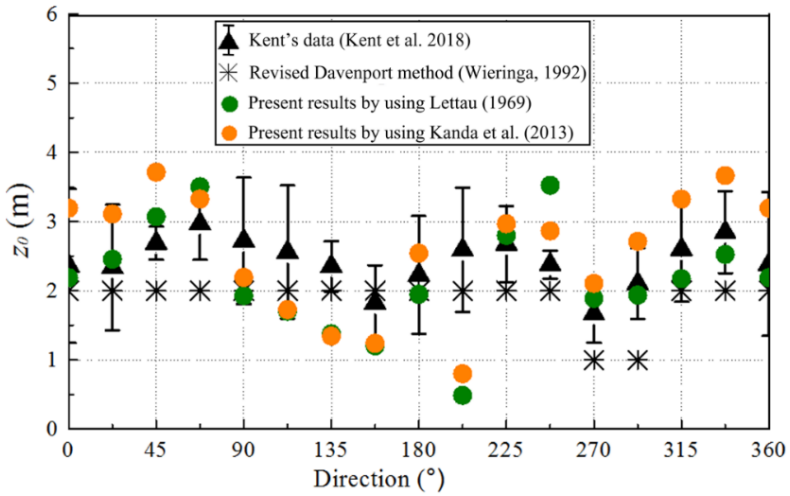

Figure 5.8 Comparison of proposed method with analytical / empirical results - Case I: London, UK.

Values of z_0 estimated by both formulas are somewhat lower for the directions of 135º and 202.5º. This is caused by the presence of the river, which makes the average roughness lower than that for other directions. It can thus be concluded that the upstream fetch of 1000 m is sufficient to determine z_0 in a large city center, but a longer upstream fetch is required for exposure with lower roughness, e.g. rivers or other open spaces. This is consistent with ASCE 7 (2022) that the

considered upstream fetch of Flat exposure type should be longer than that of Urban/Suburban, - 1524 m vs 1000 m respectively.

In order to better demonstrate differences and agreements, the deviation of proposed method results from the analytical / empirical results are also displayed – see Figure 5.9. Most of the estimated z_0 by the proposed results are within 30% deviation compared with Kent's results. It can be concluded that the proposed method by using either Lettau's or Kanda's approach can yield a reasonable estimation of z_0 in this area. The determination of exposure types using the revised Davenport's classification method is made by analyzing the map. The maximum z_0 is 2 m for chaotic exposure type, which fails to estimate the exposure roughness of a large city center. Moreover, there is no middle z_0 value between 1 m and 2 m in Davenport's method, which misses the value of z_0 in reality.

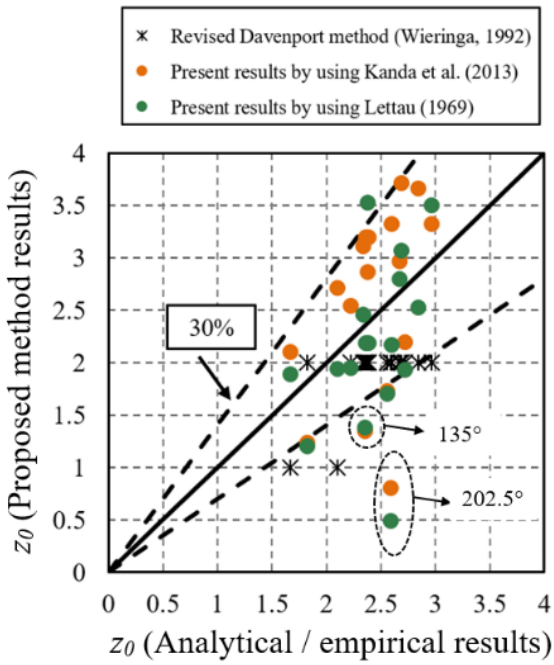

Figure 5.9 Deviation of z_0 between proposed method and analytical / empirical results - Case I: London, UK. Dashed black lines represent 30% deviations, as indicated. (Unit: m)

5.5.2 Case II: Tampa International Airport, Florida

The estimated z_0 of proposed method based on the upstream fetch of 1524 m are compared with that of (Masters et al. 2010) and revised Davenport's classification method (Wieringa 1992). The fetch length is determined according to the ASCE 7-16 that the maximum of 1524 m and 20 h should be considered for Flat exposure type, in which h is the average height of buildings or structure. The map of the investigated area from Google Earth Pro and the wind directions to be considered are shown in Figure 5.10.

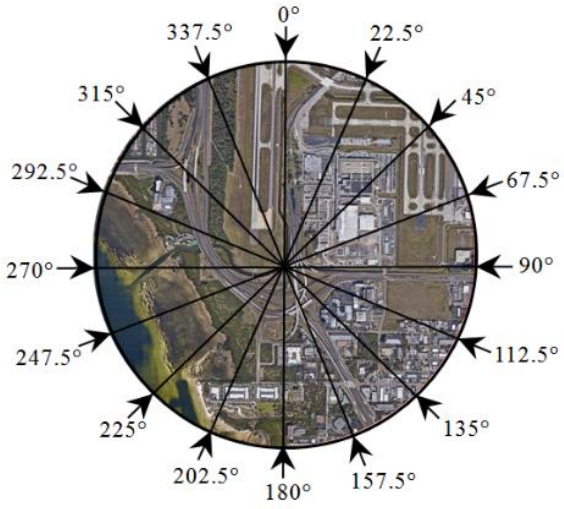

Figure 5.10 Map of Tampa International Airport, Florida. (from Google Earth Pro)

The variations of λ_f and λ_P with different wind directions are displayed in Figure 5.11. The values of both parameters in the wind direction of 202.5° – 270° are smaller than others, where the water dominates most of the area. For the directions of 0° and 90°, most of the structures are low-rise buildings with large span roofs, resulting in smaller λ_f and larger λ_P. Conversely, the majority of the structures in the directions of 135° and 157.5° are mid-rise buildings with small roof area, so the values of λ_f are larger and the values of λ_P are smaller.

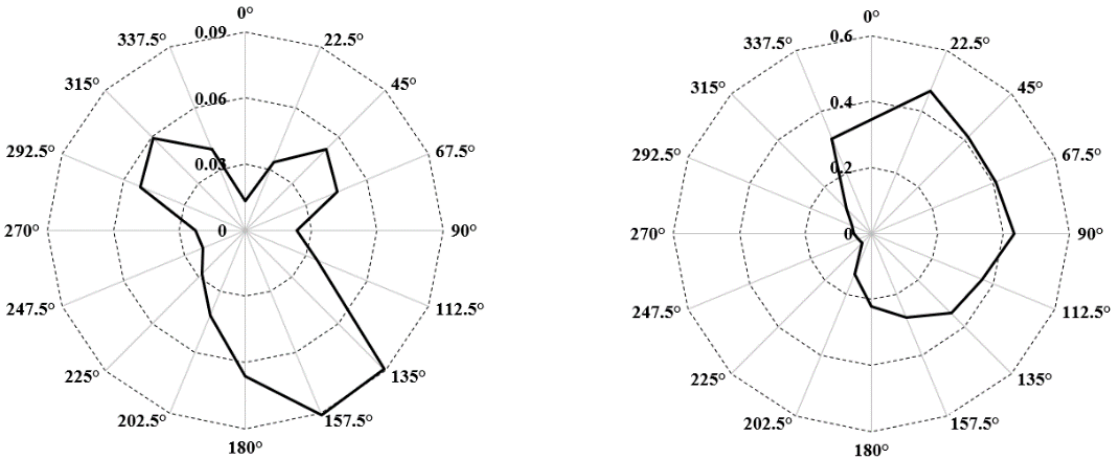

(a) The variation of λ_f with wind direction. (b) The variation of λ_P with wind direction.

Figure 5.11 Morphometric parameters of λ_f and λ_P extracted from 3D model – Case II: Tampa International Airport, Florida.

Figure 5.12 shows the comparison of estimated z_0 values similar to Figure 5.8. According to Powell et al. (1996a, b), non-standardized data can introduce surface-layer wind speed errors of the order of 30% – 40% due to terrain effects. Similar errors have appeared for gusts in (Masters et al., 2010), for which the data are given in the form of a range.

The comparison results show that the proposed method can provide a reasonable estimation of roughness length in this area. The estimated z_0 values of the proposed method fit well with Masters' field measurement data except for the wind directions of 112.5° – 180°. This deviation may be due to an error in the field measurement results, as it can be seen from the map that these areas are covered with dense low-rise and medium-rise buildings and trees with heights ranging from about 5 m to 25 m. However, the estimated z_0 from field measurements are lower than that for 247.5° and 270°, where the exposure roughness is apparently lower.

Figure 5.12 also shows that results of Kanda's formula are always lower for most of the directions compared with those of Lettau (1969) and field measurement data. This is probably due to the

consideration of skimming flow effects (Hussain and Lee 1980) of buildings in Kanda's formula. When buildings are far from each other, the vortex formed behind the buildings causes a drag to the wind. As the density increases and the buildings come closer, there will be sheltering effects from each other. The flow seems to be skimming on the top of buildings. In this case, the wind velocity is assumed to be zero near the ground under the height of z_d and the zero surface is lifted. Consequently, the exposure surface becomes smoother, and the drag reduces. On the contrary, Lettau's formula does not considered the skimming effects. For this area, the buildings and structures are fewer and far from each other, so there is no obvious skimming effect. That may be the reason why the estimated values of z_0 of Kanda's formula are always smaller. It can be inferred that Lettau's formula is more suitable for the area with low exposure roughness.

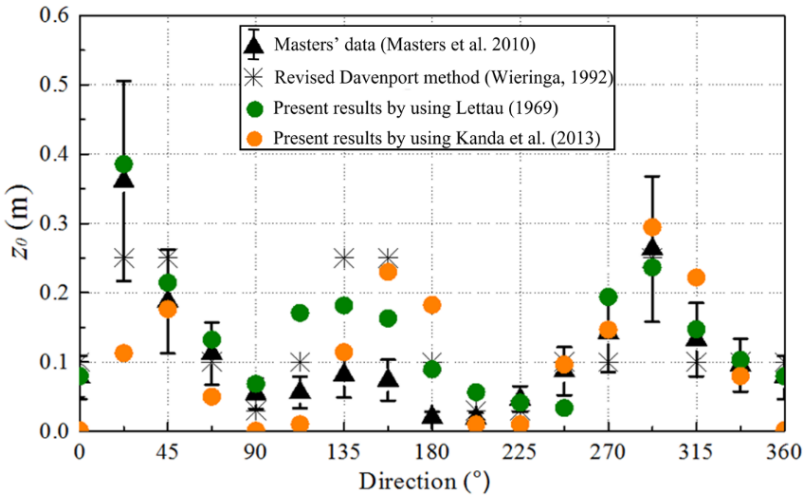

Figure 5.12 Comparison of proposed method with analytical / empirical results – Case II: Tampa International Airport, Florida.

Figure 5.13 shows the deviation of proposed method results to the field measurement results, most of the estimated z_0 by proposed method are within 30% discrepancy. The upper points beyond the 30% error are for the wind directions of 112.5° – 180°, which may be due to the possible errors in the field measurement results. The lower points by using Kanda's formula may be due to the

consideration of skimming effect. The results indicate that the proposed method with Lettau's formula can provide more accurate results in suburban area.

Results are also compared with revised Davenport's classification method, which can also make a good estimation, as it covers 8 exposure types from flat terrain to large city center. However, the accuracy is based on the designers' experience.

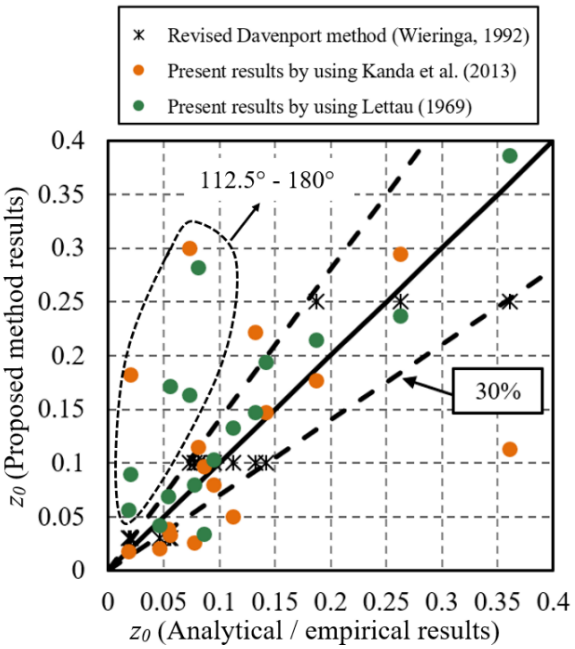

Figure 5.13 Deviation of z_0 between proposed method and analytical / empirical results – Case II: Tampa International Airport, Florida. Dashed black lines represent 30% deviations, as indicated. (Unit: m)

5.6 Summary and Conclusions

Exposure roughness length (z_0) is an important parameter in the estimation of wind load on buildings and other structures, as well as in research relative to urban environment. There are mainly three methods to estimate z_0, namely using the exposure categories of wind load code, the anemometric method, and the morphometric method. Subjective judgement of z_0 by the designers according to wind load code may lead to inaccurate results. Long-term observation data of anemometric methods is costly and time-consuming; also, it may not be available in the relevant

area and it may not keep up with the quick development of urban areas. In comparison, the morphometric method is relatively accurate and convenient, but the dimensional parameters of a large-scale upstream area are not available.

This thesis offers an innovative approach to estimate the value of z_0 in an efficient and inexpensive way. This method uses the morphometric formulas of Lettau and Kanda with the assistance of Google Earth Pro, a well-known GIS software. A 3-dimensional modeling method, which can convert the images captured from Google Earth Pro to three-dimensional models, has been presented. The accuracy of the proposed method has been demonstrated by comparison with available case studies of London, UK and Tampa International Airport, US, as well as the revised Davenport's classification method.

Comparison results show that the proposed method can make a reasonable estimation of z_0 for both Urban/Suburban and Flat exposure types, the errors of most of the estimate values are within 30% compared with analytical / empirical results. Lettau's formula is more accurate for the area that buildings are orderly arranged and with similar heights, while Kanda's formula estimates well in staggered areas with large deviation of building height. Moreover, an appropriate upstream fetch should be used to make an accurate z_0 estimation. This method is more accurate than the revised Davenport's classification method, which fails to estimate z_0 for Large City Centers. Moreover, this method can avoid the potential subjective errors made by designers of the revised Davenport's classification method.

Compared with previous application of morphometric formulas, the proposed methodology could be applied to almost anywhere in the world with adequate high-resolution imagery available on Google Earth Pro. The low cost of this method is particularly attractive for many developing

countries where other sources of long-term wind speed observation data and aerial photography are unavailable. Besides, this method is efficient and easy to use.

The proposed method has great potential on the investigation of exposure roughness. The accurate estimation of z_0 can avoid errors in subsequent analysis. Moreover, the proposed three-dimensional modeling methodology is valuable and has the potential for broader application concerning wind engineering and city environment.

Chapter 6 Influence of Upstream Fetch for Environmental Wind Engineering Applications

6.1 General

Chapter 5 has presented a new methodology on the estimation of the roughness length, z_0, for the exposure effect based on Google Earth, which is convenient and freely available. The validation of this method was carried out by comparison with field measurement data. However, the importance of the upstream fetch on approaching wind characteristics and wind environmental conditions was not addressed. The selected length of upstream exposure fetch will influence the estimation of z_0 or the assessment of PLW comfort. However, the specified fetch in various wind load provisions are different, as discussed in Chapter 2. For instance, the maximum value of 729 m and 20 H is suggested in ASCE 7 (2022), maximum value of 1000 m and 20 H is suggested in NBCC (2020), 1000 m – 3000 m is suggested in AS/NZS 1170.2 (2021), and 200 m – 20,000 m is suggested in EN 1991-1-4 for the estimation of wind load on buildings.

The objective of this chapter is to investigate the influence of different upstream fetch lengths on environmental wind engineering applications. The method proposed in Chapter 5 is adopted to investigate the consideration of different upstream exposure areas on the estimation of z_0 taking the Westmount, Montreal and Kowloon, Hong Kong as case studies, which are two different cases with the exposure type of typical suburban and urban roughnesses. The case study of Westmount, Montreal is covered with sparsely distributed low-rise to mid-rise buildings, while the case study of Kowloon, Hong Kong is a heavy urban area with high-rise buildings. These two case studies have been adopted because experimental data were available from previous projects carried out by the author.

Further to the computational methodology proposed in Chapter 5, the CFD method, as an alternative to the wind tunnel approach, was also adopted for the investigation of the influence of different ranges of upstream fetch on PLW of both Westmount, Montreal and Kowloon, Hong Kong. Compared with its application in the field of structural wind engineering, the CFD method performs better on wind environmental problems. Details of the adopted CFD method can be found in Appendix A.

6.2 Case studies of environmental wind engineering

6.2.1 Westmount, Montreal

The case study of Westmount, Montreal belongs to suburban exposure type consisting of low-rise to mid-rise sparsely distributed buildings. The experimental and numerical setup of this case study is introduced in Chapter 4. There will be a proposed building in the center of this area, which is shown by the red rectangular in Figure 6.1. Three upstream fetch length of 100 m, 200 m, and 300 m are adopted to analysis the influence of upstream exposure on environmental engineering, - see the red circles in Figure 6.1. The corresponding areas with building layout is shown in Figure 6.2. According to the wind observation data obtained at a height of 10 m at the Trudeau International Airport, the probability distribution of hourly mean wind speed at 300 m over Montreal for daylight hours during summer and winter in shown in Figure 6.3. Six most critical wind directions are selected for investigation, namely N, NNE, NE, SW, WSW, and W. Firstly, the influence of different upstream fetch lengths on the determination of z_0 at the building site was analyzed by the methodology proposed in Chapter 5. In addition, the influence of the proposed building on the wind comfort of pedestrian level height should always be assessed according to the wind comfort criteria. The PLW velocities in this area are also compared with different upstream fetch lengths by the CFD method. Sixteen (16) locations on the main street and secondary street close to the proposed

building site are selected to observe the PLW velocity. The wind directions and the locations of the observation points are shown in Figure 6.4.

Figure 6.1 Westmount, Montreal case with different upstream fetches.

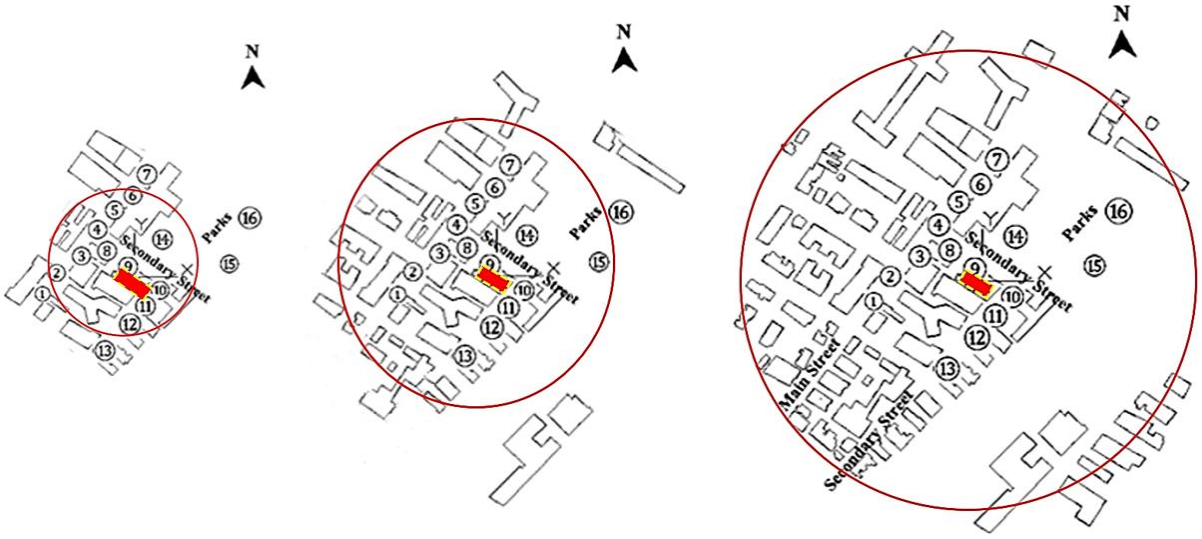

(a) Size A, R = 100 m (b) Size B, R = 200 m (c) Size C, R = 300 m

Figure 6.2 Models of different upstream fetch lengths.

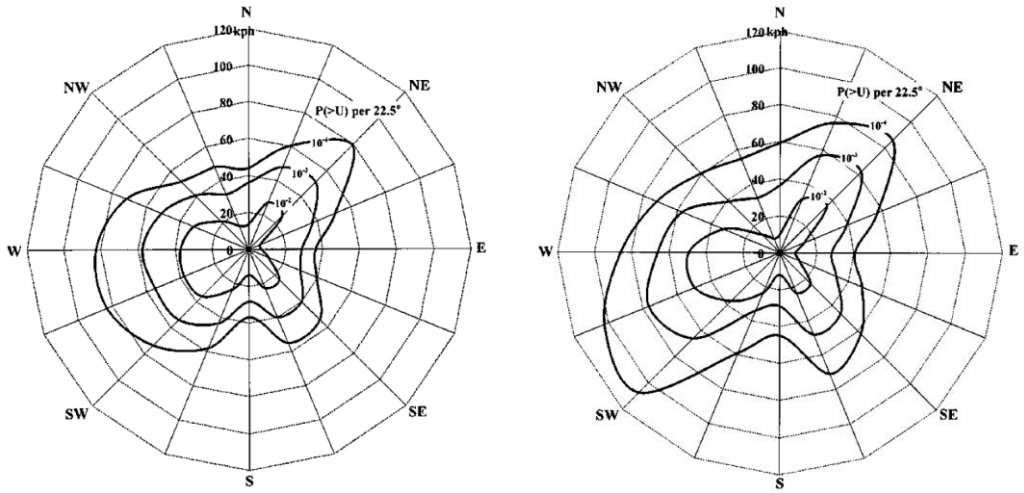

(a) Summer (b) Winter

Figure 6.3 Probability distribution of hourly mean wind speed at 300m over Montreal for daylight hours.

(derived from a 10-year record of wind data obtained at a height of 10 m at Trudeau International Airport)

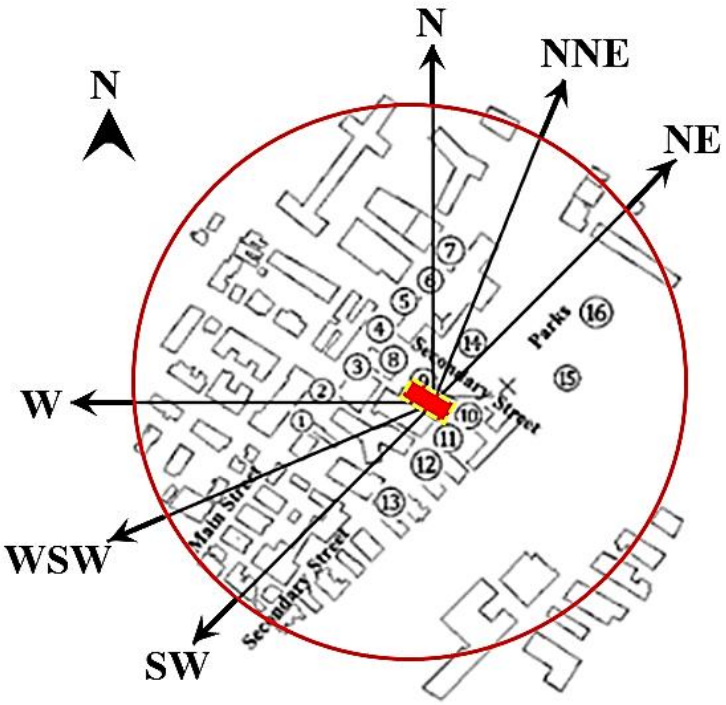

Figure 6.4 Wind directions and observation points adopted in the Westmount, Montreal case study.

6.2.2 Kowloon, Hong Kong

The case study of Kowloon, Hong Kong is a typical urban area with densely distributed high-rise buildings. The setup of wind tunnel test is introduced in Chapter 4. This area is selected for the assessment of the wind environment around existing buildings, the PLW velocity in the small red circle with the radius of 450 m in Figure 6.5 is observed by Irwin probe (Irwin, 1981) in wind tunnel test. According to the observation data at Hong Kong Observation (https:// www. weather. gov. hk/en/cis/region _ climat/windrose) during the year of 1991 – 2020, the annual wind rose is depicted, as shown in Figure 6.6. The number in the inner circle is the percentage frequency of occurrence of calm and variable winds. Different colors represent the wind speed with the units of km/h. Figure 6.7 shows that there are two most critical wind directions, which are W and E. The upstream exposure in the E wind direction is open sea, so that wind direction of 260° is selected to investigate the influence of upstream urban exposure on wind environment. The upstream urban exposure in this wind direction is as long as 3300 m, - see Figure 6.5. The corresponding wind tunnel test model can be found in Chapter 4. Fifty (50) locations for observation uniformly distributed in this area has been selected - see Figure 6.7. It should be noted that in this study, experiments were carried out in two wind tunnel tests of different case studies are adopted which are conducted in the wind tunnel of Building Aerodynamics Laboratory at Concordia University and XNJD-III boundary layer wind tunnel at Southwest Jiaotong University, so that there is diversity of the results yielding to a more credit conclusion.

Figure 6.5 Kowloon, Hong Kong case study with different upstream fetches.

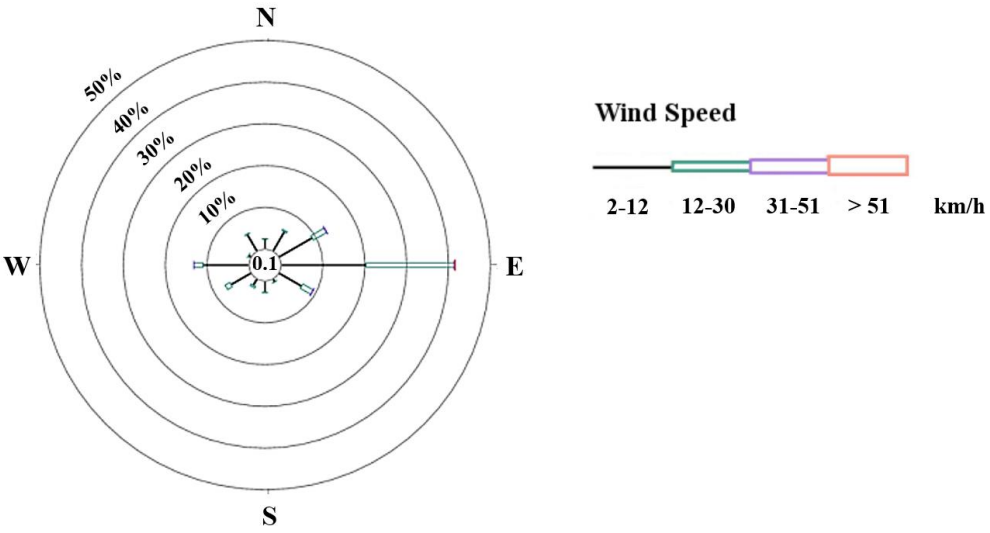

Figure 6.6 Annual wind rose of Hong Kong during 1991 – 2020.

Figure 6.7 Critical wind direction and observation points.

6.3 Influence of upstream fetch on the determination of z_0

In this section, the proposed methodology of estimation z_0 in the last chapter is applied to environmental applications to see the influence of different upstream fetch length on the determination of z_0 in both suburban and urban exposure. The results will also be compared with suggested minimum upstream fetch length in current wind load provisions, as discussed in Chapter 2. The selected upstream fetch length for the estimation of z_0 is a subject of great significance not only in environmental wind engineering applications, but also structural wind engineering applications, as it represents the influence of exposure roughness on the modification of approaching wind profile which determines the wind load on structures.

6.3.1 Case study of Westmount, Montreal

The regenerated models of Westmount, Montreal with different upstream fetch lengths are built in Agisoft Metashape by the proposed method in Chapter 5. The dense point models and the corresponding mesh files are shown in Figures 6.8 – 6.10. The red circles are the areas with the radius of upstream fetch exposure length of 100 m, 200 m and 300 m, respectively. It should be noted that when estimating the values of z_0, the buildings on the boundaries of the regenerated models are also accounted for.

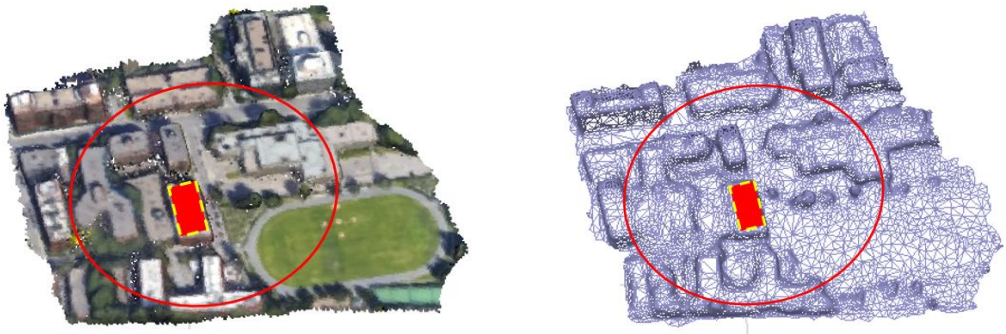

(a) Dense points model (b) Mesh model

Figure 6.8 Regenerated model of Westmount, Montreal: model with upstream fetch of 100 m.

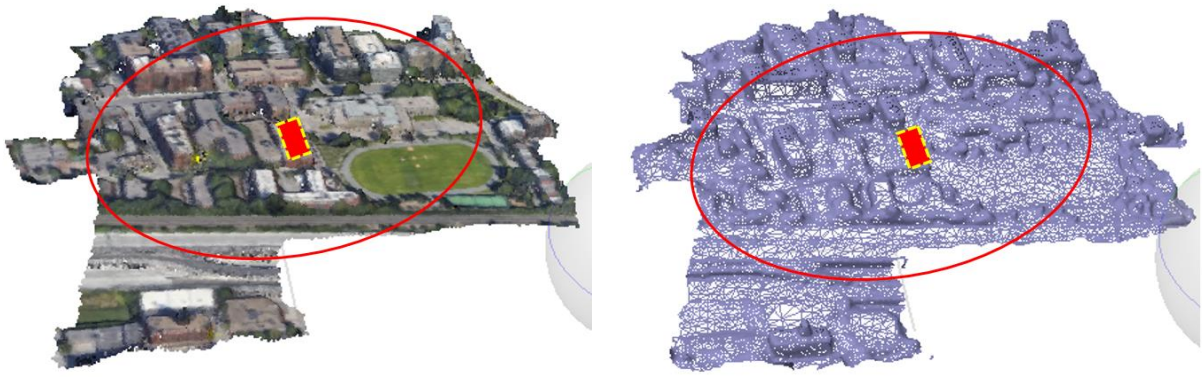

(a) Dense points model (b) Mesh model

Figure 6.9 Regenerated model of Westmount, Montreal: model with upstream fetch of 200 m.

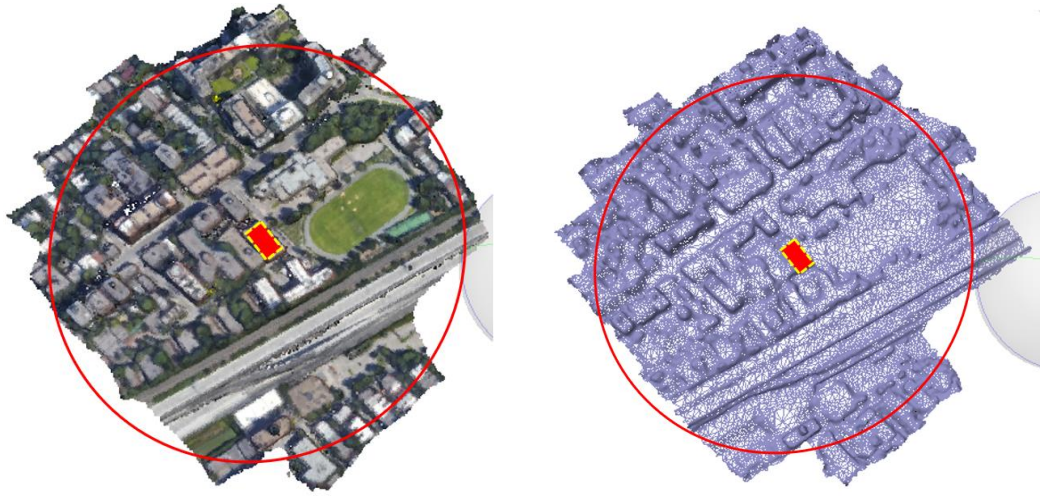

(a) Dense points model (b) Mesh model

Figure 6.10 Regenerated model of Westmount, Montreal: model with upstream fetch of 300 m.

Lettau's morphology formula is adopted with the proposed methodology to calculate the z_0 of different upstream fetch length for the six wind directions considered – see Figure 6.4. The results of different upstream fetch length, as well as the average value are shown in Table 6.1. The large values of z_0 appear for the wind directions of SW and WSW when the upstream fetch length of 100 m is considered. The estimated z_0 are 0.51 m and 0.57 m, respectively, which corresponds to the exposure type of Very Rough of the revised Davenport classification method with the suggested value of 0.5 m (Davenport et al. 2000). The estimated z_0 values reduce when a longer upstream fetch is considered, due to the decreasing of building height that far from the proposed building. Another large value of z_0 appears at the NE wind direction when the upstream fetch length of 200 m is considered, which is due to the appearance of high-rise buildings in the fetch of 100 m – 200 m upstream of the proposed building. The smallest z_0 of 0.17 m appears for the wind direction of N when the upstream fetch length of 300 m is considered, corresponding to Roughly open exposure type with the z_0 value of 0.1 m and Rough exposure type with the z_0 value of 0.25 m in the revised Davenport classification method, because the buildings are low-rise and sparsely distributed in this wind direction.

For most of the selected six wind directions, the variation tendency of the estimated z_0 value gradually becomes steady with the increasing of upstream fetch length. The deviation of the z_0 value estimated by both 200 m and 300 m upstream fetch length to the average estimated value is relatively small. Although the selected upstream fetch length should be as long as possible ideally, it will be time-consuming and expensive to consider a too large upstream fetch. The results of this case study show that for suburban exposure types, the estimated z_0 value from the 200 m upstream fetch is generally (for most critical wind directions) very near the average of the three different

cases examined. This result is close to the specification of EN 1991-1-4 (2005) that the upstream fetch length of 200 m is suggested for low-rise buildings with the height of 5 m.

Table 6.1 z_0 calculated by Lettau's formula of Westmount, Montreal (Unit: m)

Direction / Radius	N	NNE	NE	SW	WSW	W
100 m	0.27	0.46	0.28	0.51	0.57	0.42
200 m	0.21	0.43	0.52	0.27	0.5	0.48
300 m	0.17	0.3	0.34	0.23	0.37	0.37
Average	0.22	0.39	0.38	0.34	0.48	0.42

6.3.2 Case study of Kowloon, Hong Kong

The case study of Westmount, Montreal shows that the value of estimated z_0 is influenced mainly by the proximity surroundings, say about 200 m, which is much shorter than the specified minimum fetch length in current wind load provisions. In this case study, the influence of upstream fetch length on the estimation of z_0 in urban exposure is investigated in the large city center of Kowloon, Hong Kong. In the selected critical wind direction of 260°, most of the buildings are densely arranged high-rise with large height deviation. The value of z_0 with the upstream fetch length of 450 m and 3300 m are estimated. The heights of buildings are estimated through the mesh file in MATLAB. The regenerated dense points and mesh models in Agisoft Metashape are shown in Figure 6.11 and Figure 6.12.

The value of estimated z_0 with the upstream fetch of 450 m and 3300 m are 1.15 m and 1.31 m, respectively, - see Table 6.2. The estimate value corresponds well with the values specified in wind load provisions of EN 1991-1-4 (2005) and GB 50009 (2012) that the z_0 value of large city center is 1. The deviation between the estimated z_0 values from different upstream fetch length is 12%. The adopted upstream fetch lengths have significant difference, the fetch length of 450 m is smaller than most of the specified minimum upstream fetch length; in contrast, the fetch length of 3300 m is much larger than most of the specified values, while the estimated z_0 value from the two upstream fetch is close. It can be concluded that for urban areas, the minimum upstream fetch length of 450 m can yield a reasonable estimation of z_0. Both case studies of Westmount, Montreal, and Kowloon, Hong Kong indicate that the minimum upstream fetch length suggested in current wind provisions are generally larger for the estimation of z_0 in suburban/urban exposure.

Table 6.2 z_0 calculated by Lettau's formula of Kowloon, Hong Kong (Unit: m)

Radius	450 m	3300 m
z_0	1.15	1.31

(a) Dense points model

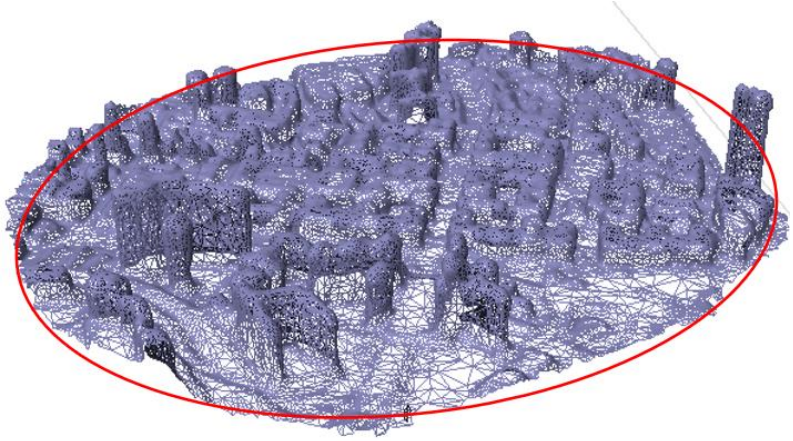

(b) Mesh model

Figure 6.11 Regenerated model of Kowloon, Hong Kong: model with upstream fetch of 450 m.

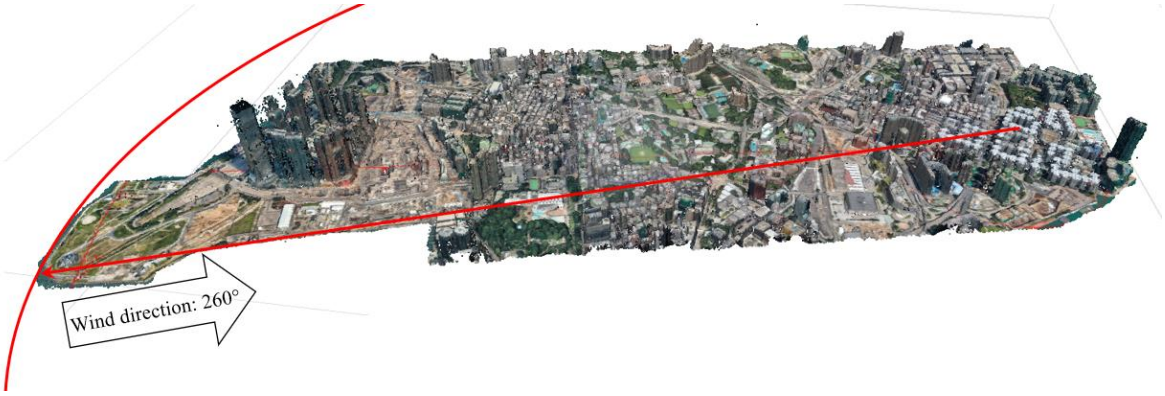

(a) Dense points model

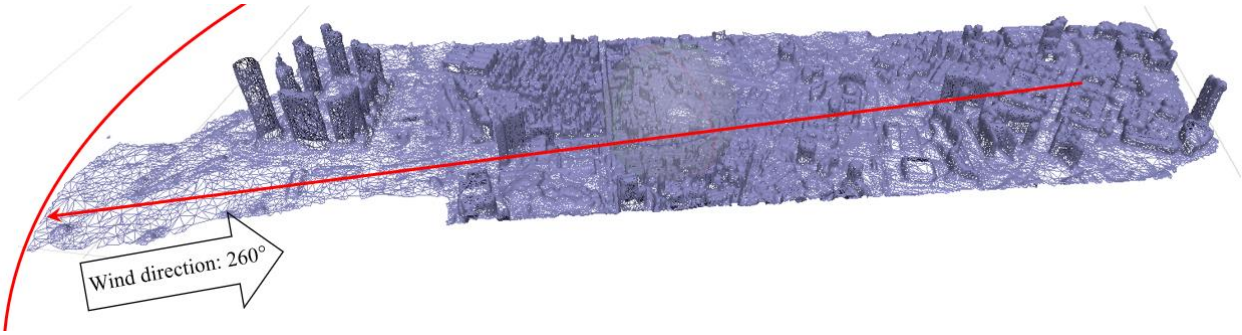

(b) Mesh model

Figure 6.12 Regenerated model of Kowloon, Hong Kong: model with upstream fetch of 3300 m.

6.4 The influence of upstream fetch on PLW environment

6.4.1 Case study of Westmount, Montreal

The application of upstream fetch on environmental wind problems of Westmount, Montreal is conducted by numerical simulation method. The influence of two different upstream fetch lengths of 100 m and 300 m on PLW velocity has been investigated. The wind directions are divided into N, NNE, and NE group and S, WSW, and SW group to illustrate the results. The PLW velocities with the two different upstream fetch lengths are compared and the influence of the proposed building on PLW comfort is investigated.

To examine the influence of different upstream fetch lengths on PLW, the velocity ratio R_i is adopted, - see Eq. 6.1. The larger the value of R_i, the stronger the increase of PLW velocity, with longer upstream fetch length.

$$R_i = V_{upstream\ fetch\ of\ 300m} / V_{upstream\ fetch\ of\ 100m} \tag{6.1}$$

where R_i is the velocity ratio at the observation point i.

In Figures 6.13 - 6.14, observation locations of each wind directions are colored by the value of R_i to illustrate the influence of different upstream fetch lengths. For the wind directions of N, NNE, and NE, $R_i < 1$ for most of the locations, means that the PLW velocity of 300 m upstream fetch length is smaller than that with the upstream fetch of 100 m. In these wind directions, most of the observation locations are sheltered by the upstream buildings from the approaching wind, and the shelter effect of the upstream fetch of 300 m is clearly larger than that of 100 m with the increasing of upstream buildings, except some increasing at the section where the wind accelerates due to the interaction of wake flow.

When the wind approaching from SW, WSW and W, the shelter effect of upstream buildings is not that much stronger as most of the selected locations are on the main and secondary street. In these

wind directions, $R_i > 1$ for lots of the observation points along the main and secondary street, there are even some red dots with $2 < R_i < 4$, means that the PLW velocity with the upstream fetch length of 300 m is much larger than that with the upstream fetch length of 100 m. This may be due to the "channeling effects" in the passage between buildings which is usually considered as high wind area. (Ishizaki and Sung, 1971, Wiren, 1975). When the wind directions is almost aligned with the main street and secondary street, the channeling effect may become stronger with the increasing of the street length as more flow is converging in the street, this is consistent with the experimental investigation results of Stathopoulos and Stroms (1984) that the most critical wind velocity conditions occur for a wind direction of 30° from the passage centre line.

Figures 6.15 – 6.16 show the differences of PLW velocity with upstream fetch of 100 m *versus* 300 m, and 200 m *versus* 300 m. The deviations between the results of the upstream fetch length of 200 m and 300 m is much smaller than that of the upstream fetch length of 100 m and 300 m, means that the variation of PLW velocity becomes steady with the increasing of fetch length. Although there are shelter and channeling effects for different wind directions, the deviation of PLW velocities of the upstream fetch length of 200 m and 300 m at most locations are within 30%.

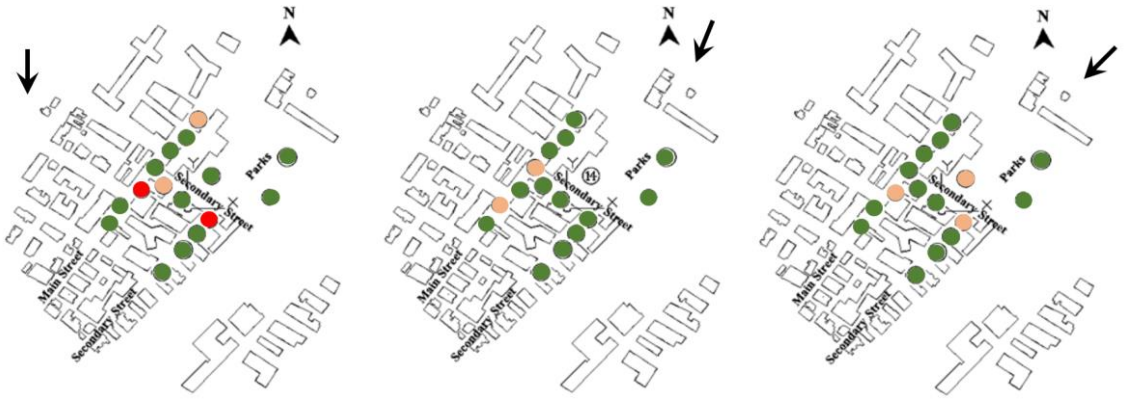

(a) N wind direction (b) NNE wind direction (c) NE wind direction

Figure 6.13 Observation locations colored by R_i in the wind directions of N, NNE and NE.

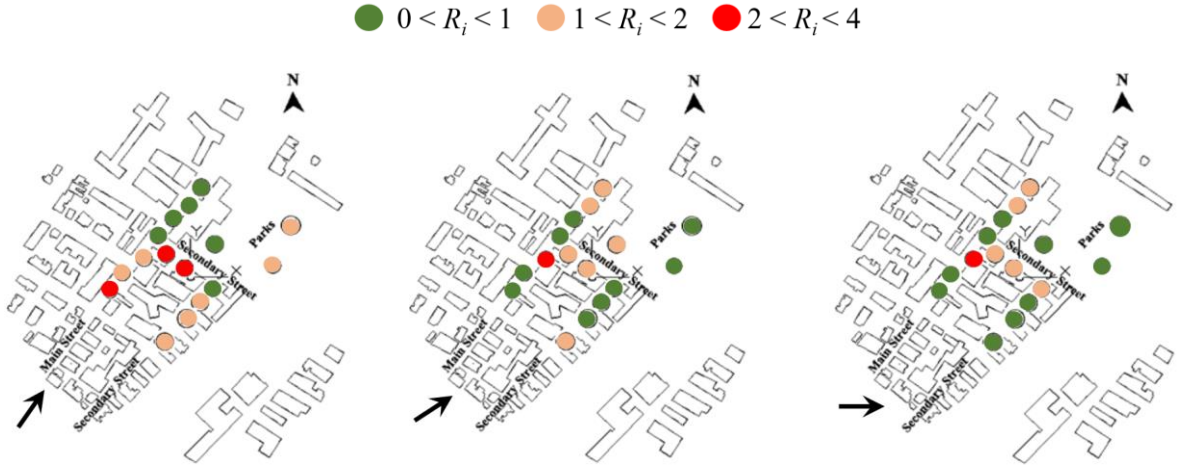

(a) SW Wind direction (b) WSW Wind direction (c) W Wind diretion

Figure 6.14 Observation locations colored by R_i in the wind directions of SW, WSW and W.

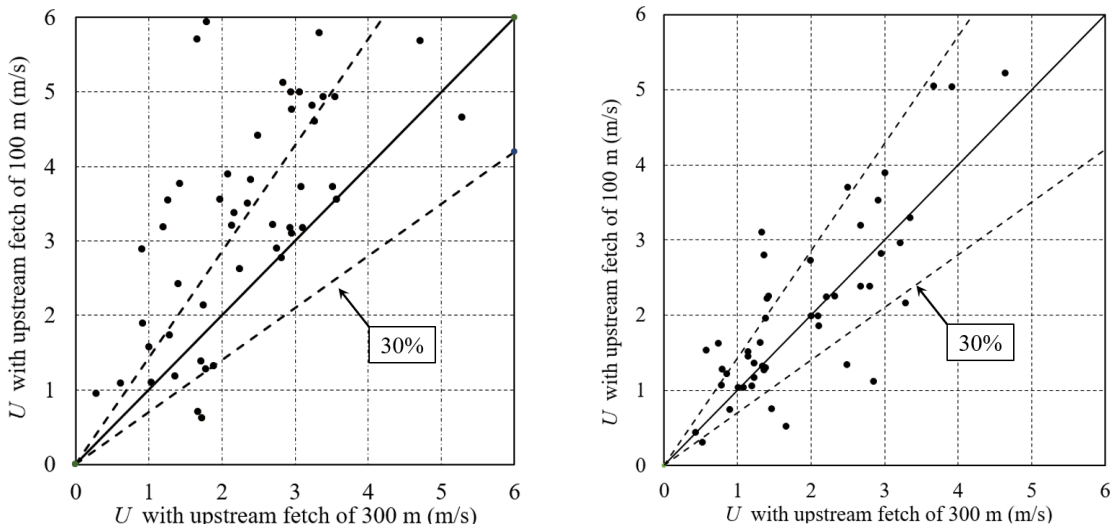

(a) Wind directions of N, NNE and NE (b) Wind directions of SW, WSW and W

Figure 6.15 Comparison of R_i with upstream fetch length of 100 m *versus* 300 m. Dashed black lines represent 30% deviations, as indicated.

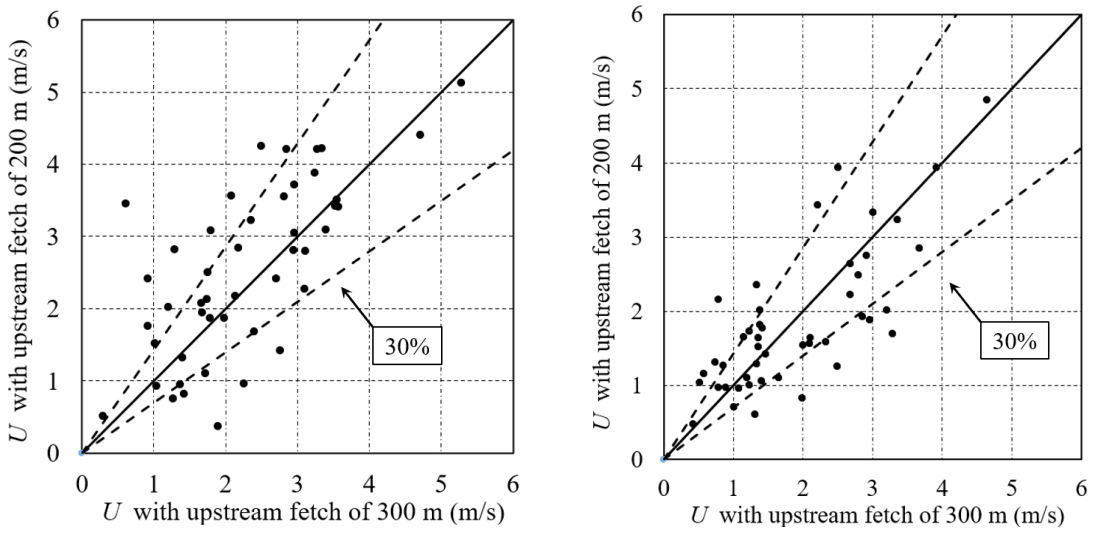

(a) Wind directions of N, NNE and NE (b) Wind directions of SW, WSW and W

Figure 6.16 Comparison of R_i with upstream fetch length of 200 m *versus* 300 m. Dashed black lines represent 30% deviations, as indicated.

In environmental wind engineering, the designers are concerned about the influence of a new proposed building on the PLW comfort. The ratio of PLW velocity with the proposed building to that without the proposed building, C_i, is adopted to represent the influence of different upstream fetch on wind comfort, - see Eq. 6.2. The deviation of value of C_i to 1 implies the extent of the influence of different upstream fetch length.

$$C_i = U_{with\ proposed\ building}/U_{without\ proposed\ building} \tag{6.2}$$

where C_i is the PLW velocity ratio at the observation point of i.

The results of C_i with the upstream fetch length of 100 m and 300 m that have a deviation larger than 30% is colored in black in Figure 6.17 – 6.18, which equals to the value of $C_i < 0.7$ and $C_i > 1.3$. These figures show that the variation of upstream fetch length from 100 m to 300 m affects the wind comfort assessment of few points near the proposed builidng with a deviation larger than 30%.

To further investigate the influence of the variation of upstream fetch length on the assessment of wind comfort, the deviations of C_i with upstream fetch length of 100 m *versus* 300 m and 200 m *versus* 300 m are shown in Figure 6.19 – 6.20. Compared with Figure 6.15 – 6.16, it can be concluded that the different upstream fetch length has less affect on the wind comfort assessment of the proposed building. Again, the deviation of C_i between the results of 200 m and 300 m upstream fetch lengths is much smaller than that between 200 m and 300 m upstream fetch lengths. The affect on the assessment of PLW comfort gradually becomes stable with the increasing of upstream fetch length.

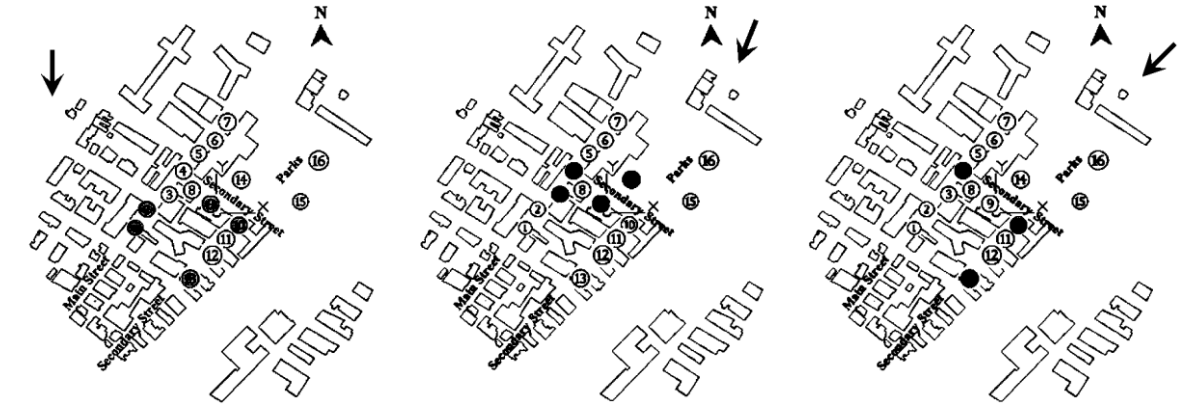

(a) N wind direction (b) NNE wind direction (c) NE wind direction

Figure 6.17 Observation locations colored by $C_i < 0.7$ and $C_i > 1.3$ in the wind directions of N, NNE and NE.

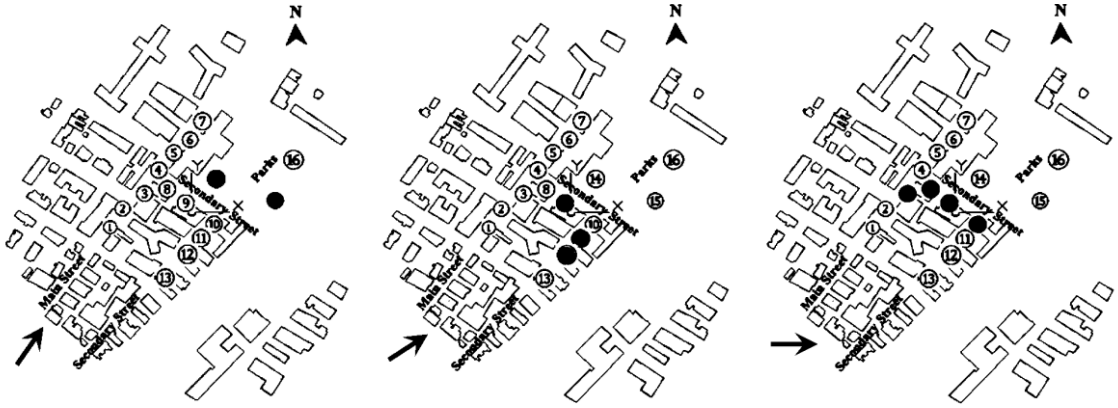

(a) SW Wind direction (b) WSW Wind direction (c) W Wind diretion

Figure 6.18 Observation locations colored by $C_i < 0.7$ and $C_i > 1.3$ in the wind directions of SW, WSW and W.

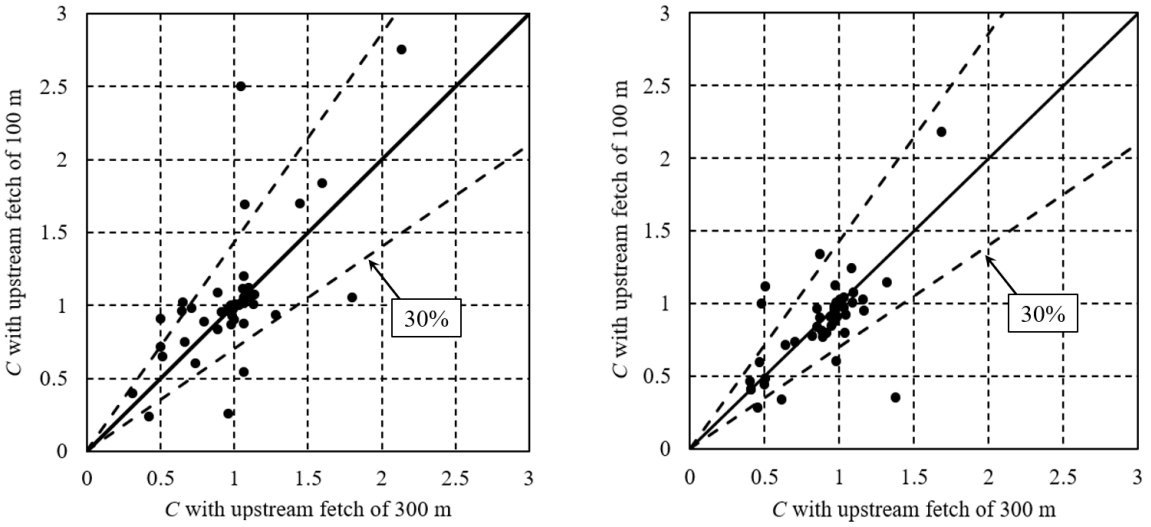

(a) Wind directions of N, NNE and NE (b) Wind directions of SW, WSW and W

Figure 6.19 Comparison of C_i with upstream fetch length of 100 m versus 300 m. Case study of Westmount, Montreal. Dashed black lines represent 30% deviations, as indicated.

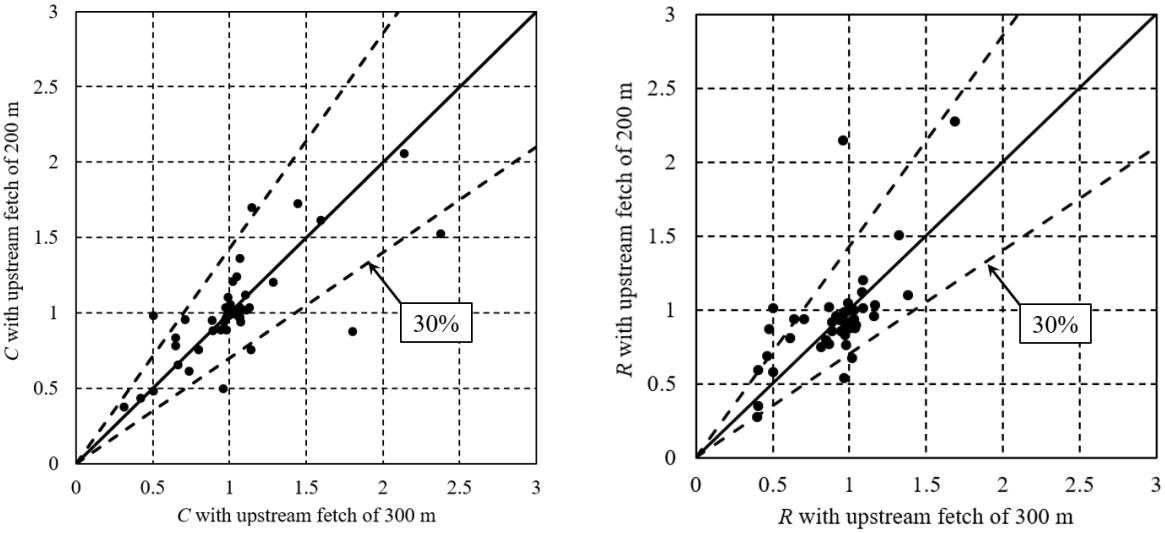

(a) Wind directions of N, NNE and NE (b) Wind directions of SW, WSW and W

Figure 6.20 Comparison of C_i with upstream fetch length of 200 m versus 300 m. Case study of Westmount, Montreal. Dashed black lines represent 30% deviations, as indicated.

6.4.2 Case study of Kowloon, Hong Kong

The objective of the case study of Hong Kong is to assess the wind environment of existing urban areas. Only the velocity ratio *R* of different upstream fetch length has been studied. This case study has been carried out experimentally in the XNJD-III wind tunnel of Southwest Jiaotong University, Chengdu, China. The PLW velocity is measured at the height of 4 mm corresponding to 3.2 m in full scale. The selected area is a typical exposure type of urban environment. Two upstream fetch length of 450 m and 3300 m were adopted. The velocity ratio R_i of the PLW velocity of the two upstream fetch lengths is used for investigation - see Eq. 6.3.

$$R_i = V_{upstream\ fetch\ of\ 3300m} / V_{upstream\ fetch\ of\ 450m} \tag{6.3}$$

Figure 6.21 is the observation locations colored by the value of R_i. The figure illustrates that when the upstream fetch length increasing from 450 m to 3300 m, the PLW velocity for most of the observation locations on the street along the wind directions increase slightly, while some of the observation locations on the street perpendicular to the wind directions decrease slightly. The increasing of the PLW velocity may be due to the channeling effects of the upstream buildings which is explained in the case study of Westmount, Montreal, and the decreasing may be due to some sheltering effects.

The comparison of PLW velocities of different upstream fetch length is illustrated in Figure 6.22. It should be noted that although the PLW velocity is influenced by different upstream fetch length, the deviations of most observation locations are within 30%, which means that the assessment of wind environment in urban exposure with the consideration of the upstream fetch of 450 m is reliable.

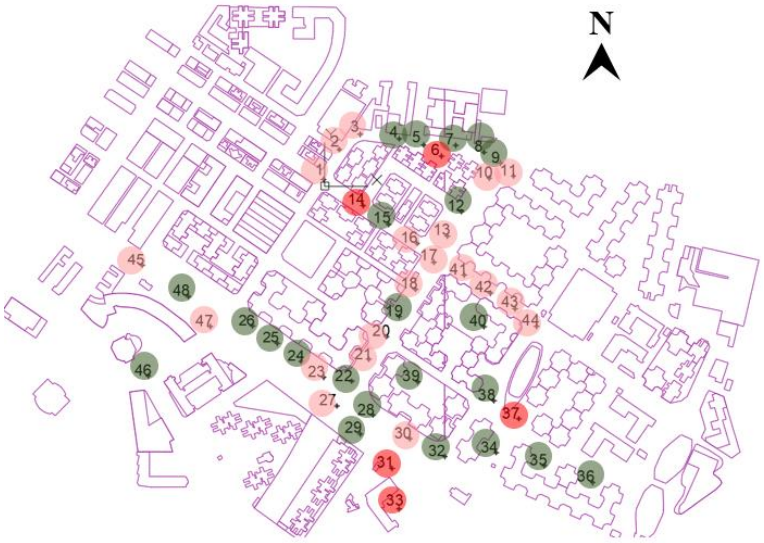

Figure 6.21 Observation locations colored by PLW velocity ratio.

$0 < R_i < 1$ $1 < R_i < 2$ $2 < R_i < 4$

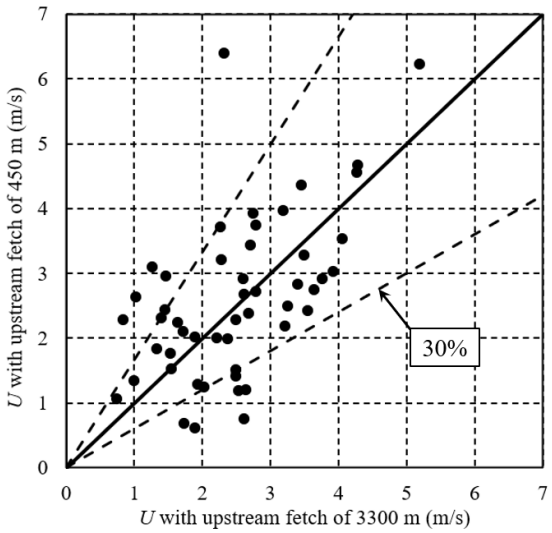

Figure 6.22 Comparison of PLW velocity with different upstream fetch length: Case study of Kowloon, Hong Kong. Dashed black lines represent 30% deviations, as indicated.

6.5 Summary and conclusions

The minimum upstream fetch length specified in current wind load provisions is based on previous research and has been always focused on the wind load on buildings. This chapter examines the influence of this parameter on environmental wind engineering problems. If the considered upstream fetch length is not large enough, the assessment of the wind environment may not be accurate. In contrast, if the considered upstream fetch length is too large, the computational efficiency will be reduced.

Two very different case studies of Westmount, Montreal and Kowloon, Hong Kong have been adopted, with the upstream fetch of 100 m, 200 m and 300 m and 450 m versus 3300 m, respectively. Firstly, the influence of upstream fetch of the determination of z_0 is examined by the method proposed in Chapter 5. Secondly, the numerical method is adopted for the Westmount case and experimental method is adopted for the Kowloon case respectively to investigate the influence of upstream fetch on the PLW.

It can be concluded from the simulated results that the PLW velocity is more sensitive to upstream fetch length than the assessment of wind comfort around proposed buildings. Except the relatively large deviation of the estimated z_0 and PLW velocity of the case study of Westmount, Montreal with the upstream fetch of 100 m and 200 m, the deviations of those values of Westmount, Montreal with the upstream fetch of 200 m and 300 m and of Kowloon, Hong Kong with the upstream fetch of 450 m and 3300 m are within 30% for most observation locations. The results show that the specifications of minimum upstream fetch in current wind load provisions are too large for suburban/urban exposure.

Chapter 7 Conclusions, Contributions, and Future Work

7.1 General

The assessment of exposure is a subject of great significant in wind engineering. The upstream exposure has an impact on the characteristic of approaching wind, thus influences the wind environment at the area of interest, as well as the wind load on buildings. Compared with the large amounts of investigations of wind loads on structures, the contributions of the exposure study to the development of wind engineering is significant in many aspects.

In practical engineering, the influence of exposure is usually determined according to the specifications in current wind load provisions of various countries. However, there are discrepancies and inconsistencies among various provisions leading to different results. Moreover, the solution of complex exposure coefficient in current wind load provisions is not adequate. Other methodologies to determine exposure coefficients is field measurement, wind tunnel test, and numerical simulation. Most of these methods are expensive, time consuming and not always feasible. A reasonable selection of upstream fetch length for the assessment of exposure will increase the accuracy and efficiency of wind engineering applications.

This thesis focuses on the investigations of upstream exposure roughness through both experimental and numerical methodologies. Firstly, the specifications of exposure factors in current wind provisions of ASCE 7 (2022), NBCC (2020), AS/NZS 1170.2 (2021), EN 1991-1-4 (2005), and GB 50009 (2012) are discussed in terms of homogeneous and non-homogeneous exposures. The discrepancies and inconsistencies are discussed. Secondly, previous investigations related to the estimation method of upstream exposure, as well as the influence of upstream exposure are reviewed. After that, a novelty method of estimating z_0 based on the GIS software of

Google Earth Pro was proposed and proven efficient, in addition to being freely available. Finally, the effects of upstream exposure on environmental wind engineering problems are investigated in terms of estimating of z_0 and PLW velocity. An upstream fetch length of 100 m, 200 m and 300 m for Westmount, Montreal, and that of 450 m and 3300 m for Kowloon, Hong Kong are adopted as case studies

7.2 Concluding remarks

This investigation intended to contribute to the exposure assessment for the evaluation of exposure parameters in wind engineering. The major conclusions of the study can be organized as follows:

1. For homogeneous exposure in various wind load provisions, the upstream roughness is generally divided in 3-5 categories, namely Flat or Sea, Open, Urban/Suburban, and Large City Center. However, there are discrepancies and inconsistencies of the specified roughness length, z_0 value, across different provisions, as well as compared with the revised Davenport's classification method. The morphometric formulas of Lettau (1969) are suggested by ASCE 7 (2022) for the exposure with easy acquisition of the upstream layout and dimensions yielding a reasonable result.

2. For the minimum upstream fetch, the specifications of 1524 m for Flat exposure type and 792 m for Urban/Suburban exposure type in the provision of ASCE 7 (2022) and the specification of 1000 m for all exposure types in NBCC (2020) and AS/NZS 1170.2 (2021) is close to the findings of field measurement studies that the upstream fetch of 1000 m - 1500 m should be considered for Flat Terrain, as well as those of the wind tunnel test that 750 m -1000 m should be considered in Urban/Suburban cases. In contrast, the specifications of 20,000 m of high-rise buildings in EN 1991-1-4 (2005) is too large.

3. For non-homogeneous exposure, the formulas suggested in wind load provisions account for small-scale roughness change and have been assessed by comparing with existing wind tunnel test

results of a low-rise building. ASCE 7 (2022), NBCC (2020) and AS/NZS 1170.2 (2021) all fit well with the experimental results, with an average deviation of 4.5%, 8% and 15% respectively. AS/NZS 1170.2 (2021) over-estimates o-r case because the influence of upstream terrain is considered equally, while only the exposure 300 m - 400 m directly upstream has an impact on the wind load of low-rise building. EN 1991-1-4 (2012) always over-estimates wind loads because the lowest roughness length is adopted to calculate exposure factor. This is in general conservative.

4. An innovative approach to estimate z_0 in an efficient and inexpensive way was proposed, which is based on the morphometric formulas of Lettau and Kanda with the assistance of Google Earth Pro. The comparison with available case studies of London, UK and Tampa International Airport, US shows that the proposed method can make a reasonable estimation of z_0 for both Urban/Suburban and Flat exposure types.

5. The effect of different upstream fetch length on the estimation of z_0 is investigated by both numerical and experimental methodologies. The results show that in suburban area, the fetch length of 200 m can yield relatively reasonable results, and this is consistent with the specification of EN 1991-1-4 (2005) that the upstream fetch length of 200 m is appropriate for low-rise buildings with the height of 5 m. In the exposure of large city center, the adoption of the upstream fetch length of 450 m leads to a z_0 estimation deviation of 12% compared with the adopted upstream fetch of 3300 m.

6. For the PLW velocity of suburban exposure, the deviation of PLW velocities of the upstream fetch length of 200 m and 300 m at most locations are within 30%. In large city center, the upstream fetch length of 450 m can be adopted, which results in a deviation within 30% compared with the upstream fetch of 3300 m for most of the locations. For the wind comfort assessment of the proposed buildings, the locations with large deviations are those close to the proposed building.

7.3 Contributions

Contributions of the present study are summarized as follows:

1. The specifications of exposure roughness in current wind load provisions are discussed and compared with previous research results in terms of homogeneous and non-homogeneous exposure. Inconsistencies and discrepancies are illustrated. The conclusions can promote the future compilation of wind load provisions.

2. An innovative approach, which is efficient and freely available, to estimate the value of z_0 based on Google Earth Pro is proposed. This approach could be applied to almost anywhere in the world with adequate high-resolution imagery available on Google Earth Pro. The low cost of this method is particularly attractive for many developing countries where other sources of long-term wind speed observation data and aerial photography are unavailable. Besides, it has great potential on broader application concerning wind engineering and city environment.

3. The effect of upstream exposure on environmental wind engineering problems has been investigated. Appropriate fetch lengths for the estimation of z_0, PLW velocity, as well as the wind comfort assessment have been suggested for suburban/urban exposure. The results will promote the application of upstream exposure in the field of environmental wind engineering.

7.4 Recommendations for future work

Possible extensions and potential improvements of the present research investigations are:

1. Full-scale field measurement in urban exposure should be conducted in the future to further validate the proposed models and investigate the influence of upstream exposure on both approaching wind characteristics and wind environment.

2. The formulas for small-scale roughness change in wind load provisions are only assessed by the wind load on the roof of existing low-rise buildings. The accuracy on mid-rise and high-rise buildings should also be assessed.
3. The present study has only investigated the influence of the upstream fetch length of 100 m, 200 m, 300 m, 450 m, and 3300 m on suburban/urban wind environment. More upstream fetch lengths should be considered. In addition, the influence of different upstream exposure on wind environment on flat/open exposure should be studied.
4. The influence of upstream mountainous terrain on the characteristics of approaching wind profile and the wind environment is also a subject worth researching.
5. The results of the present investigations can be adopted for future compilation of exposure-related wind load provisions.

References

1. Abu-Zidan Y, Mendis P, Gunawardena T. (2020) Impact of atmospheric boundary layer inhomogeneity in CFD simulations of tall buildings. *Heliyon*; 6(7): e04274.
2. Adamek K, Vasan N, Elshaer A, et al. (2017) Pedestrian level wind assessment through city development: A study of the financial district in Toronto. *Sustainable Cities and Society*; 35: 178-190.
3. AIJ-RLB. (2004) Recommendations for loads on buildings. *Architectural Institute of Japan*; Tokyo, Japan.
4. Ai Z T, Mak C M. (2016) Large eddy simulation of wind-induced interunit dispersion around multistory buildings. *Indoor Air*; 26(2): 259-273.
5. Ai Z T, Mak C M. (2014) Modeling of coupled urban wind flow and indoor air flow on a high-density near-wall mesh: Sensitivity analyses and case study for single-sided ventilation. *Environmental Modelling & Software*; 60: 57-68.
6. ASCE. (2012). Wind tunnel testing for buildings and other structures. ASCE 49-12. Reston, VA: ASCE.
7. ASCE/SEI 7-16 (2022). Minimum Design Loads for Buildings and Other Structures. Structural Engineering Institute of ASCE, Reston, VA.
8. AS/NZS 1170.2 (2021) Australian/New Zealand Standard for Structural Design Actions, part 2: Wind Actions. Sydney, New South Wales, Australia: Standards Australia and Standards New Zealand.
9. Antonia R A, Luxton R E. (1971) The response of a turbulent boundary layer to a step change in surface roughness Part 1. Smooth to rough. *Journal of Fluid Mechanics*; 48(4): 721-761.
10. Antonia R A, Luxton R E. (1972) The response of a turbulent boundary layer to a step change in surface roughness. Part 2. Rough-to-smooth. *Journal of Fluid Mechanics*; 53(4): 737-757.
11. Allegrini J., Lopez B. (2016) The influence of angular configuration of two buildings on the local wind climate. *Journal of Wind Engineering and Industrial Aerodynamics*; 156: 50-61.
12. Allegrini J, Kubilay A. (2017) Wind sheltering effect of a small railway station shelter and its impact on wind comfort for passengers. *Journal of Wind Engineering and Industrial Aerodynamics*; 164: 82-95.
13. Asfour O. S. (2010) Prediction of wind environment in different grouping patterns of housing blocks. *Energy and Buildings*; 42(11): 2061-2069.

14. Barthelmie, R. J., Palutikof, J. P., Davies, T. D. (1993). Estimation of sector roughness lengths and the effect on prediction of the vertical wind speed profile. *Boundary-Layer Meteorology*; 66(1-2), 19-47.
15. Blocken B, Carmeliet J. (2004) Pedestrian wind environment around buildings: Literature review and practical examples. *Journal of Thermal Envelope and Building Science*; 28(2): 107-159.
16. Blocken B, Stathopoulos T, Carmeliet J. (2007) CFD simulation of the atmospheric boundary layer: wall function problems. *Atmospheric Environment*; 41(2): 238-252.
17. Blocken B., Stathopoulos T., Carmeliet J. (2008) Wind environmental conditions in passages between two long narrow perpendicular buildings. *Journal of Aerospace Engineering*; 21(4): 280-287.
18. Blocken B, Persoon J. (2009) Pedestrian wind comfort around a large football stadium in an urban environment: CFD simulation, validation and application of the new Dutch wind nuisance standard. *Journal of Wind Engineering and Industrial Aerodynamics*; 97(5-6): 255-270.
19. Blocken B, Gualtieri C. (2012) Ten iterative steps for model development and evaluation applied to Computational Fluid Dynamics for Environmental Fluid Mechanics. *Environmental Modelling & Software*; 33:1-22.
20. Blocken B. (2014) 50 years of computational wind engineering: past, present and future. *Journal of Wind Engineering and Industrial Aerodynamics*; 129: 69-102.
21. Blocken B, Stathopoulos T, Van Beeck J. (2016) Pedestrian-level wind conditions around buildings: Review of wind-tunnel and CFD techniques and their accuracy for wind comfort assessment. *Building and Environment*; 100: 50-81.
22. Blocken B. (2018) LES over RANS in building simulation for outdoor and indoor applications: A foregone conclusion? *Building Simulation*; 11(5): 821-870.
23. Bradbury L.J.S., I.P. Castro I.P. (1971) A pulsed wire technique for velocity measurements in highly turbulent flows. *Journal of Fluid Mechanics*; 49:657.
24. Britter R.E., Hunt J.C.R. (1979) Velocity measurements and order of magnitude estimates of the flow between two buildings in a simulated atmospheric boundary layer, *Journal of Wind Engineering and Industrial Aerodynamics*; 4 (2): 165-182.
25. Britter R E, Hanna S R. (2003) Flow and dispersion in urban areas. *Annual Review of Fluid Mechanics*; 35(1): 469-496.
26. Brozovsky J, Simonsen A, Gaitani N. (2021)Validation of a CFD model for the evaluation of urban microclimate at high latitudes: A case study in Trondheim, Norway. *Building and Environment*; 205: 108175.

27. Bottema, M., 1995. Aerodynamic roughness parameters for homogeneous building groups-part 2: Results. Document SUB-MESO# 23. *Ecole Centrale de Nantes, France*; *80*.
28. Bottema M. (1997) Urban roughness modelling in relation to pollutant dispersion. *Atmospheric Environment*; 31(18): 3059-3075.
29. Bottema M. (2000) A method for optimisation of wind discomfort criteria. *Building and Environment*; 35(1): 1-18.
30. Buccolieri R, Santiago J L, Martilli A. (2021) CFD modelling: The most useful tool for developing mesoscale urban canopy parameterizations. *Building Simulation;* 14(3): 407-419.
31. Carpentieri M., Robins A. G., Baldi S. (2009) Three-dimensional mapping of air flow at an urban canyon intersection. *Boundary-layer Meteorology*; 133(2): 277-296.
32. Castro I.P. (1992) Pulsed-wire anemometry. *Experimental Thermal and Fluid Science*; 5: 770-780.
33. Cook, N. J. (1986). Designers guide to wind loading of building structures. Part 1.
34. Counehan, J. (1971) Wind tunnel determination of the roughness length as a function of the fetch and the roughness density of three-dimensional roughness elements. *Atmospheric Environment*; 5 (8): 637–642.
35. Choi D S, Showman A P, Brown R H. (2009) Cloud features and zonal wind measurements of Saturn's atmosphere as observed by Cassini/VIMS. *Journal of Geophysical Research: Planets*; 114 (4).
36. Darmanto, N. S., A. C. Varquez, and M. Kanda. (2017) Urban roughness parameters estimation from globally available datasets for mesoscale modeling in megacities. *Urban Clim*ate; 21 (9): 243–261.
37. Davenport, A. (1960). Rationale for determining design wind velocities. *Journal of the Structure Division-ASCE.* 86 (1960): 39-68.
38. Davenport, A., Grimmond, S., Oke, T., Wieringa, J. (2000). The revised Davenport roughness classification for cities and sheltered country. The *3rd Symposium on the Urban Environment*, Am Meteorological Soc, Davis, CA: August 14.
39. Deaves, D. M. . (1981). Computations of wind flow over changes in surface roughness. *Journal of Wind Engineering and Industrial Aerodynamics;* 7(1): 65-94.
40. Di Sabatino, S., L. S. Leo, R. Cataldo, C. Ratti, and R. E. Britter. (2010) Construction of digital elevation models for a southern European city and a comparative morphological analysis with respect to northern European and North American cities. *Journal of Applied Meteorology and Climatology*; 49 (7): 1377–1396.

41. Di Sabatino, S., E. Solazzo, P. Paradisi, and R. Britter. (2008) A simple model for spatially averaged wind profiles within and above an urban canopy. *Boundary-Layer Meteorology*; 127 (1): 131–151.
42. Di Sabatino S, Leo L S, Cataldo R, et al. (2010) Construction of digital elevation models for a southern European city and a comparative morphological analysis with respect to Northern European and North American cities. *Journal of Applied Meteorology and Climatology*; 49(7): 1377-1396.
43. Dobre, A., Arnold, S. J., Smalley, R. J., Boddy, J. W. D., Barlow, J. F., Tomlin, A. S., & Belcher, S. E. (2005). Flow field measurements in the proximity of an urban intersection in London, UK. *Atmospheric Environment*; 39(26): 4647-4657.
44. Du Y, Mak C M, Liu J, et al. (2017) Effects of lift-up design on pedestrian level wind comfort in different building configurations under three wind directions. *Building and Environment*; 117: 84-99.
45. Du Y, Mak C M, Kwok K, et al. (2017) New criteria for assessing low wind environment at pedestrian level in Hong Kong. *Building and Environment*; 123: 23-36.
46. Du Y, Mak C M. (2018) Improving pedestrian level low wind velocity environment in high-density cities: A general framework and case study. *Sustainable Cities and Society*; 42: 314-324.
47. EN 1991-1-4 (European Standard). Eurocode 1. (2005). Actions on structures-Part 1-4: General actions –Wind actions, European Standard, B-100 Brussels, Belgium.
48. Engineering Sciences Data Unit International ESDU. (1993). Strong winds in the atmospheric boundary layer. Part 2: Discrete gust speeds, Item 83045, Issued November 1983 with Amendments A and B. ESDU International, London, U.K.
49. Franke J, Hirsch C, Jensen A G, et al. (2004) Recommendations on the use of CFD in predicting pedestrian wind environment. *Cost action C*; 14.
50. Franke J, Hellsten A, Schlunzen H A, et al. (2010) The Best Practise Guideline for the CFD simulation of flows in the urban environment: an outcome of COST 732. *The Fifth International Symposium on Computational Wind Engineering;* 1-10.
51. Freidooni F, Sohankar A, Rastan M R, et al. (2021) Flow field around two tandem non-identical-height square buildings via LES. *Building and Environment*; 201: 107985.
52. Garratt, J. (1992). The Atmospheric Boundary Layer. Cambridge Atmospheric and Space Science Series. Cambridge University Press, Cambridge; 444.
53. García-Sánchez C, van Beeck J, Gorlé C. (2018) Predictive large eddy simulations for urban flows: Challenges and opportunities. *Building and Environment*; 139: 146-156.

54. Gandemer J. Wind environment around buildings; Aerodynamics concepts, (1975) The 4th Int Conf. on Wind Effects on Buildings and Structures, London.
55. GB 50009 (National Standard of the People's Republic of China). (2012). Load code for the design of building structures, part 2: Wind Actions. Revision group of national standard code for building load. China, Beijing.
56. Grimmond C S B, King T S, Roth M, et al. (1998) Aerodynamic roughness of urban areas derived from wind observations. *Boundary-Layer Meteorology*; 89(1): 1-24.
57. Grimmond, C. S. B., & Oke, T. R. (1999). Aerodynamic properties of urban areas derived from analysis of surface form. *Journal of Applied Meteorology and Climatology*; 38(9), 1262-1292.
58. Grimmond C S B, Oke T R. (1995) Comparison of heat fluxes from summertime observations in the suburbs of four North American cities. *Journal of Applied Meteorology and Climatology*; 34(4): 873-889.
59. Godłowska, J., and W. Kaszowski. (2019) Testing various morphometric methods for determining the vertical profile of wind speed above Krakow, Poland. *Boundary-Layer Meteorology*; 172 (1): 107–132.
60. Gu Z. L., Zhang Y. W., Cheng Y., et al. (2011) Effect of uneven building layout on air flow and pollutant dispersion in non-uniform street canyons. *Building and Environment*; 46(12): 2657-2665.
61. Hanna S R, Chang J C. (1992) Boundary-layer parameterizations for applied dispersion modeling over urban areas. *Boundary-Layer Meteorology*; 58(3): 229-259.
62. Hang J., Li Y., Buccolieri R., et al. (2012) On the contribution of mean flow and turbulence to city breathability: the case of long streets with tall buildings. *Science of the Total Environment*; 416: 362-373.
63. Hang J, Li Y. (2010) Ventilation strategy and air change rates in idealized high-rise compact urban areas. *Building and Environment*; 45(12): 2754-2767.
64. Harris R I, Deaves D M. (1980) The structure of strong winds. *Proceedings of the CIRIA Conference*, London, 12-13.
65. He, Y. C., P. W. Chan, and Q. S. Li. (2017) Estimation of roughness length at Hong Kong International Airport via different micrometeorological methods. *Journal of Wind Engineering and Industrial Aerodynamics*; 171 (12): 121–136.
66. He L., Hang J., Wang X., et al. (2017) Numerical investigations of flow and passive pollutant exposure in high-rise deep street canyons with various street aspect ratios and viaduct settings. *Science of the Total Environment*; 584: 189-206.

67. He Y., Tablada A., Wong N. H. (2018) Effects of non-uniform and orthogonal breezeway networks on pedestrian ventilation in Singapore's high-density urban environments. *Urban Climate*; 24: 460-484.
68. He B. J., Ding L., Prasad D. (2019) Enhancing urban ventilation performance through the development of precinct ventilation zones: A case study based on the Greater Sydney, Australia. *Sustainable Cities and Society*; 47: 101472.
69. HKBD (Hong Kong Buildings Department). (2004) Code of practice on wind effects in Hong Kong.
70. Hsieh C M, Jan F C, Zhang L. (2016) A simplified assessment of how tree allocation, wind environment, and shading affect human comfort. *Urban Forestry & Urban Greening*; 18: 126-137.
71. Huang T. L., Kuo C. Y., Tzeng C. T., et al. (2020) The influence of high-rise buildings on pedestrian-level wind in surrounding street canyons in an urban renewal project. *Energies*; 13(11): 2745.
72. Hunt J C R, Poulton E C, Mumford J C. (1976) The effects of wind on people; new criteria based on wind tunnel experiments. *Building and Environment*; 11(1): 15-28.
73. Hussain M, Lee B E. (1980) A wind tunnel study of the mean pressure forces acting on large groups of low-rise buildings. *Journal of Wind Engineering and Industrial Aerodynamics*; 6(3-4): 207-225.
74. Irwin H.P.A.H., (1981) A simple omnidirectional sensor for wind-tunnel studies of pedestrian-level winds, *Journal of Wind Engineering and Industrial Aerodynamics*; 7(3): 219-239
75. Irwin, P. A. (2006). Exposure categories and transitions for design wind loads. *Journal of Structural Engineering*; *132*(11), 1755-1763.
76. Iqbal Q .M. Z., Chan A. L. S. (2016) Pedestrian level wind environment assessment around group of high-rise cross-shaped buildings: Effect of building shape, separation and orientation. *Building and Environment*; 101: 45-63.
77. Ishizaki H. and Sung I.W. (1971) Influence of adjacent buildings to wind. Proceeding 3rd International Conference on Wind Effects on Buildings and Structures, Tokyo, Japan. 1(15):1-8.
78. Isyumov N., Davenport A.G., (1975) Comparison of full-scale and wind tunnel wind speed measurements in the commerce court plaza. *Journal of Wind Engineering and Industrial Aerodynamics*; 1:201-212.
79. Isyumov, N. (Editor) (1999). Wind Tunnel Studies of Buildings and Structures. ASCE Manuals and Reports on Engineering Practice No. 67, Aerodynamics Committee.
80. Jacob J, Sagaut P. (2018) Wind comfort assessment by means of large eddy simulation with lattice Boltzmann method in full scale city area. *Building and Environment*; 139: 110-124.

81. Jakeman A J, Letcher R A, Norton J P. (2006) Ten iterative steps in development and evaluation of environmental models. *Environmental Modelling & Software*; 21(5): 602-614.
82. Jamieson N.J., Carpenter P., Cenek P.D. (1992) The effect of architectural detailing on pedestrian level wind speeds. *Journal of Wind Engineering and Industrial Aerodynamics*; 44 (13) 2301-2312.
83. Janssen W, Blocken B, van Hooff T, et al. (2013) Use of CFD simulations to improve the pedestrian wind comfort around a high-rise building in a complex urban area. *13th Conference of International Building Performance Simulation Association*. August 16.
84. Jegede, O. O., & Foken, T.. (1999). A study of the internal boundary layer due to a roughness change in neutral conditions observed during the linex field campaigns. *Theoretical & Applied Climatology*; 62(1-2), 31-41.
85. Jiang D., Jiang W., Liu H., et al. (2008) Systematic influence of different building spacing, height and layout on mean wind and turbulent characteristics within and over urban building arrays. *Wind and Structures*; 11(4): 275-290.
86. Jones W P, Launder B E. (1972) The prediction of laminarization with a two-equation model of turbulence. *International Journal of Heat and Mass Transfer*; 15(2): 301-314.
87. Kanda, M., A. Inagaki, T. Miyamoto, M. Gryschka, and S. Raasch. (2013). A new aerodynamic parametrization for real urban surfaces. *Boundary-Layer Meteorology;* 148 (2): 357–377
88. Kang G, Kim J J, Kim D J, et al. (2017) Development of a computational fluid dynamics model with tree drag parameterizations: Application to pedestrian wind comfort in an urban area. *Building and Environment*; 124: 209-218.
89. Kang G, Kim J J, Choi W. (2020) Computational fluid dynamics simulation of tree effects on pedestrian wind comfort in an urban area. *Sustainable Cities and Society*; 56: 102086.
90. Kataoka H, Ono Y, Enoki K. (2020) Applications and prospects of CFD for wind engineering fields. *Journal of Wind Engineering and Industrial Aerodynamics*; 205: 104310.
91. Ketterer, C., M. Gangwisch, D. Fröhlich, and A. Matzarakis. (2017) Comparison of selected approaches for urban roughness determination based on voronoi cells. *International Journal of Biometeorology*; 61 (1): 189–198.
92. Kent, C.W., C. S. B. Grimmond, D. Gatey, and J. F. Barlow. (2018) Assessing methods to extrapolate the vertical wind-speed profile from surface observations in a city center during strong winds. *Journal of Wind Engineering and Industrial Aerodynamics*; 173 (2): 100–111.
93. Kent, C. W., S. Grimmond, J. Barlow, D. Gatey, S. Kotthaus, F. Lindberg, and C. H. Halios. (2017). Evaluation of urban local-scale aerodynamic parameters: implications for the vertical profile of wind speed and for source areas. *Boundary-Layer Meteorology*; 164 (2): 183–213.

94. Kiefer, H., & Plate, E. J. (1998). Modelling of mean and fluctuating wind loads in built-up areas. *Journal of Wind Engineering and Industrial Aerodynamics;* 74: 619-629.
95. Kim Y.C., Yoshida A., Tamura Y. (2012). Characteristics of surface wind pressures on low-rise building located among large group of surrounding buildings. *Engineering Structures*; 35(1): 18-28.
96. Kim Y.C., Tamura Y., Yoon S.W. (2015). Proximity effect on low-rise building surrounded by similar-sized buildings. *Journal of Wind Engineering and Industrial Aerodynamics*. 146(2015):150-162.
97. King T, Grimmond C S B. (1997) Transfer mechanisms over an urban surface for water vapor, sensible heat, and momentum. *Preprints, 12th Symp. on Boundary Layers and Turbulence*, Vancouver, BC, Canada, Amer. Meteor. Soc., 455-456.
98. Kondo J, Yamazawa H. (1986) Aerodynamic roughness over an inhomogeneous ground surface. *Boundary-Layer Meteorology*; 35(4): 331-348.
99. Korobeynikova, A., Danilina, N., & Makisha, N. (2021). Sustainable Development of the Slope Lands of the Russian Arctic: Investigation of the Relationship between Slope Aspects, Wind Regime and Residential Wind Comfort. *Land;* 10(4), 354.
100. Koss, H. H. (2006). On differences and similarities of applied wind comfort criteria. *Journal of Wind Engineering and Industrial Aerodynamics*, 94(11), 781-797.
101. Kotthaus S, Grimmond C S B. (2012) Identification of Micro-scale Anthropogenic CO2, heat and moisture sources–Processing eddy covariance fluxes for a dense urban environment. *Atmospheric Environment*; 57: 301-316.
102. Kotthaus S, Grimmond C S B. (2014) Energy exchange in a dense urban environment–Part II: Impact of spatial heterogeneity of the surface. *Urban Climate*; 10: 281-307.
103. Kubota T., Miura M., Tominaga Y., et al. (2008)Wind tunnel tests on the relationship between building density and pedestrian-level wind velocity: Development of guidelines for realizing acceptable wind environment in residential neighborhoods. *Building and Environment*; 43(10): 1699-1708.
104. Kutzbach, J. E. (1961). Investigations of the modification of wind profiles by artificially controlled surface roughness. *Studies of the Three Dimensional Structure of the Planetary Boundary Layer*, 71-113.
105. Kuo C. Y., Tzeng C. T., Ho M. C., et al. (2015) Wind tunnel studies of a pedestrian-level wind environment in a street canyon between a high-rise building with a podium and low-level attached houses. *Energies*; 8(10): 10942-10957.

106. Lawson T. V., Penwarden A. D. (1975) The effects of wind on people in the vicinity of buildings. *In: Proceedings the 4th international conference on wind effects on buildings and structures.*

107. Lettau, H. (1969). Note on aerodynamic roughness-parameter estimation on the basis of roughness-element description. *Journal of Applied Meteorology*;m8(5), 828-832.

108. Letchford, C., Gardner, A., Howard, R., & Schroeder, J. (2001). A comparison of wind prediction models for transitional flow regimes using full-scale hurricane data. *Journal of Wind Engineering and Industrial Aerodynamics*; 89(10), 925-945.

109. Leo, L. S., Buccolieri, R., & Di Sabatino, S. (2018). Scale-adaptive morphometric analysis for urban air quality and ventilation applications. *Building Research & Information*; 46(8), 931-951.

110. Li B., Luo Z., Sandberg M., et al. (2015) Revisiting the 'Venturi effect' in passage ventilation between two non-parallel buildings. *Building and Environment*; 94: 714-722.

111. Li B., Cunyan J., Lu W., et al. (2019) A parametric study of the effect of building layout on wind flow over an urban area. *Building and Environment*; 160: 106-160.

112. Lin, M., Hang, J., Li, Y., Luo, Z., & Sandberg, M. (2014). Quantitative ventilation assessments of idealized urban canopy layers with various urban layouts and the same building packing density. *Building and Environment*; 79, 152-167.

113. Lindberg F, Grimmond C S B. (2011) The influence of vegetation and building morphology on shadow patterns and mean radiant temperatures in urban areas: model development and evaluation. *Theoretical and Applied Climatology*; 105(3): 311-323.

114. Liu S, Pan W, Zhang H, et al. (2017) CFD simulations of wind distribution in an urban community with a full-scale geometrical model. *Building and Environment*; 117: 11-23.

115. Lombardo, F. T., & Krupar III, R. J. (2017). Characterization and comparison of aerodynamic roughness lengths using ground-based photography and sonic anemometry. *Journal of Structural Engineering*; 143(7), 04017049.

116. Macdonald, R. W., Griffiths, R. F., & Hall, D. J. (1998). An improved method for the estimation of surface roughness of obstacle arrays. *Atmospheric Environment*; 32(11), 1857-1864.

117. Masters, F. J., Vickery, P. J., Bacon, P., & Rappaport, E. N. (2010). Toward objective, standardized intensity estimates from surface wind speed observations. *Bulletin of the American Meteorological Society*; 91(12), 1665-1682.

118. Matzarakis A, Matuschek O. (2011) Sky view factor as a parameter in applied climatology-rapid estimation by the SkyHelios model. *Meteorologische Zeitschrift*; 20(1): 39.

119. Melbourne, W. H. (1978). Criteria for environmental wind conditions. *Journal of Wind Engineering and Industrial Aerodynamics*; *3*(2-3), 241-249.

120. Menter F R. (1994) Two-equation eddy-viscosity turbulence models for engineering applications. *AIAA Journal*; 32(8): 1598-1605.
121. Miller, C., Balderrama, J. A., & Masters, F. (2015). Aspects of observed gust factors in landfalling tropical cyclones: gust components, terrain, and upstream fetch effects. *Boundary-Layer Meteorology*; 155(1), 129-155.
122. Mittal H, Sharma A, Gairola A.(2018) A review on the study of urban wind at the pedestrian level around buildings. *Journal of Building Engineering*; 18: 154-163.
123. Mittal H., Sharma A., Gairola A. (2019) Numerical simulation of pedestrian level wind flow around buildings: effect of corner modification and orientation. *Journal of Building Engineering*; 22: 314-326.
124. Mittal H., Sharma A., Gairola A. (2020) Numerical simulation of pedestrian level wind conditions: effect of building shape and orientation. *Environmental Fluid Mechanics*; 20(4): 663-688
125. Mochida A, Tominaga Y, Murakami S, et al. (2002) Comparison of various *k-ε* models and DSM applied to flow around a high-rise building-report on AIJ cooperative project for CFD prediction of wind environment. *Wind and Structures*; 5(23): 227-244.
126. Montazeri H, Blocken B. (2013) CFD simulation of wind-induced pressure coefficients on buildings with and without balconies: validation and sensitivity analysis. *Building and Environment*; 60: 137-149.
127. Montazeri, H., & Montazeri, F. (2018). CFD simulation of cross-ventilation in buildings using rooftop wind-catchers: Impact of outlet openings. *Renewable Energy*; 118, 502-520.
128. Mortezazadeh, M., & Wang, L. L. (2020). Solving city and building microclimates by fast fluid dynamics with large timesteps and coarse meshes. *Building and Environment*; 179, 106955.
129. Murakami, S., Iwasa, Y., & Morikawa, Y. (1986). Study on acceptable criteria for assessing wind environment at ground level based on residents' diaries. *Journal of Wind Engineering and Industrial Aerodynamics*; 24(1), 1-18.
130. Nakajima, K., Ooka, R., & Kikumoto, H. (2018). Evaluation of *k-ε* Reynolds stress modeling in an idealized urban canyon using LES. *Journal of Wind Engineering and Industrial Aerodynamics*; 175, 213-228.
131. NBCC (National Building Code of Canada). (2020). User's Guide-NBCC 2015. Structural Commentaries (Part 4). Issued by the Canadian Commission on Buildings and Fire Codes, National Research Council of Canada, Ottawa.
132. Oke, T. R. (1988). Street design and urban canopy layer climate. *Energy and Buildings*; 11(1-3), 103-113.

133. Panofsky, H. A., Larko, D., Lipschut, R., Stone, G., Bradley, E. F., Bowen, A. J., & Højstrup, J. (1982). Spectra of velocity components over complex terrain. *Quarterly Journal of the Royal Meteorological Society*; 108(455), 215-230.
134. Petersen, R. L. (1997). A wind tunnel evaluation of methods for estimating surface roughness length at industrial facilities. *Atmospheric Environment*; 31(1), 45-57.
135. Penwarden, A. D., Grigg, P. F., & Rayment, R. (1978). Measurements of wind drag on people standing in a wind tunnel. *Building and Environment*; 13(2), 75-84.
136. Powell, M. D., Houston, S. H., & Reinhold, T. A. (1996). Hurricane Andrew's landfall in south Florida. Part I: Standardizing measurements for documentation of surface wind fields. *Weather and Forecasting*; *11*(3), 304-328.
137. Powell, M. D., & Houston, S. H. (1996). Hurricane Andrew's landfall in south Florida. Part II: Surface wind fields and potential real-time applications. *Weather and Forecasting*; 11(3), 329-349.
138. Ratcliff, M. A., & Peterka, J. A. (1990). Comparison of pedestrian wind acceptability criteria. *Journal of Wind Engineering and Industrial Aerodynamics;* 36, 791-800.
139. Ratti, C., Di Sabatino, S., & Britter, R. (2006). Urban texture analysis with image processing techniques: winds and dispersion. *Theoretical and Applied Climatology*; 84(1), 77-90.
140. Rafailidis, S. (1997). Influence of building areal density and roof shape on the wind characteristics above a town. *Boundary-layer Meteorology*; 85(2), 255-271.
141. Raupach, M. R. (1994). Simplified expressions for vegetation roughness length and zero-plane displacement as functions of canopy height and area index. *Boundary-Layer Meteorology;* 71(1-2), 211-216.
142. Raymer, W. G. (1962). Wind resistance of conifers. Teddington, UK: National Physical Laboratory.
143. Ricci, A., Kalkman, I., Blocken, B., Burlando, M., Freda, A., & Repetto, M. P. (2017). Local-scale forcing effects on wind flows in an urban environment: Impact of geometrical simplifications. *Journal of Wind Engineering and Industrial Aerodynamics*; 170, 238-255.
144. Ricci, A., Kalkman, I., Blocken, B., Burlando, M., Freda, A., & Repetto, M. P. (2018). Large-scale forcing effects on wind flows in the urban canopy: Impact of inflow conditions. *Sustainable Cities and Society*; *42*, 593-610.
145. Ricci, A., Burlando, M., Repetto, M. P., & Blocken, B. (2019). Simulation of urban boundary and canopy layer flows in port areas induced by different marine boundary layer inflow conditions. *Science of the Total Environment*; 670, 876-892.

146. Ricci, A., & Blocken, B. (2020). On the reliability of the 3D steady RANS approach in predicting microscale wind conditions in seaport areas: The case of the IJmuiden sea lock. *Journal of Wind Engineering and Industrial Aerodynamics*; *207*, 104437.

147. Ricci, A., Kalkman, I., Blocken, B., Burlando, M., & Repetto, M. P. (2020). Impact of turbulence models and roughness height in 3D steady RANS simulations of wind flow in an urban environment. *Building and Environment*; 171, 106617.

148. Ricci, A., Guasco, M., Caboni, F., Orlanno, M., Giachetta, A., & Repetto, M. P. (2022). Impact of surrounding environments and vegetation on wind comfort assessment of a new tower with vertical green park. *Building and Environment*; 207, 108409.

149. Richards, P. J., & Hoxey, R. P. (1993). Appropriate boundary conditions for computational wind engineering models using the *k-ε* turbulence model. *Journal of Wind Engineering and Industrial Aerodynamics*; 46, 145-153.

150. Roth, M., & Oke, T. R. (1993). Turbulent transfer relationships over an urban surface. I. Spectral characteristics. *Quarterly Journal of the Royal Meteorological Society*; 119(513), 1071-1104.

151. Santiago, J. L., Martilli, A., & Martín, F. (2007). CFD simulation of airflow over a regular array of cubes. Part I: Three-dimensional simulation of the flow and validation with wind-tunnel measurements. *Boundary-layer Meteorology*; 122(3), 609-634.

152. Sanz-Andres, A., & Cuerva, A. (2006). Pedestrian wind comfort: Feasibility study of criteria homogenisation. *Journal of Wind Engineering and Industrial Aerodynamics*; 94(11), 799-813.

153. Schmid, H. P., & Bünzli, B. (1995). The influence of surface texture on the effective roughness length. *Quarterly Journal of the Royal Meteorological Society*; 121(521), 1-21.

154. Shih, T. H., Liou, W. W., Shabbir, A., Yang, Z., & Zhu, J. (1995). A new *k-ε* eddy viscosity model for high reynolds number turbulent flows. *Computers & Fluids*; 24(3), 227-238.

155. Shishegar, N. (2013). Street design and urban microclimate: analyzing the effects of street geometryand orientation on airflow and solar access in urban canyons. *Journal of Clean Energy Technologies*; 1(1).

156. Shirzadi, M., Tominaga, Y., & Mirzaei, P. A. (2020). Experimental study on cross-ventilation of a generic building in highly-dense urban areas: Impact of planar area density and wind direction. *Journal of Wind Engineering and Industrial Aerodynamics*; 196, 104030.

157. Shui, T., Liu, J., Yuan, Q., Qu, Y., Jin, H., Cao, J., & Chen, X. (2018). Assessment of pedestrian-level wind conditions in severe cold regions of China. *Building and Environment*; *135*, 53-67.

158. Spalding, D. B., Launder, B. E., Morse, A. P., & Maples, G. (1974). Combustion of hydrogen-air jets in local chemical equilibrium: A guide to the CHARNAL computer program. No. REPT-73-1.

159. Stathopoulos, T. (1984). Wind loads on low-rise buildings: a review of the state of the art. *Engineering Structures*; 6(2), 119-135.
160. Stathopoulos, T. (1984). Design and fabrication of a wind tunnel for building aerodynamics. *Journal of Wind Engineering and Industrial Aerodynamics*; 16(2-3), 361-376.
161. Stathopoulos, T. (1985). Wind environmental conditions around tall buildings with chamfered corners. *Journal of Wind Engineering and Industrial Aerodynamics*; 21(1), 71-87.
162. Stathopoulos, T., & Storms, R. (1986). Wind environmental conditions in passages between buildings. *Journal of Wind Engineering and Industrial Aerodynamics*; 24(1), 19-31.
163. Stathopoulos, T. (2006). Pedestrian level winds and outdoor human comfort. *Journal of Wind Engineering and Industrial Aerodynamics*; 94(11), 769-780.
164. Stathopoulos, T., Zisis, I., & Wang, K. (2009). Terrain classification and exposure factor in the 2005 National Building Code of Canada. Taipei: TW.
165. Stathopoulos, T., & Blocken, B. (2016). Pedestrian wind environment around tall buildings. *In Advanced Environmental Wind Engineering* Springer, Tokyo; 101-127.
166. Simiu, E., & Scanlan, R. H. (1996). *Wind effects on structures: fundamentals and applications to design* (Vol. 688). New York: John Wiley.
167. Schmid, H. P., & Oke, T. R. (1990). A model to estimate the source area contributing to turbulent exchange in the surface layer over patchy terrain. *Quarterly Journal of the Royal Meteorological Society*; 116(494), 965-988.
168. Spalart, P., & Allmaras, S. (1992). A one-equation turbulence model for aerodynamic flows. In *30th Aerospace Sciences Meeting and Exhibit*; 439.
169. Soulhac, L., Garbero, V., Salizzoni, P., Mejean, P., & Perkins, R. J. (2009). Flow and dispersion in street intersections. *Atmospheric Environment*; 43(18), 2981-2996.
170. Takano, Y., & Moonen, P. (2013). On the influence of roof shape on flow and dispersion in an urban street canyon. *Journal of Wind Engineering and Industrial Aerodynamics*; 123, 107-120.
171. Takemi, T., Yoshida, T., Horiguchi, M., & Vanderbauwhede, W. (2020). Large-eddy-simulation analysis of airflows and strong wind hazards in urban areas. *Urban Climate*; 32, 100625.
172. Tamura, Y., Suda, K., Sasaki, A., Miyashita, K., Iwatani, Y., Maruyama, T., ... & Ishibashi, R. (2001). Simultaneous wind measurements over two sites using Doppler sodars. *Journal of Wind Engineering and Industrial Aerodynamics*; 89(14-15), 1647-1656.
173. Taylor, P. A. (1988). Turbulent wakes in the atmospheric boundary layer. In *Flow and Transport in the Natural Environment: Advances and Applications*. Springer, Berlin, Heidelberg. 270-292.

174. Tolias, I. C., Koutsourakis, N., Hertwig, D., Efthimiou, G. C., Venetsanos, A. G., & Bartzis, J. G. (2018). Large Eddy Simulation study on the structure of turbulent flow in a complex city. *Journal of Wind Engineering and Industrial Aerodynamics*; 177, 101-116.

175. Tominaga, Y., Yoshie, R., Mochida, A., Kataoka, H., Harimoto, K., & Nozu, T. (2005). Cross comparisons of CFD prediction for wind environment at pedestrian level around buildings. *Part*, *2*, 2661-2670.

176. Tominaga, Y., Mochida, A., Yoshie, R., Kataoka, H., Nozu, T., Yoshikawa, M., & Shirasawa, T. (2008). AIJ guidelines for practical applications of CFD to pedestrian wind environment around buildings. *Journal of Wind Engineering and Industrial Aerodynamics*; 96(10-11), 1749-1761.

177. Tominaga, Y., Akabayashi, S. I., Kitahara, T., & Arinami, Y. (2015). Air flow around isolated gable-roof buildings with different roof pitches: Wind tunnel experiments and CFD simulations. *Building and Environment*; 84, 204-213.

178. Tsang, C. W., Kwok, K. C., & Hitchcock, P. A. (2012). Wind tunnel study of pedestrian level wind environment around tall buildings: Effects of building dimensions, separation and podium. *Building and Environment*; 49, 167-181.

179. Tse, K. T., Zhang, X., Weerasuriya, A. U., Li, S. W., Kwok, K. C., Mak, C. M., & Niu, J. (2017). Adopting 'lift-up' building design to improve the surrounding pedestrian-level wind environment. *Building and Environment*; 117, 154-165.

180. Tsichritzis, L., & Nikolopoulou, M. (2019). The effect of building height and façade area ratio on pedestrian wind comfort of London. *Journal of Wind Engineering and Industrial Aerodynamics*; 191, 63-75.

181. Tsutsumi, J., Katayama, T., & Nishida, M. (1992). Wind tunnel tests of wind pressure on regularly aligned buildings. *Journal of Wind Engineering and Industrial Aerodynamics*; 43(1-3), 1799-1810.

182. Uematsu, Y., Yamada, M., Higashiyama, H., & Orimo, T. (1992). Effects of the corner shape of high-rise buildings on the pedestrian-level wind environment with consideration for mean and fluctuating wind speeds. *Journal of Wind Engineering and Industrial Aerodynamics*; 44(1-3), 2289-2300.

183. Van Beeck, J. P. A. J., Dezsö, G., & Planquart, P. (2009). Microclimate assessment by sand erosion and Irwin probes for atmospheric boundary layer wind tunnels. *Proceedings of the PHYSMOD2009, Rhode-Saint-Genése*.

184. Verkaik, J. W., & Holtslag, A. A. M. (2007). Wind profiles, momentum fluxes and roughness lengths at Cabauw revisited. *Boundary-layer Meteorology*; 122(3), 701-719.

185. Vita, G., Shu, Z., Jesson, M., Quinn, A., Hemida, H., Sterling, M., & Baker, C. (2020). On the assessment of pedestrian distress in urban winds. *Journal of Wind Engineering and Industrial Aerodynamics*; 203, 104200.

186. Wamser, C., Moller, H., & Panofsky, H. A. (1977). On the spectral scale of wind fluctuations within and above the surface layer. *Quarterly Journal of the Royal Meteorological Society*; 103(438), 721-730.

187. Wang, K., & Stathopoulos, T. (2006). The impact of exposure on wind loading of low buildings. In *Structures Congress 2006: Structural Engineering and Public Safety* ; 1-10.

188. Wang, K., & Stathopoulos, T. (2007). Exposure model for wind loading of buildings. *Journal of Wind Engineering and Industrial Aerodynamics*; 95(9-11), 1511-1525.

189. Weng, W., Taylor, P. A., & Salmon, J. R. (2010). A 2-D numerical model of boundary-layer flow over single and multiple surface condition changes. *Journal of Wind Engineering and Industrial Aerodynamics*; 98(3), 121-132.

190. Wu, H., & Stathopoulos, T. (1994). Further experiments on Irwin's surface wind sensor. *Journal of Wind Engineering and Industrial Aerodynamics*; 53(3), 441-452.

191. Wiren B.G., (1975). A wind-tunnel study of wind velocities in passages between and through buildings. Proceeding 4th International Conference on Wind Effects on Buildings and Structures, Heathrow, United Kingdom. 465-475.

192. Wieringa, J. (1980). Representativeness of wind observations at airports. *Bulletin of the American Meteorological Society*; 61(9), 962-971.

193. Wieringa, J. (1992). Updating the Davenport roughness classification. *Journal of Wind Engineering and Industrial Aerodynamics*; 41(1-3), 357-368.

194. Wiernga, J. (1993). Representative roughness parameters for homogeneous terrain. *Boundary-Layer Meteorology*; 63(4), 323-363.

195. Xie, Z. T., Coceal, O., & Castro, I. P. (2008). Large-eddy simulation of flows over random urban-like obstacles. *Boundary-layer Meteorology*; 129(1), 1-23.

196. Xu, Y., Ren, C., Ma, P., Ho, J., Wang, W., Lau, K. K. L., ... & Ng, E. (2017). Urban morphology detection and computation for urban climate research. *Landscape and Urban Planning*; 167, 212-224.

197. Xu, X., Yang, Q., Yoshida, A., & Tamura, Y. (2017). Characteristics of pedestrian-level wind around super-tall buildings with various configurations. *Journal of Wind Engineering and Industrial Aerodynamics*; 166, 61-73.

198. Yamamura, S., & Kondo, Y. (1993). Numerical study on relationship between building shape and ground-level wind velocity. *Journal of Wind Engineering and Industrial Aerodynamics*; 46, 773-778.

199. Yakhot, V., & Orszag, S. A. (1986). Renormalization group analysis of turbulence. I. Basic theory. *Journal of Scientific Computing*; 1(1), 3-51.

200. Yim, S. H. L., Fung, J. C. H., Lau, A. K. H., & Kot, S. C. (2009). Air ventilation impacts of the "wall effect" resulting from the alignment of high-rise buildings. *Atmospheric Environment*; 43(32), 4982-4994.

201. Yoshie, R., Jiang, G., Shirasawa, T., & Chung, J. (2011). CFD simulations of gas dispersion around high-rise building in non-isothermal boundary layer. *Journal of Wind Engineering and Industrial Aerodynamics*; 99(4), 279-288.

202. Yu, J., Stathopoulos, T., & Li, M. (2021). Estimating Exposure Roughness Based on Google Earth. *Journal of Structural Engineering*; 147(3), 04020353.

203. Zaki, S. A., Hagishima, A., Tanimoto, J., & Ikegaya, N. (2011). Aerodynamic parameters of urban building arrays with random geometries. *Boundary-layer Meteorology*; 138(1), 99-120.

204. Zhang, A., Gao, C., & Zhang, L. (2005). Numerical simulation of the wind field around different building arrangements. *Journal of Wind Engineering and Industrial Aerodynamics*; 93(12), 891-904.

205. Zhang, X., Tse, K. T., Weerasuriya, A. U., Li, S. W., Kwok, K. C., Mak, C. M., ... & Lin, Z. (2017). Evaluation of pedestrian wind comfort near 'lift-up' buildings with different aspect ratios and central core modifications. *Building and Environment*; 124: 245-257.

206. Zhang, X., Weerasuriya, A. U., Zhang, X., Tse, K. T., Lu, B., Li, C. Y., & Liu, C. H. (2020). Pedestrian wind comfort near a super-tall building with various configurations in an urban-like setting. In *Building simulation.* Tsinghua University Press. 13 (6): 1385-1408.

207. Zheng, X., & Yang, J. (2021). CFD simulations of wind flow and pollutant dispersion in a street canyon with traffic flow: Comparison between RANS and LES. *Sustainable Cities and Society*; 75, 103307.

Appendix Background of Numerical Work and Validation Procedure

The applications of CFD in urban wind environment were started with regular or staggered arranged idealized urban-like obstacles (Santiago et al. 2007, Du et al. 2018, and Nakajima et al. 2018). The numerical investigation of wind flow in complex area were started in the last twenty years, as the flow filed are more complex and a fine quality mesh and high-performance computer is required. To ensure the accuracy of CFD simulation, several best practice guidelines were established (Franke et al. 2004, Tominage et al. 2008, Jakeman et al. 2006). The guidelines are briefly summarised as follows:

(1) The numerical models should include all buildings and structures that have an impact on the flow at the location of interest.

(2) The computational domain should be large enough to avoid the artificial acceleration. The size can be determined from the height of the tallest building and the blockage ratio.

(3) The computational grid of hexahedral or prismatic cells near solid boundaries are preferable. A grid-sensitivity test of at least three different sizes should be conducted.

(4) The boundary conditions should be consistent.

(5) At least second-order discretization schemes should be adopted.

Improving the accuracy of numerical simulation method on PLW in urban area is still being challenged. In the last couple of decades, the factors that influence the accuracy of CFD simulation were studied by comparing with wind tunnel tests or field measurement data, which are computational domain size, turbulence model, ground surface roughness, inlet boundary conditions, meshing strategy, et al. Most of this research are conducted with steady-state RANS turbulence

model, with the advantage of lower requirement of meshing size and higher computational efficiency compared with LES turbulence model. The deficiency of RANS turbulence model is the underestimation of wind speed in the wake region (Tominaga et al. 2008, Blocken et al. 2012).

As the accuracy of CFD simulations of flow field in complex urban area are intensively studied, the application of CFD in the microclimates simulations has become part of the urban design process to guide the construction of the urban (Brozovsky et al. 2021). Initial use of CFD applications for environmental issues is the prediction of pedestrian wind environment. Since then, the numerical methodology has been extended to the application of dust dispersion from building site. These applications are based on the RANS turbulence model (Kataoka et al. 2020). With the development of high-performance computer, the LES model is used to predict the unsteady flow field related problems and aerodynamic wind load on structures. According to the comparison with wind tunnel test and field measurement data, the proper execution of CFD is equivalent to the wind tunnel experiment. CFD is the most useful tool for developing mesoscale urban canopy parameterizations (Buccolieri et al. 2021).

Blocken et al. (2004, 2009, 2012) conducted numerical simulation to investigate the PLW comfort in passage between tall buildings, around a large football stadium, and the Eindhoven University campus. Montazeri et al. (2013, 2018) conducted CFD analysis of wind comfort on high-rise building balconies. Janssen et al. (2013) conducted 3D RANS simulations to compare different wind comfort criteria based on whole-flow field data for a complex case study. Stathopoulos and Blocken (2016), Zhang et al. (2020) and Zhang (2017) conducted numerical simulations to influence the impact of tall building, super tall building, and megatall building on PLW comfort, respectively. Blocken et al. (2016) reviewed the wind tunnel test and CFD techniques on PLW conditions around buildings and their accuracy for wind comfort assessment. Hsieh et al. (2016),

Kang et al.(2017, 2020) investigate the influence of trees on the wind comfort. Allegrini and Kubilay (2017) conducted CFD simulations to study the Wind sheltering effect of a small railway station shelter and its impact on wind comfort for passengers. Adamek et al. (2017) took the case study of the financial district in Toronto for the pedestrian level wind assessment through city development. Du et al. (2018) conducted four RANS models test and found that the RNG turbulence models yields better results in predicting PLW while SKE model cannot provided adequate predicted results. Shui et al. (2018) evaluated PLW conditions in severe cold region of China. Tsichritzis and Nikolopoulou (2019) investigated the effect of building height and façade area ratio on pedestrian wind comfort. Tsichritzis and Nikolopoulou (2019) adopted the CFD simulation method to investigate the effect of building height and façade area ratio on pedestrian wind comfort of London, UK, et al. Korobeynikova et al. (2021) adopted CFD method to investigate the relationship between slope aspects, wind regime and residential wind comfort. Zheng et al. (2021) adopted k-ε turbulence model to investigate the characteristics of wind flow around a building with different surrounding building layer. Ricci et al. (2020, 2022) found that the turbulence model had larger impact on the urban wind flow than the setup of ground roughness, he also investigate the impact of surrounding environments and vegetation on wind comfort assessment of a new tower with vertical green park by 3D RANS calculations. The wind comfort assessment methodology of wind tunnel test and CFD techniques has been reviewed by Blocken et al. (2014, 2016) and Jacob and Saguat (2018).

The accuracy of the CFD methodology is validated by wind tunnel test introduced in Chapter 4. The CFD results of the wind directions of W, WSW, W are combined, as well as the wind directions of N, NNE, NE. The numerical simulation results are compared with the corresponding wind tunnel test results in the scatter plot, - see Figure A.1. The root-mean-square error (RMSE) value

of these two groups are 1.26 and 1.55, respectively and the mean absolute error (MAE) of both groups are 36.5% and 46.5% respectively. Figure A.1 shows that most locations with large deviation are in the range of low PLW velocity less than 4 m/s. In the investigation of PLW, it is the high velocity that affect the wind comfort and being concerned, so the CFD results are assumed to be acceptable.

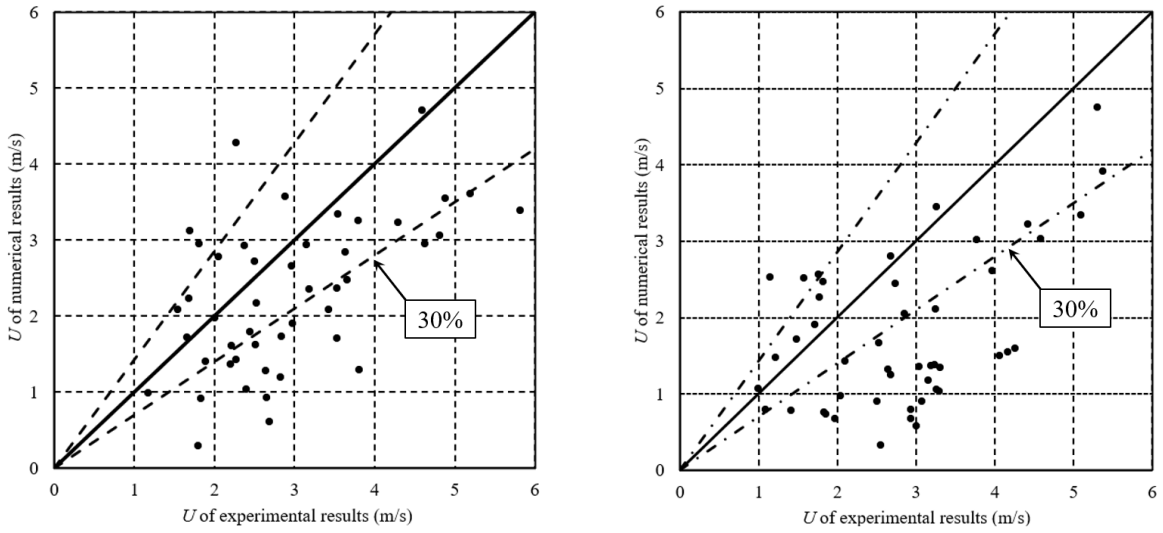

(a) Wind directions of N, NNE and NE (b) Wind directions of SW, WSW and W

Figure A.1 Deviation of PLW velocity between experimental and numerical method. Dashed black lines represent 30% deviations, as indicated.

The wind velocity and vector contour at the pedestrian level height, as well as the locations with large deviations of each wind direction are summarized in Figure A.2 – A.3. The location with the deviation of $0.5 > U_{CFD}/U_{WT}$ and $U_{CFD}/U_{WT} > 1.5$ are circled in red. The velocity vector contours show that these locations with large deviations with the wind tunnel test are the locations at the wake flow. This may due to the reason that the RANS turbulence model is less accurate in the prediction of the turbulence at the wake flow. It should be noted that most of the deviations appears at the low wind velocity, while it is the high PLW velocity that affects the wind comfort and

pedestrian safety. The two figure also show that there are more locations with large deviations in the wind directions of SW, WSW, and W than the wind directions of N, NNE, and NE. The reason is that most of observation points are sheltered in the wind directions of SW, WSW, and W, so the evaluation metrics of RMSE and MAE of these wind directions is worse than the wind directions of N, NNE, and NE.

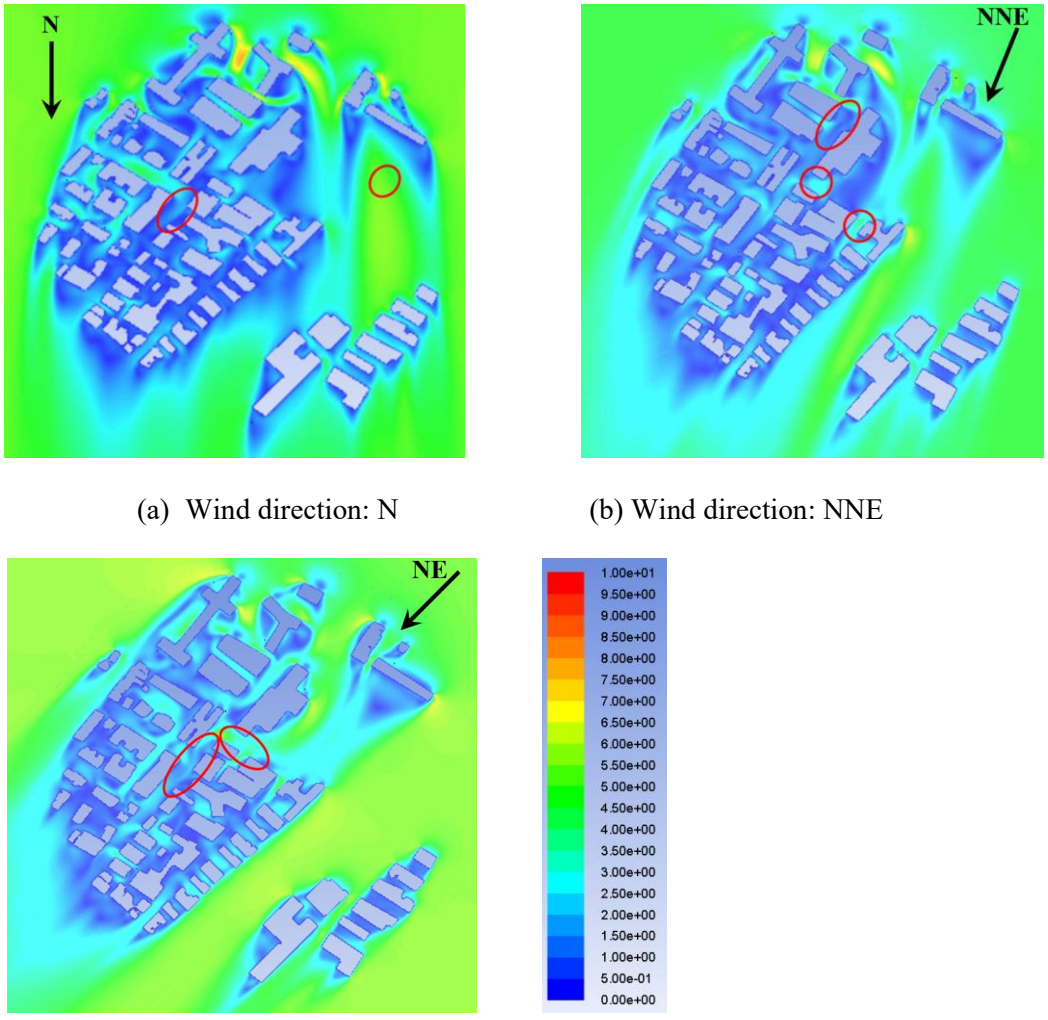

(a) Wind direction: N

(b) Wind direction: NNE

(c) Wind direction: NE

Figure A.2 The velocity contour at the pedestrian height for the wind directions of N, NNE and NE.

(Unit: m/s)

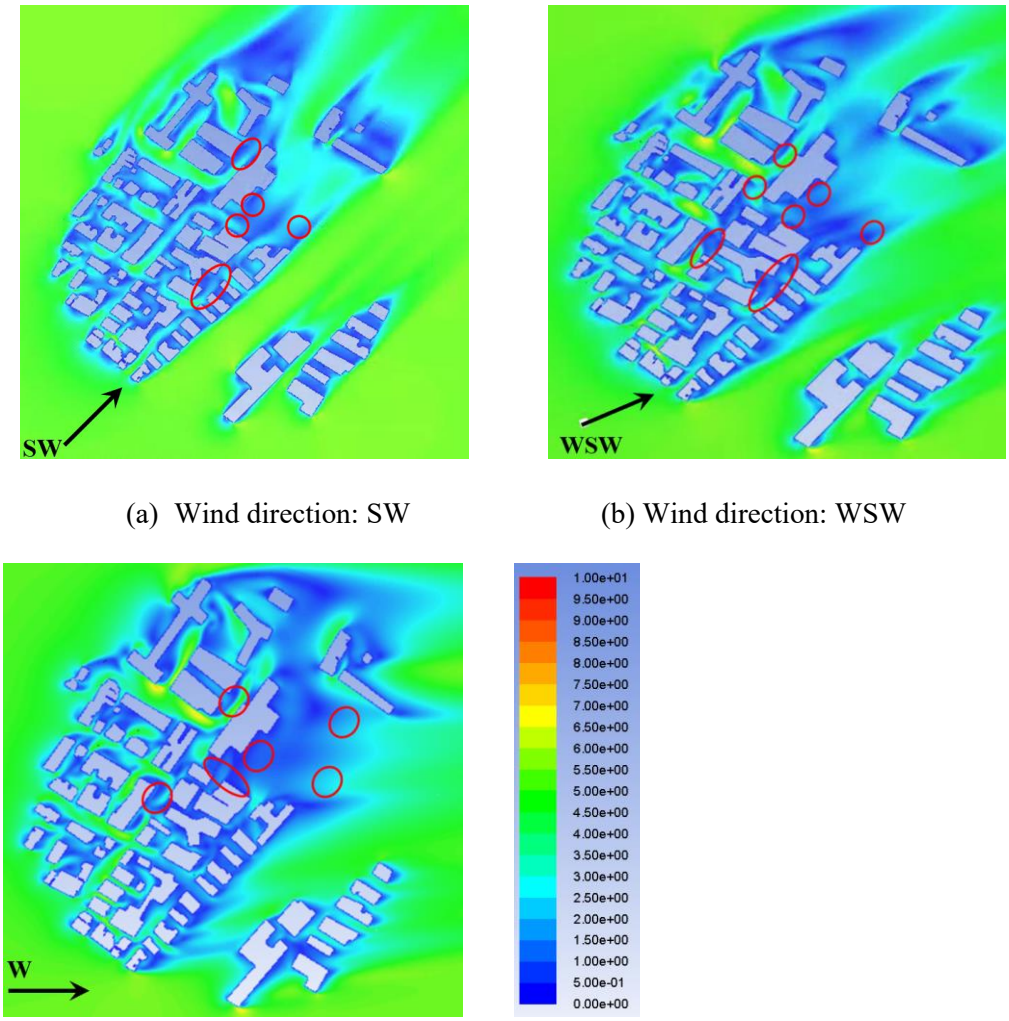

(a) Wind direction: SW

(b) Wind direction: WSW

(c) Wind direction: W

Figure A.3 The velocity contour at the pedestrian height for the wind directions of SW, WSW and W.

(Unit: m/s)